UDK 66:54(05) CODEN HMIDA 8 ISSN 0367–598X

4

Hemijska industrija

Vol. 78

Časopis Saveza hemijskih inženjera Srbije

Chemical Industry

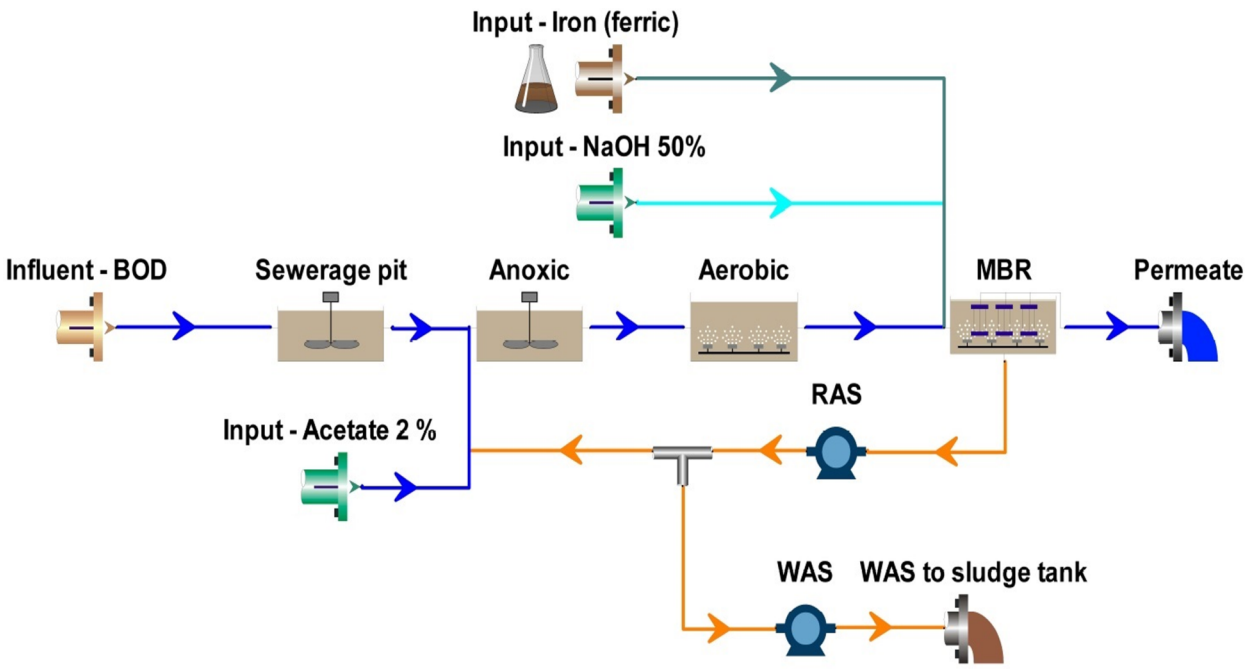

BEOGRAD, OKTOBAR-DECEMBAR 2024. HMIDA 8, 78(4) 315-372 (2024)

Aktivnosti Saveza hemijskih inženjera Srbije pomažu:

**MINISTARSTVO NAUKE,
TEHNOLOŠKOG RAZVOJA
I INOVACIJA
REPUBLIKE SRBIJE**

Tehnološko-metalurški fakultet
Univerziteta u Beogradu

Prirodno-matematički fakultet
Univerziteta u Novom Sadu

Institut za tehnologiju nuklearnih i
drugih mineralnih sirovina, Beograd

Tehnološki fakultet
Univerziteta u Novom Sadu

Institut za hemiju, tehnologiju i metalurgiju
Univerziteta u Beogradu

Fakultet tehničkih nauka
Univerziteta u Novom Sadu

Tehnološki fakultet
Univerziteta u Nišu, Leskovac

Fakultet tehničkih nauka
Univerziteta u Prištini
Kosovska Mitrovica

Institut IMS, Beograd

DCP HEMIGAL
Leskovac

Barič

Elixir Prahovo

Chemical Industry
Химическая промышленность

Hemijska industrija

Časopis Saveza hemijskih inženjera Srbije
Journal of the Association of Chemical Engineers of Serbia
Журнал Союза химических инженеров Сербии

VOL. 78 **Beograd, oktobar – decembar 2024.** **Broj 4**

Izdavač
Savez hemijskih inženjera Srbije
Beograd, Kneza Miloša 9/I

Glavni urednik
Bojana Obradović

Zamenica glavnog i odgovornog urednika
Emila Živković

Pomoćnik glavnog i odgovornog urednika
Ivana Drvenica

Urednici
Jelena Bajat, Dejan Bezbradica, Ivana Banković-Ilić, Dušan Mijin, Marija Nikolić, Đorđe Veljović, Tatjana Volkov-Husović

Članovi uredništva
Nikolaj Ostrovski, Milorad Cakić, Željko Čupić, Miodrag Lazić, Slobodan Petrović, Milovan Purenović, Aleksandar Spasić, Dragoslav Stoiljković, Radmila Šećerov-Sokolović, Slobodan Šerbanović, Nikola Nikačević, Svetomir Milojević

Članovi uredništva iz inostranstva
Dragomir Bukur (SAD), Jiri Hanika (Češka Republika), Valerij Meshalkin (Rusija), Ljubiša Radović (SAD), Constantinos Vayenas (Grčka)

Likovno-grafičko rešenje naslovne strane
Milan Jovanović

Redakcija
11000 Beograd, Kneza Miloša 9/I
Tel/fax: 011/3240-018
E-pošta: shi@ache.org.rs
www.ache.org.rs

Izlazi kvartalno, rukopisi se ne vraćaju

Za izdavača: Ivana T. Drvenica

Sekretar redakcije: Slavica Desnica

Izdavanje časopisa pomaže
Republika Srbija, Ministarstvo nauke, tehnološkog razvoja i inovacija

Uplata pretplate i oglasnog prostora vrši se na tekući račun Saveza hemijskih inženjera Srbije, Beograd, broj 205-2172-71, Komercijalna banka a.d., Beograd

Menadžer časopisa i kompjuterska priprema
Aleksandar Dekanski

Štampa
Razvojno-istraživački centar grafičkog inženjerstva, Tehnološko-metalurški fakultet, Univerzitet u Beogradu, Karnegijeva 4, 11000 Beograd

Indeksiranje
Radovi koji se publikuju u časopisu *Hemijska Industrija* ideksiraju se preko *Thompson Reuters Scietific®* servisa *Science Citation Index - Expanded™* i *Journal Citation Report (JCR)*

SADRŽAJ/CONTENTS

Special topic: New methods in the process industry
Specijalna tema: Nove metode u procesnoj industriji
Guest Editor/Gost urednik: Mirjana Kijevčanin

New methods in the process industry

Mirjana Kijevčanin

University of Belgrade, Faculty of Technology and Metallurgy, Karnegijeva 4, Belgrade, Serbia

EDITORIAL

UDC: 66:681.5.015.23

Hem. Ind. **78(4)** 315 (2024)

Available on-line at the Journal web address: http://www.ache.org.rs/HI/

Keywords: Vaste valorization; green solvents; biofuels; water treatment; circular economy.

We are happy to launch a new special topic with the aim of introducing new methods and procedures for optimizing industrial processes. These works highlight the industry's ongoing commitment to sustainability, efficiency, and environmental responsibility.

In this issue, the first paper [1] examines the thermodynamic properties of green solvents, such as terpenes, as potential substitutes for toxic organic solvents. By investigating mixtures of terpenes with 1-propanol, researchers have provided insights into their non-ideal behavior. This research could lead to advancements in biofuels and environmentally friendly industrial applications.

The second paper [2] explores the use of waste streams to obtain valuable raw materials, specifically addressing the global challenge of phosphorus scarcity. Ash derived from the incineration of municipal wastewater sludge, revealing its high P2O5 content, opens the door to its use as an alternative raw material in mineral fertilizer production. This study is highly relevant since it supports circular economy principles and sustainable development.

The third paper [3] tackles sanitary wastewater treatment from an energy facility, which exhibits atypically high total nitrogen and biochemical oxygen demand ratios. Process adjustments, including ferric chloride dosing and increased sludge recirculation, significantly reduced nitrogen and phosphorus concentrations in the effluent, demonstrating the potential for improved wastewater management.

These contributions underscore the transformative potential of innovative methodologies in the process industry. By leveraging waste materials, advancing green chemistry, and optimizing water treatment processes, the research presented on this special topic sets a benchmark for sustainable industrial practices. We look forward to practically implementing these findings, driving progress in environmental stewardship and industrial efficiency.

REFERENCES

[1] Đorđević IA, Grozdanić ND, Kijevčanin MLj, Radović IR, Thermodynamic properties of binary mixtures of terpenes and 1-propanol in the temperature range from 288.15 to 323.15 K at atmospheric pressure. *Hem Ind.* 2024; 78(4): 317-328. https://doi.org/10.2298/HEMIND240415023D

[2] Salkunić A, Stanojević Lj, Belobaba N, Bogdanović S, Salkunić B, Circular chemistry in response to the phosphate crisis. *Hem Ind.* 2024; 78(4): 329--335. https://doi.org/10.2298/HEMIND240414022S

[3] Mitrinović DS, Perović MS, Kovačević SR, Popović MR, Radibratović ZZ, Modelling of sanitary wastewater composition and operation of a small membrane bioreactor wastewater treatment plant with denitrification and nitrification. *Hem Ind.* 2024; 78(4): 337-349. https://doi.org/10.2298/HEMIND240423025M

E-mail: mirjana@tmf.bg.ac.rs

Thermodynamic properties of binary mixtures of terpenes and 1-propanol in the temperature range from 288.15 to 323.15 K at atmospheric pressure

Ivona A. Đorđević, Nikola D. Grozdanić, Mirjana Lj. Kijevčanin and Ivona R. Radović

University of Belgrade, Faculty of Technology and Metallurgy, Belgrade, Republic of Serbia

Abstract

Terpenes are the most abundant class of chemical compounds present in essential oils. They are considered green solvents, and come from natural sources such as plants, citrus fruits, but also from tree leaves or pinecones. They find wide commercial uses in food industry as natural flavors and food additives, as well as in pharmaceutical and cosmetics industries. In order to study thermodynamic properties of binary mixtures of terpenes (α-pinene, p-cymene and linalool) with 1-propanol, density and viscosity of these mixtures were determined experimentally. Experimental measurements were done over the temperature range from 288.15 to 323.15 K at atmospheric pressure, over the entire composition range. Excess molar volumes, viscosity deviations and thermal expansion coefficients were calculated based on the experimental results of densities and viscosities. Experimentally measured properties were correlated using the Heritz-Brewer-Jouyban-Acree model, while the Redlich-Kister polynomial was used to correlate the derrived properties. All the experimentally obtained data and the derived values were used to analyze non-ideal behavior of the selected mixtures. The Heritz-Brewer-Jouyban-Acree model successfully correlated the experimental values for all three binary systems, while the Redlich-Kister successfully correlated the derived quantities.

Keywords: Density; viscosity; excess properties; modeling.

Available on-line at the Journal web address: http://www.ache.org.rs/HI/

ORIGINAL SCIENTIFIC PAPER

UDC: 621.1.016.7:54-185

Hem. Ind. **78(4)** 317-328 (2024)

1. INTRODUCTION

Most of the current industrial processes rely on organic solvents, which are often highly volatile and toxic. Terpenes, regarded as green solvents, offer a solution to many of these issues. These compounds are present in many natural sources and exhibit a diverse range of chemical structures, leading to varying methods for their extraction and purification. Having that in mind, understanding the thermodynamic properties of various terpenes is crucial. Additionally, incorporating solvents like 1-propanol into terpene mixtures is valuable for advancing extraction techniques [1-3]. Combining 1-propanol with terpenes can enhance extraction efficiency and provide a more environmentally friendly solvent option. Accurate thermodynamic calculations are crucial for predicting the behavior of these mixtures, optimizing the extraction conditions, and preventing issues like phase separation, leading to more effective and sustainable industrial processes.

The first investigated terpene was (*1S*)-(-)-*α*-pinene, later referred as α-pinene (IUPAC: (1S)-2,6,6-trimethylbicyclo-[3.1.1]-hept-2-ene), one of the two possible isomers of pinene. It is a bicyclic monoterpene with a highly reactive ring in its structure, commonly extracted from pine wood remnants and also found in pinecones. *α*-pinene is used in cosmetic and pharmaceutical industries due to its anti-inflammatory and antimicrobial effects. For many years, it has also been used in the treatment of respiratory tract infections. Also, due to many suitable properties of pinene dimers, there is a high possibility of using them in mixtures with renewable, biodegradable biofuels, which could be a green alternative to commercial diesel [4,5].

Corresponding authors: Nikola D. Grozdanić, University of Belgrade, Faculty of Technology and Metallurgy, Belgrade, Republic of Serbia
Paper received: 15 April 2024; Paper accepted: 13 December 2024; Paper published: 18 January 2025.
E-mail: ngrozdanic@tmf.bg.ac.rs
https://doi.org/10.2298/HEMIND240415023D

p-Cymene (IUPAC: 1-methyl-4-(propan-2-yl)benzene), is an aromatic hydrocarbon consisting of a para-substituted benzene ring with methyl and isopropyl groups. In addition to the only progeneric *p*-cymene, there are also two significantly less common geometric isomers, ortho- and meta-cymene. This terpene is used as an intermediate in various organic syntheses, with a particularly notable application being the addition of p-cymene to liquid fuels that lack other aromatic compounds [6]. Furthermore, *p*-cymene shows significant antimicrobial effect in a wide spectrum of actions [7,8].

Linalool (IUPAC: 3,7-dimethylocta-1,6-dien-3-ol) is a representative of terpene alcohols, which can be found in a large number of different flowers and herbs. It is estimated that over 200 plant species produce this alcohol in nature, while in *Lavandula sp.* [9], *Ocinum Basilicum* L. [10] and *Coriandrum sativum* L. [11] it is present at higher concentrations. It is used as an aroma in the production of soaps, fragrances, various food additives, in a large number of household products, but also in insecticides. Like pinene, it has anti-inflammatory properties, and it can be also converted into suitable dimers for use as a fuel [12].

Expanding the database of thermodynamic properties is vital for designing industrial processes, as the accuracy of calculations depends heavily on the consistency of the available data. Furthermore, these properties enhance understanding of molecular interactions in binary systems [13], as solvent mixtures often deviate from ideal behavior. In this work, densities and viscosities for three binary mixtures of terpenes (α-pinene, p-cymene and linalool) with 1-propanol were determined over the entire composition range, for T = 288.15 to 323.15 K and at atmospheric pressure. Furthermore, the excess properties and deviations, the excess molar volumes, the viscosity deviations and thermal expansion coefficients were calculated from the obtained density and viscosity data. The densities and viscosities were correlated by using the Heric-Brewer-Jouyban-Acree single mathematical model, while the excess properties were correlated as a function of the mole fraction by using the Redlich-Kister equation.

2. EXPERIMENTAL

2. 1. Materials

Within this work pure terpenes (*α*-pinene, *p*-cymene and linalool) were products supplied by Acros Organics (Belgium), while the pure solvent 1-propanol was purchased from Fisher Scientific (United Kingdom) (Table 1). The supplied chemicals were used without additional purification.

Table 1. *Sample details*

Chemical name	Supplier	Molar mass, g mol^{-1}	CAS registry Nº	Initial mass fraction purity
(*1S*)-(-)-*α*-pinene	Acros organics	136.23	7785-26-4	0.98
p-cymene	Acros organics	134.21	99-87-6	0.99
linalool	Acros organics	154.25	78-70-6	0.97
1-propanol	Fisher scientific	60.09	71-23-8	0.99

2. 2. Apparatus and procedure

Density (*ρ*) and viscosity (*η*) of binary mixtures of selected terpenes (*α*-pinene, *p*-cymene, linalool) with 1-propanol were measured by using an Anton Paar SVM 3000/G2 viscometer (Anton Paar, Austria) with rotating cylinders. Measurements were performed in the temperature range from 288.15 to 323.15 K with 5 K increment. A detailed explanation of the characteristics of the apparatus and measurement methods used can be found in our previous work [14].

All chemicals were stored in dark bottles in a separate room when not used, due to terpenes sensitivity to the direct light. The mixtures were prepared gravimetrically using a Mettler AG 204 balance (Mettler Toledo, Switzerland) with a precision of 0.10 μg in the whole range of compositions with the step of 0.01 μg. The standard uncertainty in the mole fraction calculation was less than ±10^{-4}, with all molar quantities derived from the IUPAC relative atomic mass table. The combined expanded uncertainties in the density and viscosity measurements are estimated to 2 kg m^{-3} and 0.007 mPa s, respectively.

2. 3. Comparison with literature

Experimental values of densities and viscosities for pure terpenes and 1-propanol were compared with literature data at several temperatures. Table 2 provides the experimental data and literature values, including their percent deviations.

Table 2. *Experimental and literature values of densities, viscosities of the pure components and deviation at atmospheric pressure*

Component	T^b / K	ρ^c / g m^{-3}		η^d / mPa s		Deviation at atmospheric pressure[a], %	
		Exp.	Lit.	Exp.	Lit.	Density	*V*iscosity
(1S)-(-)-α-pinene	288.15	0.8643	0.862393 [15]	1.548	1.5542 [15]	0.22	0.40
	293.15	0.8603	0.858276 [15] 0.8585 [16]	1.410	1.4403 [15]	0.24 0.21	2.15
	298.15	0.8562	0.854151 [15] 0.8548 [16] 0.85403 [17]	1.288	1.3096 [15] 1.293 [21]	0.24 0.16 0.25	1.68 0.39
	303.15	0.8521	0.850019 [15] 0.8519 [16]	1.182	1.2110 [15]	0.24 0.02	2.45
	308.15	0.8480	0.845876 [15] 0.8469 [16] 0.84579 [17]	1.087	1.1223 [15]	0.25 0.13 0.26	3.25
	313.15	0.8438	0.841722 [15] 0.8429 [16]	0.999	1.0423 [15]	0.25 0.11	4.33
	318.15	0.8396	0.837556 [15] 0.8394 [16] 0.83864 [17]	0.9248	0.9711 [15]	0.24 0.02 0.11	5.01
	323.15	0.8354	0.833377 [15] 0.8352 [16]	0.859	0.9065 [15]	0.24 0.02	5.53
p-cymene	288.15	0.8614	0.860963 [15]	0.917	0.9358 [15]	0.05	2.05
	293.15	0.8575	0.856962 [15] 0.8561 [16]	0.847	0.8719 [15]	0.06 0.16	2.94
	298.15	0.8536	0.852953 [15] 0.8521 [16] 0.85347 [17]	0.793	0.8073 [15] 0.798 [21]	0.08 0.18 0.02	1.80 0.63
	303.15	0.8496	0.848934 [15] 0.8486 [16]	0.744	0.7595 [15]	0.08 0.12	2.08
	308.15	0.8456	0.844907 [15] 0.8445 [16]	0.697	0.7126 [15]	0.08 0.13	2.24
	313.15	0.8415	0.840873 [15] 0.8406 [16]	0.647	0.6672 [15]	0.07 0.11	3.12
	318.15	0.8374	0.836826 [15] 0.83846 [17]	0.613	0.6321 [15]	0.07 0.13	3.12
	323.15	0.8334	0.832768 [15] 0.8326 [16]	0.579	0.5971 [15]	0.08 0.10	3.13
linalool	293.15	0.8613	0.8618 [18]	5.431	5.53 [18]	0.06	1.82
	298.15	0.8572	0.8577 [18] 0.85809 [20] 0.85760 [21]	4.362	4.47 [18] 4.3493 [19] 4.4640 [20] 4.3810 [21]	0.06 0.10 0.05	2.48 0.29 2.34 0.44
	303.15	0.8531	0.8533 [18]	3.584	3.63 [18]	0.02	1.28
	313.15	0.8446	0.8448 [18] 0.84543 [21]	2.505	2.541 [18] 2.552 [20]	0.02 0.10	1.44 1.88
	323.15	0.8359	0.8362 [18]	1.844	1.868 [18]	0.04	1.30
1-propanol	288.15	0.8074	0.80754 [22]	2.502	2.5150 [23]	0.02	0.52
	293.15	0.8035	0.80362 [24]	2.194	2.198 [25]	0.01	0.18
	298.15	0.7996	0.79956 [22] 0.79941 [24]	1.968	1.970 [25]	0.01 0.02	0.10
	303.15	0.7956	0.79527 [24]	1.750	1.745 [24]	0.04	0.29
	308.15	0.7915	0.79146 [22]	1.560	1.5050 [23]	0.01	3.53
	313.15	0.7875	0.78662 [24]	1.366	1.361 [25]	0.11	0.37
	318.15	0.7832	0.78319 [22]	1.250	1.2253 [26]	<0.01	1.98
	323.15	0.7791	0.77391 [24]	1.125	1.115 [25]	0.67	0.89

Standard uncertainties u for each variable are: [a]$u(p)$ = 0.005 MPa, [b]$u(T)$ = 0.01 K and the combined expanded uncertainties U_c are [c]$U_c(\rho)$ = 2 kg m^{-3}, [d]$U_c(\eta)$ = 0.007 mPa s with 0.95 level of confidence (k = 2)

The results show that the largest density deviation of 0.67 % occurs for 1-propanol at 323.15 K, whereas the smallest deviation of less than 0.01 % is observed for 1-propanol at 318.15 K. Conversely, the largest viscosity deviation of 5.53 % is observed for α-pinene at 323.15 K, while the smallest deviation of 0.10 % is recorded for 1-propanol at 298.15 K.

3. RESULTS AND DISCUSSION

Experimentally determined densities and viscosities for binary mixtures at different temperatures in the investigated temperature range are shown in the Table S1 (Supplementary material) and represented graphically in Figures 1 and 2, respectively.

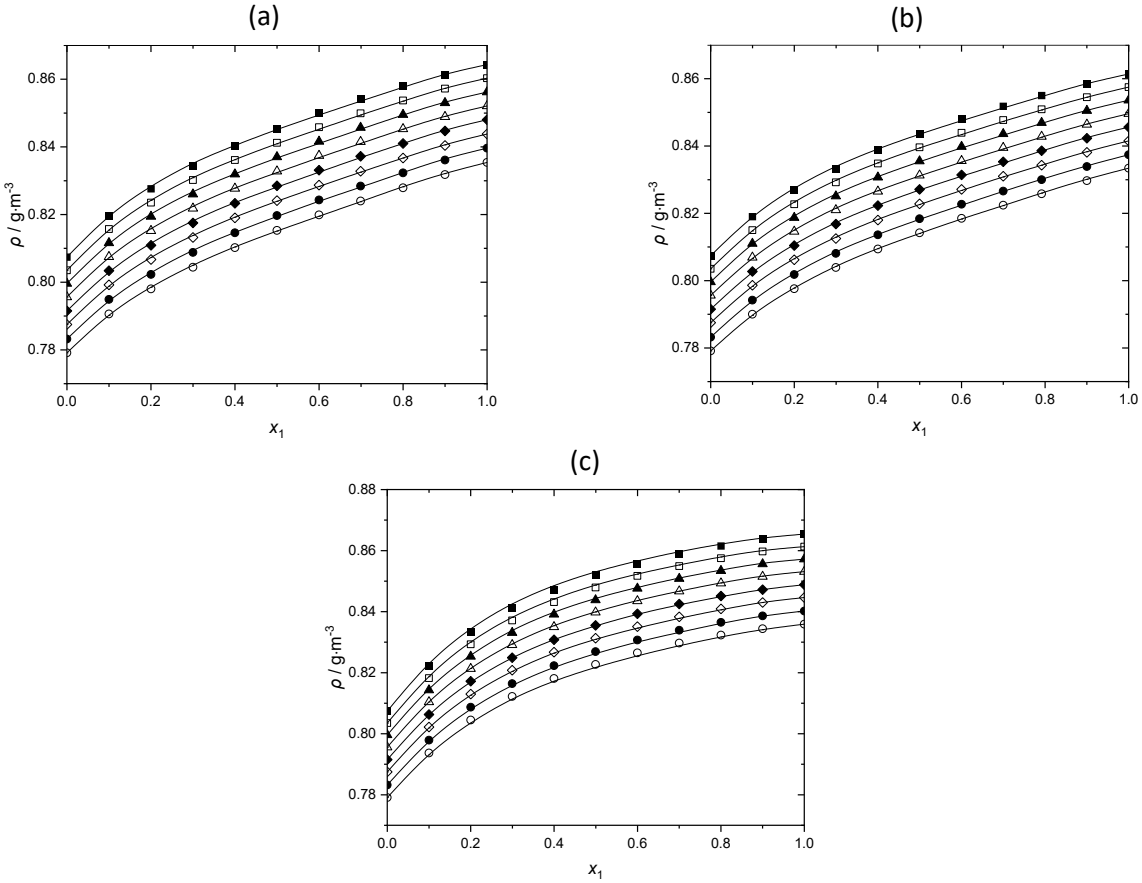

Figure 1. *Experimental values of density ρ as a function of molar fraction x_1 for the binary systems: (a) α-pinene (1) + 1-propanol (2); (b) p-cymene (1) + 1-propanol (2); (c) linalool (1) + 1-propanol (2); at following temperatures: ■ -288.15 K, □ - 293.15 K, ▲ - 298.15 K, Δ - 303.15 K, ♦ - 308.15 K, (◊) 313.15 K, ● - 318.15 K, ○ - 323.15 K; ⟶ - predictions by the Heric-Brewer-Jouyban-Acree model*

From the Figure 1 it is apparent that for all three systems density decreases with increasing temperature but increases as the amount of a terpene in the binary mixture increases. All the systems investigated show similar density values following the same trend.

Similarly to density, viscosities also decrease with the increase in temperature for all the analyzed systems. Among all the investigated terpenes only pure linalool shows higher viscosity than 1-propanol (Figure 2c), consequently viscosities increase with increasing the concentration of linalool in mixtures. For the other two systems viscosities decrease as the amount of a terpene increases.

Experimental thermodynamics properties (density and viscosity) of the investigated binary mixtures were mathematically described using the Heric-Brewer-Jouyban-Acree model, Equation (1) [27,28]:

$$\ln Y_{m,T} = x_1 \ln Y_{1,T} + x_2 \ln Y_{2,T} + J_0\left[\frac{x_1 x_2}{T}\right] + J_1\left[\frac{x_1 x_2 (x_1 - x_2)}{T}\right] + J_2\left[\frac{x_1 x_2 (x_1 - x_2)^2}{T}\right] \quad (1)$$

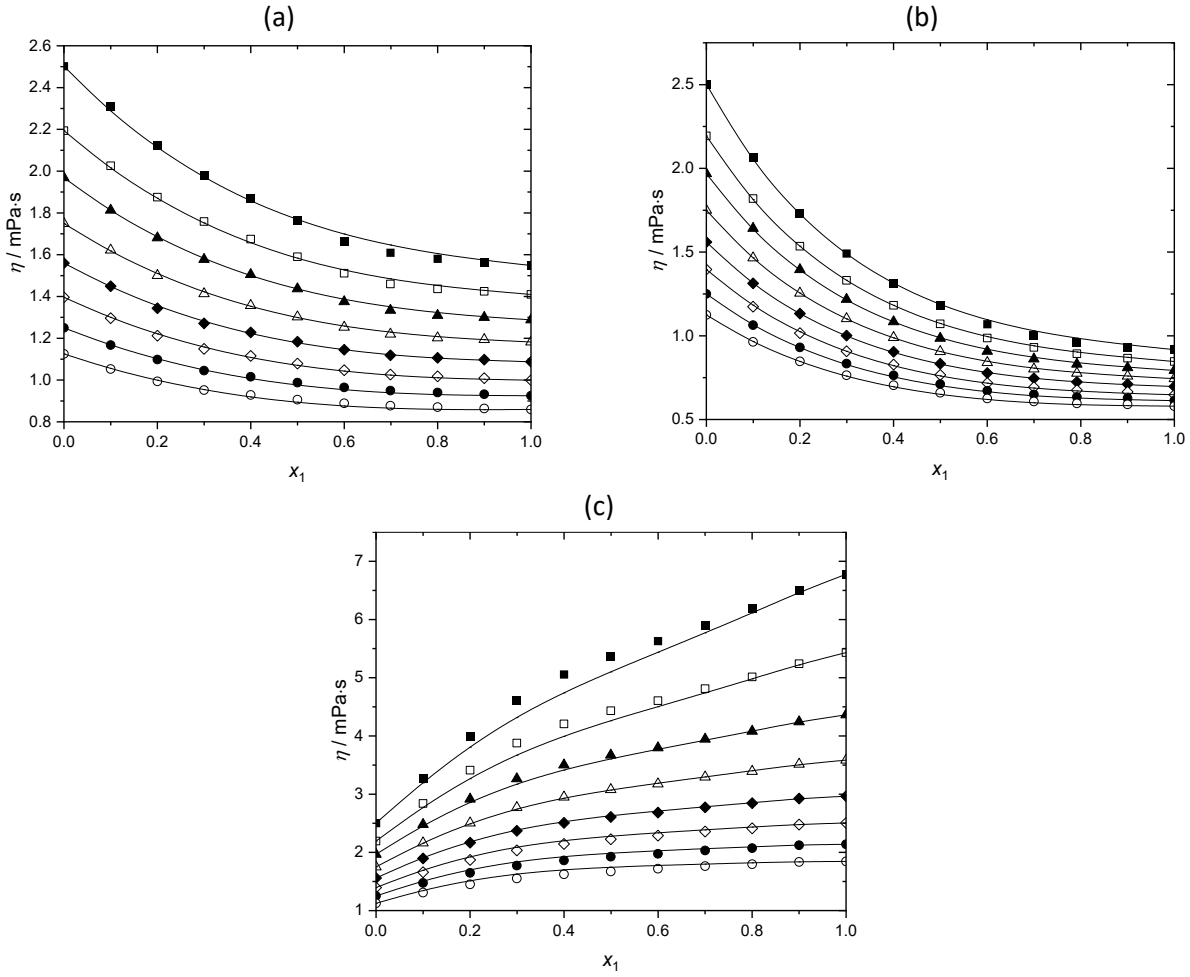

Figure 2. *Experimental values of dynamic viscosity η as a function of molar fraction x_1 for the binary systems: (a) α-pinene (1) + 1-propanol (2); (b) p-cymene (1) + 1-propanol (2); (c) linalool (1) + 1-propanol (2); at following temperatures: ■ - 288.15 K, □ - 293.15 K, ▲ - 298.15 K, Δ - 303.15 K, ♦ - 308.15 K, ◊ - 313.15 K, ● - 318.15 K, ○ - 323.15 K; ⟶ - predictions by the Heric-Brewer-Jouyban-Acree model*

$Y_{m,T}$, $Y_{1,T}$ and $Y_{2,T}$ represent the values of the corresponding property at the temperature *T*. The subscript m denotes a mixture, while 1 and 2 correlate to the pure components of the mixtures (terpene and 1-propanol). The J_i is the model parameters obtained with the use of the least squares method, where the optimal degree of the polynomial was determined based on the minimum value of the standard deviation of the correlation, Equation (2):

$$\sigma = \left(\frac{\left(\sum_{i=1}^{n} Y_i^{\text{exp}} - Y_i^{cal} \right)^2}{n-m} \right)^{1/2} \tag{2}$$

The accuracy of the used model was evaluated by the average percent deviation, Equation (3):

$$D = \frac{100}{N} \sum_{i=1}^{n} \left(\frac{Y_i^{\text{exp}} - Y_i^{cal}}{Y_i^{\text{exp}}} \right) \tag{3}$$

In Equations (2) and (3), *N* stands for number of data points in each set, *n* is the number of experimental data, *m* is the number of model parameters, while Y_{cal} and Y_{exp} are the calculated and experimental values of the observed property, respectively.

Table 3 shows Heric-Brewer-Jouyban-Acree model parameters together with standard deviation *σ* and the average percent deviation *D*.

Table 3. *Heric-Brewer-Jouyban-Acree model parameters for density and viscosity, predictions, standard deviation, and the average deviations, at T = 288.15 to 323.15 K*

Function	A_0	A_1	A_2	σ	Deviation, %
α-pinene (1) + 1-propanol (2)					
ρ / g m^{-3}	13.287	-9.1360	7.6862	0.0004	0.0449
η / mPa·s	-122.97	19.160	11.456	0.0113	0.6518
p-cymene (1) + 1-propanol (2)					
ρ / g m^{-3}	13.142	-9.0732	6.1676	0.0003	0.0335
η /mPa·s	-279.78	57.438	25.299	0.0079	0.6464
linalool (1) + 1-propanol (2)					
ρ / g m^{-3}	23.416	-13.133	7.2450	0.0006	0.0591
η /mPa·s	247.13	-186.05	104.77	0.0941	1.9800

By the analysis of the obtained results of density and viscosity modeling (Fig. 1 and Table 3) it is apparent that the Heric-Brewer-Jouyban-Acree model with three parameters was successfully used to correlate both properties over the entire temperature range, showing a very good agreement with experimental values. All the given parameters are temperature dependent. Average percent deviations show smaller deviations for densities than for viscosities, where the highest deviation is for the system linalool + 1-propanol due to higher viscosity values of linalool, particularly at lower temperatures in the interval, such as 288.15 and 293.15 K.

The experimental data were used to calculate derived thermodynamics properties. Excess molar volume (V^E) was calculated using Equation (4):

$$V^E = \frac{x_1M_1 + x_2M_2}{\rho} - \left(\frac{x_1M_1}{\rho_1} + \frac{x_2M_2}{\rho_2} \right) \quad (4)$$

where ρ represents density of the binary mixture, ρ_1 and ρ_2 are densities of pure components, while M_1 and M_2 as well as x_1 and x_2 represent molar masses and mole fractions of components, respectively.

The viscosity deviation ($\Delta\eta$) was calculated by using the experimentally determined viscosity of the binary mixture, η, and viscosities of pure components, η_1 and η_2, Equation (5):

$$\Delta\eta = \eta - \sum_{i=1}^{2} x_i\eta_i \quad (5)$$

Isobaric thermal expansion describes the increase in a liquid's volume as its temperature rises, while the pressure remains constant. Coefficients of thermal expansion measure the extent to which a material expands in response to a change in temperature. The calculated thermal expansion coefficients for the three investigated mixtures are shown in Table S1 (Supplementary material).

Eq. (6) shows the temperature dependence of density in the mixtures using a polynomial expression; Equation (6):

$$\rho = a + bT + cT^2 \quad (6)$$

The isobaric thermal expansion coefficient (α) is obtained from a density value by the following equation:

$$\alpha = -\frac{1}{\rho}\left(\frac{\partial\rho}{\partial T} \right)_p \quad (7)$$

Table S1 (Supplementary material) indicates that α values are increasing as the temperature is increased.

Calculated values of the described quantities were correlated by using the Redlich-Kister [29] polynomial Equation (8):

$$Y = x_ix_j\sum_{p=0}^{k} A_p\left(2x_i - 1\right)^p \quad (8)$$

A_p are the adjustable parameters in the equation of the related property Y (V^E, $\Delta\eta$) and the corresponding standard deviations are calculated by Equation (2). The Redlich-Kister parameters are shown in Table 4.

Figure 3 represents experimental and correlated values of the excess molar volume, calculated by the Redlich-Kister polynomial as a function of molar fraction x_1 for the investigated binary systems at different temperatures.

Table 4. *Redlich-Kister parameters for predictions of the excess molar volume, and viscosity deviation, with the corresponding root-mean-square deviations*

Function	T/K	A_0	A_1	A_2	A_3	A_4	σ
α-pinene (1) + 1-propanol (2)							
Excess molar volume	288.15	0.3514	0.1649	-0.0993	1.5115	-2.2787	0.0092
	293.15	0.4633	0.2873	0.0616	1.4390	-2.4316	0.0115
	298.15	0.5643	0.2688	0.0336	1.5310	-2.1820	0.0097
	303.15	0.2914	0.0664	0.2003	0.4380	-3.9064	0.0090
	308.15	0.7651	0.2642	0.5456	1.7332	-3.0780	0.0103
	313.15	0.9204	0.3711	0.3794	1.5923	-2.7362	0.0095
	318.15	1.0190	0.4336	0.6423	1.6913	-0.3112	0.0105
	323.15	1.1662	0.4888	0.7789	1.6904	-3.1645	0.0077
Viscosity deviation	288.15	-1.0541	-0.0013	-0.3747	0.2663	0.7841	0.0073
	293.15	-0.8530	0.0179	-0.4772	0.3109	0.7655	0.0048
	298.15	-0.7685	0.1266	-0.3965	0.1544	0.5694	0.0029
	303.15	-0.6549	0.1794	-0.4484	0.0384	0.7388	0.0037
	308.15	-0.5589	0.2024	-0.4120	0.0153	0.6524	0.0040
	313.15	-0.4762	0.1829	-0.3074	0.0726	0.4430	0.0039
	318.15	-0.4002	0.1908	-0.1772	-0.0122	0.2436	0.0024
	323.15	-0.3434	0.1787	-0.1714	-0.0048	0.2029	0.0020
p-cymene (1) + 1-propanol (2)							
Excess molar volume	288.15	0.1126	0.4746	-0.0580	1.0743	-1.6749	0.0069
	293.15	0.2174	0.5217	0.1833	1.1024	-1.9386	0.0076
	298.15	0.3383	0.5593	0.0955	1.1302	-1.7796	0.0068
	303.15	0.4600	0.5845	-0.2671	1.1817	-1.1274	0.0076
	308.15	0.5545	0.6738	-0.1092	1.1402	-1.2112	0.0064
	313.15	0.6908	0.7023	0.0955	1.2594	-1.4969	0.0051
	318.15	0.8332	0.8380	0.1991	1.0873	-1.6091	0.0042
	323.15	0.9386	0.8852	0.2250	1.2758	-1.2538	0.0051
Viscosity deviation	288.15	-2.1400	0.8394	-0.3645	0.2124	-	0.0039
	293.15	-1.7979	0.8023	-0.4156	0.1208	0.2068	0.0016
	298.15	-1.5895	0.6446	-0.2307	0.1924	-	0.0021
	303.15	-1.3717	0.5685	-0.2091	0.1955	-	0.0017
	308.15	-1.1864	0.4955	-0.1784	0.1895	-	0.0014
	313.15	-1.0264	0.4468	-0.1977	0.2959	-	0.0020
	318.15	-0.8843	0.3784	-0.1255	0.1984	-	0.0011
	323.15	-0.7733	0.3291	-0.1134	0.1773	-	0.0011
linalool (1) + 1-propanol (2)							
Excess molar volume	288.15	-2.1111	1.0005	-0.9016	-0.4801	0.7521	0.0095
	293.15	-2.1709	0.9625	-0.6558	-0.5210	-	0.0118
	298.15	-2.1571	1.0177	-0.9836	-0.5711	0.5421	0.0085
	303.15	-2.1963	1.0367	-0.7559	-0.4565	-	0.0096
	308.15	-2.2018	0.9465	-1.3225	-0.2499	0.8333	0.0073
	313.15	-2.2090	1.0129	-1.2869	-0.4501	0.8753	0.0022
	318.15	-2.2122	1.0029	-1.3522	-0.3603	0.8720	0.0042
	323.15	-2.2626	0.9727	-1.3729	-0.5575	0.7871	0.0052
Viscosity deviation	288.15	2.9352	-2.9218	-0.2324	2.6085	-	0.0094
	293.15	2.4852	-2.5063	0.0756	1.9475	-	0.0083
	298.15	2.0260	-1.8998	0.2083	1.3468	-	0.0067
	303.15	1.6506	-1.4524	0.3658	0.9980	-	0.0064
	308.15	1.3849	-1.0783	0.4062	0.6542	-	0.0047
	313.15	1.1008	-0.8123	0.3007	0.5216	-	0.0041
	318.15	0.9265	-0.6554	0.3534	0.3188	-	0.0029
	323.15	0.7608	-0.5028	0.3332	0.2282	-	0.0032

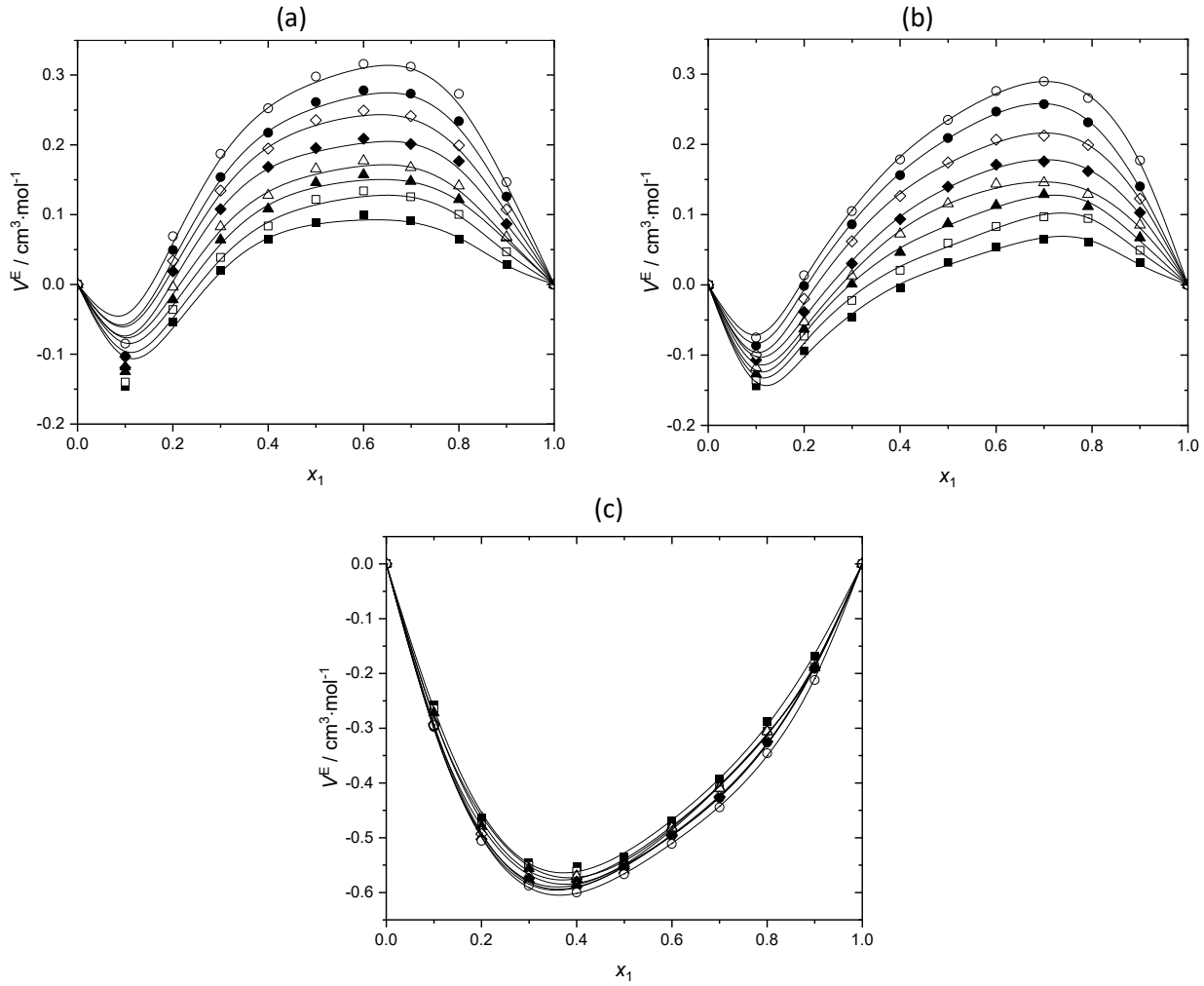

Figure 3. *Experimental values of excess molar volume V^E as a function of molar fraction x_1 for the binary systems: (a) α-pinene (1) + 1-propanol (2); (b) p-cymene (1) + 1-propanol (2); (c) linalool (1) + 1-propanol (2); at following temperatures: ■ - 288.15 K, □ - 293.15 K, ▲ - 298.15 K, Δ- 303.15 K, ♦ - 308.15 K, ◊ - 313.15 K, ● - 318.15 K, ○ 323.15 K; ⟶ - predictions by the RK equation*

The excess molar volumes show S-shape curves for binary mixtures containing *α*-pinene and *p*-cymene, while the mixtures with linalool show negative deviation from the ideal behavior over the entire composition range. The non-ideality or positive/negative V^E is the result of physical, chemical and structural characteristics of the selected mixtures. For the lower concentrations of *α*-pinene in the *α*-pinene + 1-propanol mixture apparently attractive intermolecular forces dominate causing shrinkage of volume during the mixing process. As the concentration of *α*-pinene rises above x_1 = 0.1, V^E grows positive with the maximum at x_1 = 0.6, causing the expansion in volume. The same trend occurs in the system *p*-cymene + 1-propanol. Binary mixtures containing linalool and 1-propanol show negative values for V^E with the minimum at x_1 = 0.4. In these binary mixtures attractive intermolecular forces dominate, forming hydrogen bonds between OH groups, causing negative values of V^E through the entire composition range.

Comparison of the three investigated systems shows that the temperature has the same influence, i.e the deviation from ideal behavior increases with the temperature increase.

The systems *α*-pinene + 1-propanol as well as *p*-cymene + 1-propanol show negative values for deviations in viscosities (Δ*η*) in the entire composition range (Figs 4a and 4b). Those negative values indicate that the mixtures are more viscous than the pure substances, which is more prominent for the system with *p*-cymene. Deviations grow less negative with the increase in the temperature. On the other hand, the system linalool + 1-propanol expresses asymmetrical $\Delta\eta$-x_1 function with a positive maximum at around x_1=0.4, with a lower temperature influence on Δ*η* for higher concentrations of linalool in the binary mixture.

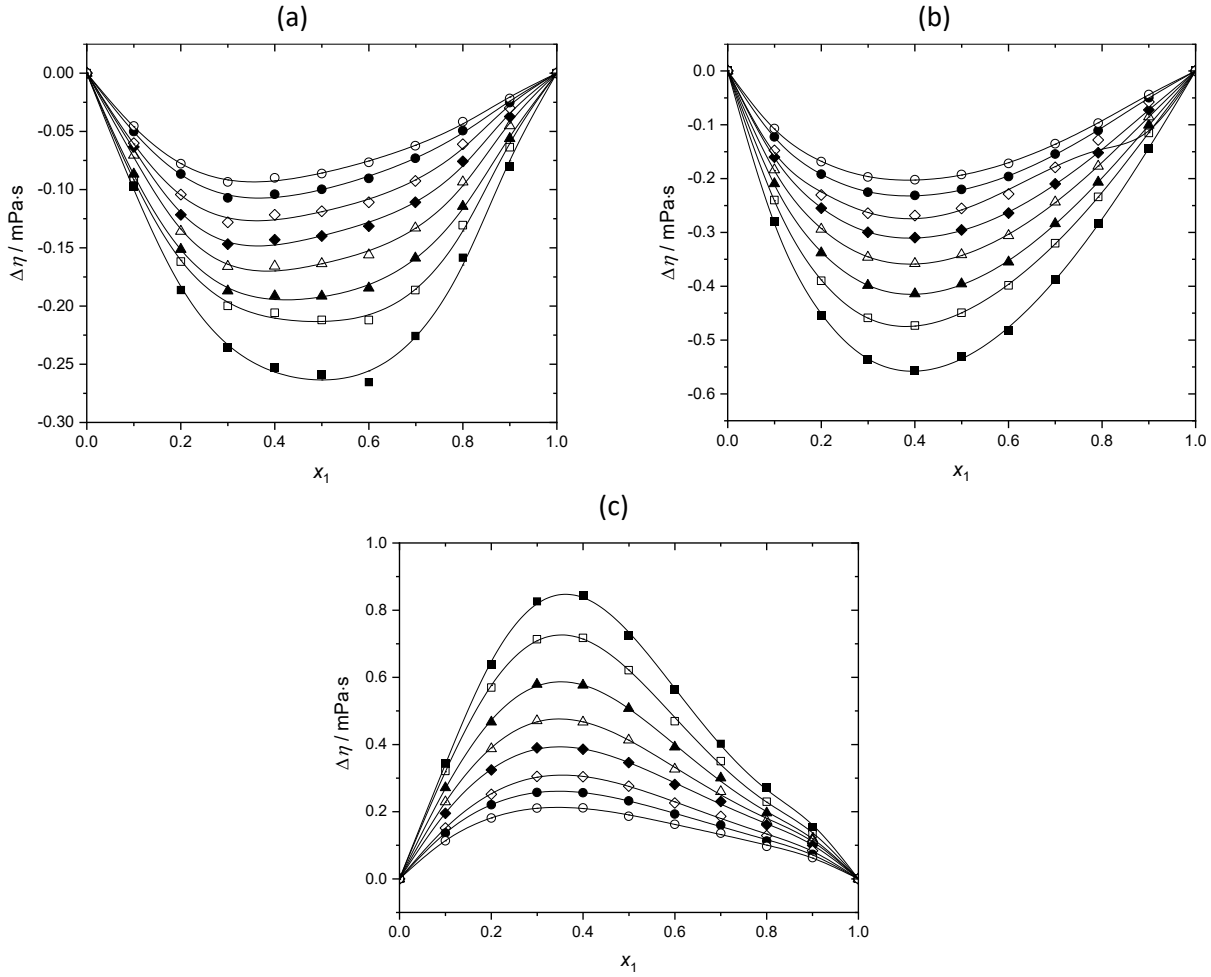

Figure 4. *Experimental values of deviations in viscosities Δη as a function of molar fraction x_1 for the binary systems: (a) α-pinene (1) + 1-propanol (2); (b) p-cymene (1) + 1-propanol (2); (c) linalool (1) + 1-propanol (2); at following temperatures: ■ - 288.15 K, □ - 293.15 K, ▲ - 298.15 K, Δ - 303.15 K, ♦ - 308.15 K, ◊ - 313.15 K, ● - 318.15 K, ○ - 323.15 K; ⎯ - predictions by the RK equation*

4. CONCLUSION

Within this paper, densities and viscosities of three binary systems, *α*-pinene + 1-propanol, *p*-cymene + 1-propanol and linalool + 1-propanol were experimentally determined in the temperature range *T* = 288.15 to 323.15 K and at atmospheric pressure over the entire composition range. Based on the experimental results the excess molar volume and viscosity deviation were calculated and fitted to the Redlich-Kister equation. Two binary mixtures, α-pinene and p-cymene with 1-propanol, showed negative values for excess molar volume for the lower concentrations of terpene in the mixture, growing positive with increasing terpene molar fractions. The system linalool + 1-propanol is the only system with positive viscosity deviation, while *α*-pinene and *p*-cymene express negative viscosity deviations in mixtures with 1-propanol. The Heric-Brewer-Jouyban-Acree model was successfully used to correlate the experimental values of the density and viscosity. For density measurements the maximum average percent deviation of 0.06 % was obtained for all three mixtures, while for the viscosity the maximum average percent deviation of 0.65 % is obtained for the α-pinene and p-cymene with 1-propanol and around 2 % for the linalool with 1-propanol. Both models successfully correlated given properties what is approved with obtained deviations.

The presented study offers valuable insights into the thermodynamic and transport properties of binary mixtures involving α-pinene, p-cymene, linalool, and 1-propanol. These findings provide a robust foundation for better understanding intermolecular interactions in systems containing terpenes and alcohols, which is critical for tailoring such mixtures for industrial applications. From a practical perspective, the distinct behavior of linalool mixtures,

especially the positive viscosity deviations, could be leveraged to optimize formulations in the pharmaceutical, cosmetic, and fragrance industries where viscosity and miscibility are essential parameters.

SUPPLEMENTARY MATERIAL

Additional data are available electronically at https://www.ache-pub.org.rs/index.php/HemInd/article/view/1134, or from the corresponding author on request.

CRediT authorship contribution statement: *Ivona A. Đorđević: experimental & writing, Nikola D. Grozdanić: modeling, Mirjana Lj. Kijevčanin: supervision, resources, Ivona R. Radović: conceptualization, writing - review & editing, supervision.*

Declaration of competing Interest: *The authors declare that they have no known competing financial interests or personal relationships that could have appeared to influence the work reported in this paper.*

Funding: *The authors gratefully acknowledge the financial support received from the Research Fund of Ministry of Education, Science and Technological Development, Republic of Serbia and the Faculty of Technology and Metallurgy, University of Belgrade (Contract No. 451-03-68/2023-14/200135).*

Acknowledgements*: This work is supported by the Ministry of Science, Technological Development, and Innovation of the Republic of Serbia, under contract 451-03-47/2023-01/200017. The authors acknowledge Dr. Thomas van Swieten and Prof. Andries Meijerink for help in obtaining photoluminescence spectra.*

REFERENCES

[1] Jiang Z, Kempinski C, Chappell J, Extraction and analysis of terpenes/terpenoids. *Curr Protoc Plant Biol*. 2006; 1(2): 345-358. https://doi.org/10.1002/cppb.20024

[2] Rodriguez-Garcia A, Hosseini S, Martinez-Chapa S, Cordell A, Multi-target activities of selected alkaloids and terpenoids. *Mini-Rev Org Chem*. 2017; 14(4): 272-279. 10.2174/1570193X14666170518151027

[3] Papada E, Gioxari A, Brieudes V, Amerikanou C, Halabalaki M, Skaltsounis L, Kaliora C. Bioavailability of terpenes and postprandial effect on human antioxidant potential. An open-label study in healthy subjects. *Mol Nut & Food Res*. 2018; 62(3): 1700751. https://doi.org/10.1002/mnfr.201700751

[4] Allenspach M, Steuer C. α-Pinene: A never-ending story. *Phytochem*. 2021; 190: 112857. https://doi.org/10.1016/j.phytochem.2021.112857

[5] Jung K, Lee Y, Choi W, Jae J, Ha M, Suh J, Lee Y. Production of high-energy-density fuels by catalytic β-pinene dimerization: effects of the catalyst surface acidity and pore width on selective dimer production. *Energy Conv and Manag*. 2016; 116: 72-79. http://dx.doi.org/10.1016/j.enconman.2016.02.053

[6] Oswald P, Whitside R, Schäffer J, Köhler M. An experimental flow reactor study of the combustion kinetics of terpenoid jet fuel compounds: Farnesane, p-menthane and p-cymene. *Fuel.* 2017; 187: 43-50. http://dx.doi.org/10.1016/j.fuel.2016.09.035

[7] Balahbib A, El Omari N, Hachlafi E, Lakhdar F, El Menyiy N, Salhi N, Bouyahya A. Health beneficial and pharmacological properties of p-cymene. *Food and Chem Tox*. 2021; 153: 112259. https://doi.org/10.1016/j.fct.2021.112259

[8] Marchese A, Arciola R, Barbieri R, Silva S, Nabavi F, Tsetegho Sokeng J., Nabavi M. Update on monoterpenes as antimicrobial agents: A particular focus on p-cymene. *Materials*. 2017; 10(8): 947. https://doi.org/10.3390/ma10080947

[9] Cheng H, Lin Y, Yeh F, Cheng S, Chang T. Potential source of S-(+)-linalool from Cinnamomum osmophloeum ct. linalool leaf: essential oil profile and enantiomeric purity. *J Agric & Food Chem*. 2012; 60(31): 7623-7628. https://doi.org/10.1021/jf302248w

[10] Hussain I, Anwar F, Sherazi H, Przybylski R. Chemical composition, antioxidant and antimicrobial activities of basil (Ocimum basilicum) essential oils depends on seasonal variations. *Food Chem*. 2008; 108(3): 986-995. https://doi.org/10.1016/j.foodchem.2007.12.010

[11] Bakkali F, Averbeck S, Averbeck D, Idaomar M. Biological effects of essential oils–a review. Food & Chem Toxic. 2008; 46(2): 446-475. https://doi.org/10.1016/j.fct.2007.09.106

[12] Meylemans A, Quintana L, Goldsmith R, Harvey G. Solvent-free conversion of linalool to methylcyclopentadiene dimers: a route to renewable high-density fuels. *Chem Sus Chem*. 2011; 4(4): 465-469. https://doi.org/10.1002/cssc.201100017

[13] Radovic I, Grozdanic N, Djordjevic B, Serbanovic S, Kijevcanin M. Prediction of excess molar volumes of binary mixtures by Prigogine-Flory-Patterson (PFP) and extended real association solution (ERAS) models, *J Serb Chem Soc*. 2017; 82: 1379-1390. http://dx.doi.org/10.2298/JSC170817103R

[14] Grozdanic N, Radovic I, Knezevic-Stevanovic A, Kijevcanin M. Volumetric properties of binary mixtures of tetrahydrofuran, dimethyl adipate, 1-butanol and 2-butanol from (288.15 to 323.15) K and modeling by Prigogine-Flory-Patterson (PFP) and Extended Real Association Solution (ERAS) models. *J Mol Liq*. 2021; 340: 117313. https://doi.org/10.1016/j.molliq.2021.117313

[15] Ilic-Pajic J, Radovic I, Grozdanic N, Stajic-Trosic J, Kijevcanin M. Volumetric and thermodynamic properties of binary mixtures of p-cymene with α-pinene, limonene and citral at atmospheric pressure and temperatures up to 323.15 K. Journal of Molecular Liquids. 2021; 344: 117486. https://doi.org/10.1016/j.molliq.2021.117486

[16] Ribeiro A, Bernardo-Gil G. Densities and refractive indices of components of pine resin. *J Chem Eng Data*. 1990; 35: 204-206. https://doi.org/10.1021/je00060a033

[17] Liao D-K, Meng X-L, Tong Z-F, Zheng D-X, Peng D-Y, Lu B. Excess Molar Enthalpies of p-cymene + α-Pinene + β-Pinene at (298.15, 308.15 and 318.15) K and at Atmospheric Pressure. *J Chem Eng Data*. 2007; 52: 808-811. http://dx.doi.org/10.1021/je060420p

[18] Clara R, Gomez Marigliano A, Solimo H. Density, Viscosity, and Refractive Index in the Range (283.15 to 353.15) K and Vapor Pressure of r-Pinene, d-Limonene, (()-Linalool, and Citral Over the Pressure Range 1.0 kPa Atmospheric Pressure. *J Chem Eng Data*. 2009; 54: 1087–1090. http://dx.doi.org/10.1021/je8007414

[19] Florido M, Andrade G, Capellini C, Carvalho H, Aracava K, Koshima C, Rodrigues C, Goncalves B. Viscosities and densities of systems involved in the deterpenation of essential oils by liquid-liquid extraction: New UNIFAC-VISCO parameters. *J Chem Thermodyn.* 2014; 72: 152-160. https://doi.org/10.1016/j.jct.2013.11.026

[20] Comelli F, Francesconi R, Castellari C. Densities, Viscosities, and Excess Molar Enthalpies of Binary Mixtures Containing Essential Oils at (298.15 and 313.15) K. The (S)-(−)-Limonene + Cineole, (S)-(−)-Limonene + Linalool, and Cineole + Linalool Systems. *J Chem Eng Data.* 2001; 46: 868–872. https://doi.org/10.1021/je010005r

[21] Comelli F, Ottani S, Francesconi R, Castellari C. Densities, Viscosities, and Refractive Indices of Binary Mixtures Containing n-Hexane + Components of Pine resins and Essential Oils at 298.15 K. *J Chem Eng Data*. 2002; 47: 93-97. https://doi.org/10.1021/je010216w

[22] Vercher E, Orchilles V, Miguel P, Martinez-Andreu A. Volumetric and Ultrasonic Studies of 1-Ethyl-3-methylimidazolium Trifluoromethanesulfonate Ionic Liquid with Methanol, Ethanol, 1-Propanol, and Water at Several Temperatures. *J Chem Eng Data*. 2007; 52: 1468-1482. https://doi.org/10.1021/je7001804

[23] Pal A, Kumar A. Viscosity of 1-Propanol + Ethylene Glycol Dimethyl, + Diethylene Glycol Dimethyl, + Triethylene Glycol Dimethyl, and + Tetraethylene Glycol Dimethyl Ethers at 288.15, 298.15 and 308.15 K. *Ind J Chem A*. 2003; 42: 2708-2716. https://nopr.niscpr.res.in/bitstream/123456789/20780/1/IJCA%2042A(11)%202708-2716.pdf

[24] Yang C, Lai H, Liu Z, Ma P. Density and Viscosity of Binary Mixtures of Diethyl Carbonate with Alcohols at (293.15 to 363.15) K and Predictive Results by UNIFAC-VISCO Group Contribution Method. *J Chem Eng Data*. 2006; 51: 1345-1351. http://dx.doi.org/10.1021/je0600808

[25] Rodriguez A, Canosa J, Dominguez A, Tojo J. Dynamic viscosities of diethyl carbonate with linear and secondary alcohols at several temperatures. *J Chem Eng Data*. 2004; 49: 157-162. http://dx.doi.org/10.1021/je0341413

[26] Saleh A, Habibullah M, Ahmed S, Uddin A, Uddin H, Khan M, Excess Molar Volumes and Viscosities of Some Alkanols with Cumene. *Phys Chem Liq.* 2006; 44: 31-43. http://dx.doi.org/10.1080/00319100500287853

[27] Jouyban A, Khoubnasabjafari M, Vaez-Gharamaleki Z, Fekari Z, Eugene Jr W. Calculation of the viscosity of binary liquids at various temperatures using Jouyban–Acree model. *Chem and Pharm Bull*. 2005; 53(5): 519-523. https://doi.org/10.1248/cpb.53.519

[28] Wan Normazlan D, Sairi A, Alias Y, Udaiyappan F, Jouyban A, Khoubnasabjafari M. Composition and temperature dependence of density, surface tension, and viscosity of EMIM DEP/MMIM DMP+ water+ 1-propanol/2-propanol ternary mixtures and their mathematical representation using the Jouyban–acree model. *J Chem Eng Data*. 2014; 59(8): 2337-2348. http://dx.doi.org/10.1021/je400576e

[29] Redlich O, Kister T. Algebraic representation of thermodynamic properties and the classification of solutions. *Ind & Eng Chem*. 1948; 40(2): 345-348. https://doi.org/10.1021/ie50458a036

Termodinamička svojstva dvokomponentnih smeša terpena i 1-propanola u intervalu temperature od 288,15 do 323,15 K na atmosferskom pritisku

Ivona A. Đorđević, Nikola D. Grozdanić, Mirjana Lj. Kijevčanin i Ivona R. Radović

Univerzitet u Beogradu, Tehnološko-metalurški fakultet, Beograd, Srbija

(Naučni rad)

Izvod

Najzastupljenija klasa hemijskih jedinjenja prisutna u esencijalnim uljima jesu terpeni. Smatraju se zelenim rastvaračima, a potiču iz prirodnih izvora poput biljaka, citrusnog voća, ali i lišća drveća ili šišarki. Pronalaze veliku komercijalnu upotrebu u granama prehrambene industrije, kao prirodne arome i dodaci hrani, a pored toga su veoma zastupljeni i u farmaceutskoj i kozmetičkoj industriji. U cilju proučavanja termodinamičkih svojstava smeša terpena (α-pinen, p-cimen i linalool) sa 1-propanolom, eksperimentalno su određene gustine i viskoznosti za navedene smeše. Eksperimentalna merenja rađena su u opsegu temperatura od 288,15 do 323,15 K na atmosferskom pritisku, za ceo opseg udela. Na osnovu eksperimentalno dobijenih rezultata za gustine i viskoznosti izračunate su vrednosti dopunske molarne zapremine, kao i vrednosti promene viskoznosti pri mešanju. Izmerene veličine (gustina i viskoznost) korelisane su korišćenjem modela Herik-Bruer-Džuben-Eikrija (Heric-Brewer-Jouyban-Acree), dok je za korelisanje dopunskih veličina (dopunska molarna zapremina, promena viskoznosti i koeficijent termičke ekspanzije) korišćen Redlih-Kisterov (Redlich-Kister) polinom. Svi eksperimentalno dobijeni podaci i njihove izvedene veličine korišćene su za analizu neidealnog ponašanja odabranih smeša. Herik-Bruer-Džuben-Eikrijev model je uspešno korelisao eksperimentalne vrednosti za sva tri binarna sistema u celom temperaturnom opsegu i na atmosferskom pritisku, dok je Redlih-Kisterov polinom uspešno korelisao izvedene veličine.

Ključne reči: gustina; viskozitet, dopunske veličine, modelovanje

Cirkularna hemija kao odgovor na krizu izazvanu nedostatkom fosfata

Alija Salkunić[1], Ljiljana Stanojević[2], Nikola Belobaba[1], Slavica Bogdanović[1] i Bajro Salkunić[2]

[1]*Elixir Zorka - Mineralna đubriva, Hajduk Veljkova 1, Šabac, Srbija*
[2]*Elixir Group, Hajduk Veljkova 1, Šabac, Srbija*

Izvod

Sirovi fosfat se koristi kao sirovina za proizvodnju đubriva na bazi fosfora, a nedostatak njegove ponude mogao bi negativno uticati na globalno snabdevanje hranom. Evropska komisija je klasifikovala ovu sirovinu kao kritičnu sa aspekta procenjenih zaliha. Godinama unazad istražuju se novi resursi koji mogu biti zamena za fosfatnu komponentu u proizvodnji đubriva i drugih proizvoda koja sadrže fosfor. Kao alternativa javila se mogućnost primene pepela dobijenog insineracijom mulja nastalog u postupku prerade komunalnih otpadnih voda. U ovom radu je kao studija slučaja analiziran sastav pepela dobijenog spaljivanjem mulja nastalog preradom komunalnih otpadnih voda u cilju određivanja potencijala za delimičnu zamenu fosfata u đubrivu. Pokazano je da pepeo sadrži P_2O_5 u velikom procentu, što čini ovu vrstu mulja atraktivnom za korišćenje u proizvodnji mineralnih đubriva kao alternativne sirovine. Prikazani rezultati imaju značaj za Republiku Srbiju gde je planirano da se do 2041. godine izgradi preko 300 postrojenja za prečišćavanje otpadnih komunalnih voda i projekcije su da će biti generisano oko 135.000 tona mulja godišnje. Prikazana analiza sastava pepela poreklom od ove vrste mulja opravdava izgradnju energana, kao što je planirana energana u Prahovu, Srbija, koje će tretirati otpad i doprineti principima cirkularne ekonomije i hemije.

Ključne reči: mineralna đubriva, cirkularna ekonomija, fosforna komponenta, valorizacija pepela.

Dostupno na Internetu sa adrese časopisa: http://www.ache.org.rs/HI/

STRUČNI RAD

UDC 543.392:631.85: 631.878

Hem. Ind. **78(4)** 329-335 (2024)

1. UVOD

Fosfor je nemetal iz 15. grupe periodnog sistema elemenata i jedan je od najvažnijih elemenata za svakodnevni život čoveka. On je gradivna supstanca DNK i RNK (u obliku fosfatnog jona PO_4^{3-}), igra bitnu ulogu u prenosu energije kroz žive ćelije kao komponenta adenozin-trifosfata (ATP), a kao gradivna komponenta fosfolipida, doprinosi stvaranju ćelijskih membrana [1]. Pored toga, znatna količina fosfora sadržana je u organizmima živih bića, pre svega u kostima i zubima, uglavnom kao kalcijum-hidroksiapatit, $Ca_{10}(PO_4)_6(OH)_2$ [2]. Prosečan ljudski organizam sadrži oko 650 g fosfora [3]. U svojoj elementarnoj formi fosfor se ne može naći slobodan u prirodi zbog velike reaktivnosti, a minerali koji sadrže fosfor (uglavnom kao fosfati) raspršeni su po celoj planeti u sedimentnim stenama (vrlo malo u stenama magmatskog porekla) [4].

Prirodno, koncentracija fosfora u zemljištu je mala i predstavlja ograničavajući faktor u rastu poljoprivrednih kultura. Fosforna đubriva su glavni unos neorganskog fosfora u poljoprivredno zemljište i približno 70 do 80 % fosfora u kultivisanim zemljištima je neorganskog porekla [5]. Đubriva su materije namenjene za direktnu ili indirektnu ishranu biljaka, a unose se u zemljište da bi mu se korigovao sastav i dodao onaj deo biogenih elemenata koji nedostaju, a u cilju profitabilne biljne proizvodnje [6]. Za značaj primene đubriva u ishrani biljaka znalo se od davnina, a ruski naučnik Prjanjišnjikov koji se smatra osnivačem moderne agrohemije, govoreći o značaju hemizacije u savremenoj zemljoradnji rekao je: „Izostavite primenu mineralnih đubriva i prinosi će opasti kao što su opadali u Nemačkoj za vreme Prvog svetskog rata (1914-1918), kada je hemijska industrija proizvodila umesto đubriva eksplozivne materije, i za 4 godine rata prinosi su se vratili na nivo od pre 75 godina“ [7].

Međutim, sve veća upotreba fosfatnih veštačkih đubriva u poljoprivredi dovela je do intenzivne ekploatacije fosfatnih ruda, pa se poslednjih godina sve više govori o mogućoj fosfatnoj krizi. Naime, najveći deo proizvodnje sirovog fosfata (proizvoda koji nastaje kada se ruda koja sadrži dovoljno fosfora podvrgne obogaćivanju) u svetu koristi se u poljoprivrednom sektoru, uglavnom kao đubrivo ili sirovina za proizvodnju mineralnih đubriva [5]. Kako se očekuje da će globalno stanovništvo ubrzano rasti narednim decenijama, potražnja za fosforom, odnosno fosfatima će se povećavati zbog sve veće potrebe za proizvodnjom hrane.

Korespodencija: Alija Salkunić, Elixir Zorka - Mineralna đubriva, Hajduk Veljkova 1, Šabac, Srbija
E-mail: alija.salkunic@elixirzorka.rs
Rad primljen: 14. aprila 2024, Rad prihvaćen: 13. decembra 2024, Rad publikovan: 30. Decembra 2024.
https://doi.org/10.2298/HEMIND240414022S

Iako brojni istraživači tvrde da se sa novootkrivenim zalihama fosfatnih sirovina kriza odložila [1,4,8,9], upitna je i raspodela svetskih rezervi fosfora. Kuper i sar. su predvideli da se „70 % globalne proizvodnje trenutno proizvodi iz rezervi koje će se potrošiti u roku od 100 godina“, i da će „Maroko, sa 73 % globalnih rezervi, morati da poveća proizvodnju za 700 % do 2075. godine“ [10].

Kako bi se osigurala sigurna proizvodnja mineralnih đubriva u budućnosti, a time i obezbedilo dovoljno hrane, mora se naći alternativa za sirovi fosfat koji se i našao na listi kritičnih sirovina u Evropskom zakonu o kritičnim sirovinama iz 2023. godine [11].

2. CIRKULARNA HEMIJA

Dosadašnji sistem linearne ekonomije koji se zasniva na „uzmi-napravi-iskoristi-odloži“ gubi primenljivost jer povećava generisanje otpada što sa sobom nosi ogromne ekološke i ekonomske troškove, a korisne materije bivaju „zarobljene“ i na taj način gube ekonomsku vrednost. Da bi budućnost bila održiva, hemija i njeni proizvodi moraju biti prilagođeni cirkularnoj ekonomiji - sistemu koji ima za cilj eliminisanje otpada, cirkulaciju i reciklažu proizvoda i uštedu resursa i zaštitu životne sredine [12].

Dok su principi ranije koncipirane zelene hemije pomogli optimizaciji linearnih procesa, sam okvir zelene hemije ne doprinosi obezbeđivanju istinske održivosti. U studiji [13] dat je odličan komentar o razlikama između zelene hemije i onoga što je nazivano cirkularnom hemijom. Autori su postavili novi set vodećih principa koji potencijalno omogućavaju holističko razmatranje prilikom dizajniranja procesa ili proizvoda. Prema principima zelene hemije proizvodnju otpada treba sprečiti, a proizvode dizajnirati tako da budu reciklabilni, bezbedni i obnovljivi. Cirkularna hemija ide korak dalje, i predlaže da nastajanje otpada ne mora da se spreči u fazi proizvodnje, već da se on mora u budućnosti koristiti kao resurs i na kraju, kao „obnovljiva sirovina“ što se dobro uklapa i u koncept cirkularne ekonomije. Pored toga, novi okvir cirkularne hemije zahteva naročitu pažnju prilikom procene prirode proizvoda, koji se smatraju „zelenim“ u svom delovanju, ali su proizvedeni korišćenjem linearnih procesa. Naime, jedan od principa zelene hemije je i proizvodnja proizvoda koji su dizajnirani tako da budu (bio)razgradljivi, ali cirkularna ekonomije i hemija, s druge strane, vrednuju obezbeđivanje dugovečnosti materijala tako što ga drže u opticaju dugo vremena. Cirkularna hemija, kao i cirkularna ekonomija, tretira sirovine (hemikalije) i energiju uskladištenu u materijalu kao dugoročnu investiciju i stoga, promoviše ponovnu upotrebu proizvoda, te čuva uskladištenu energiju umesto da zahteva dodatni unos energije. Na kraju, principi cirkularne hemije, pod uticajem cirkularne ekonomije, leže u razmatranju ne samo održivosti životne sredine, već i ekonomske dobiti.

U literaturi je predstavljeno dvanaest principa cirkularne hemije koji kombinuju koncepte iz hemije sa cirkularnom ekonomijom i održivošću [14]:

1. Sakupljanje i korišćenje otpada - Ponovna upotreba otpada kao resursa je neophodan preduslov za omogućavanje cirkularnosti. Otpad je vredan resurs koji treba pretvoriti u tržišno prihvatljive proizvode kako bi se promovisala cirkulacija elemenata, molekula i materijala.
2. Povećanje cirkularnosti atoma - Kružni procesi treba da imaju za cilj da maksimalno iskoriste sve atome u postojećim molekulima. To zahteva optimalan dizajn proizvoda koji će favorizovati efikasne korake separacije i prečišćavanja, dok se istovremeno povećavaju mogućnosti ponovne upotrebe atoma, uzimajući u obzir ekološki prihvatljiv pristup.
3. Optimizacija upotrebe prirodnih resursa - Očuvanje resursa treba da bude ciljano. Promovišući ponovnu upotrebu, sačuvaće se i pametnije koristiti ograničene sirovina.
4. Težnja energetskoj efikasnosti - U svakom koraku proizvodnje ili korišćenja proizvoda energetska efikasnost treba da bude maksimalna.
5. Poboljšanje efikasnosti procesa – Procesne inovacije treba da kontinuirano promovišu i povećavaju ponovnu upotrebu i recikliranje, bilo da otpad potiče iz procesa proizvodnje ili van njega, a po mogućnosti na licu mesta.
6. Vođenje procesa proizvodnje tako da nema negativnog efekta po životnu sredinu - Hemijski procesi ne bi trebalo da oslobađaju zagađujuća jedinjenja u životnu sredinu.
7. Opimalni dizajn proizvoda – Potrebno je dizajnirati takav proizvod koji ima najbolje mogućnosti na kraju životnog ciklusa, uzimajući u obzir separaciju, prečišćavanje i razgradnju.
8. Procena održivosti proizvoda - Procena životnog ciklusa (engl. *life cycle assessment*, LCA) treba da bude urađena za svaki proizvod kako bi se identifikovale neefikasnosti u hemijskim procesima.
9. Primena lestvica (stepena) cirkularnosti prilikom dizajniranja proizvoda - Treba težiti da proizvodi na kraju životnog veka ispoljavaju što veće mogućnosti na lestvici cirkularnosti.
10. Prodaja usluga, a ne proizvoda - Proizvođači bi trebalo da koriste poslovne modele zasnovane na uslugama, kao što je lizing hemikalija, promovišući efikasnost u odnosu na stopu proizvodnje.

11. Stvaranje uslova za cirkularnost - Poslovno i regulatorno okruženje treba da bude fleksibilno kako bi se omogućila implementacija inovacija.
12. Integracija industrije i obezbeđivanje koherentnog političkog okvira - Industrija i politika treba da budu ujedinjeni kako bi se stvorilo optimalno okruženje koje bi omogućilo primenu principa cirkularnosti u hemijskim procesima.

Važno je istaći da ovih dvanaest principa kružne hemije pokrivaju aspekte hemije, ali i aspekte ekonomije, politike i nauke o životnoj sredini, naglašavajući važnost međusobne povezanosti između ovih oblasti i potrebu za transdisciplinarnim i multidisciplinarnim pristupima, istraživanjima i praksom.

2. 1. Cirkularna hemija kao odgovor na krizu izazvanu nestašicom fosfata

Jedna od atraktivnih alternativnih sirovina koja se može koristiti kao zamena za fosfatne minerale u proizvodnji mineralnih đubriva, zbog relativno visokog sadržaja P_2O_5, jeste mulj nastao preradom komunalnih otpadnih voda, koji je u evropskoj regulativi klasifikovan kao neopasan otpad. Najjednostavniji način valorizacije fosfora iz ovog mulja je direktna upotreba mulja kao đubriva, međutim, sam transport i upravljanje visoko hidratisanim muljem (obično iznad 50 % vode) može generisati od 25 do 65 % ukupnih operativnih troškova postrojenja za prečišćavanje [15]. Takođe, ovaj mulj može sadržati značajne količine potencijalno opasnih organskih zagađujućih materija, na primer aromatične ugljovodonike, koji mogu zagaditi zemljište, kao i poljoprivredne useve koji se njime tretiraju [5]. Iz tog razloga, tehnologije za tretman mulja i indirektnu valorizaciju fosfora postaju sve popularnije, a termičke metode svakako prednjače (pre svega insineracija). Nakon termičkog tretmana mulja nastalog preradom komunalnih otpadnih voda ostaje pepeo koji je bogat fosforom pa se kao takav može koristiti kao đubrivo ili dodatak mineralnim đubrivima [16-20].

Korišćenjem pepela kao alternativne sirovine u proizvodnji mineralnih đubriva podstiče se očuvanje prirodnih resursa fosfata, a pepeo ovako korišćen nije više otpad već je dragocena sirovina. Na ovaj način se pospešuje vraćanje fosfora u životni ciklus proizvoda, a povećava mu se ekonomska vrednost, jer nema odlaganja. Dodatno, ukoliko se proces insineracije mulja nastalog preradom komunalnih otpadnih voda obavlja u blizini fabrike mineralnih đubriva i fosforne kiseline, velika količina energije oslobođena prilikom insineracije se dalje može koristiti u procesu dobijanja ovih proizvoda. Ovim putem se pravi spona između industrije đubriva i fabrika za prečišćavanje otpadnih voda, čime se prodaje usluga, a industrija postaje fleksibilna za unapređenje i inoviranje. Korišćenje pepela na najbolji način promoviše principe na kojima se zasniva cirkularna hemija, i samim tim cirkularna hemija postaje odgovor na krizu izazvanu nestašicom fosfata.

Valja napomenuti da nova regulativa Evropskog parlamenta i veća (EC 2019/1009) za đubriva [21], koja se primenjuje od jula 2022. godine, daje snažan podsticaj za ponovnu upotrebu regenerisanog fosfora iz otpada u proizvodnji mineralnih đubriva.

Na lokaciji na kojoj posluje proizvodna članica Eliksir Grupe (Elixir Group) u Prahovu, Srbija, započete su aktivnosti na izgradnji energane koja kao gorivo koristi opasan i neopasan otpad pri čemu bi se odvojeno tretirao mulj dobijen na postrojenjima za prečiscavanje otpadnih voda, i zatim nastali pepeo koristio u proizvodnji mineralnih đubriva.

U Idejnom rešenju postrojenja za energetsko iskorišćenje, insineraciju, otpada u Prahovu planira se, između ostalog, insineracija mulja koji je nastao preradom komunalnih otpadnih voda sa maksimalnim kapacitetom spaljivanja muljeva je od 10 t/h ili 80.000 t/god.

3. EKSPERIMENTALNI DEO

U ovom radu ispitivana je primena pepela kao izvora fosfora u proizvodnji veštačkih đubriva i fosforne kiseline. Urađena je karakterizacija pepela od spaljivanja mulja koji je nastao preradom komunalnih otpadnih voda, a koji je nabavljen iz Ulma (Nemačka), i rezultati su upoređeni sa sastavom sirovih fosfata koji se trenutno koriste u proizvodnim fabrikama kompanije Eliksir Grupe u Šapcu i Prahovu, Srbija. Sirovi fosfati su nabavljeni iz Egipta, i različitog su kvaliteta: 30 mas.% P_2O_5 i 28 mas.% P_2O_5 (*Misr Phosphate, Rock phosphate 30, Rock phosphate 28*; u daljem tekstu Fosfat 1 i Fosfat 2, redom).

Karakterizacija pepela i sirovih fosfata je urađena standardnim metodama. Sadržaj hlorida je određen volumetrijski u odsustvu organskog materijala (SRPS EN 16195:2013) [22], a fluorida potenciometrijski (VM 002) [23]. Sadržaj aluminijuma, кadmijuma, hroma, olova, nikla određen je primenom atomske emisione spektrometrije sa induktivno spregnutom plazmom (ICP-AES) nakon rastvaranja carskom vodom (SRPS EN 16319:2016) [24], gvožđa primenom plamene atomske apsorpcione spektrometrije (FAAS) (SRPS EN 16965:2018) [25], a silicijuma gravimetrijski [26]. Sadžaj žive određen je kombinovanjem tehnike generisanja pare (VG) i atomske apsorpcione spektrometrije nakon rastvaranja carskom vodom (SRPS EN 16320:2014) [27[, a arsena i selena hidridnom tehnikom atomske apsorpcione spektrometrije (HG/AAS) (EPA 7061A:1992 i EPA 7741A, redom) [28,29]. Manganometrijskom metodom je određen sadržaj kalcijuma nakon taloženja u obliku oksalata (SRPS EN 16196:2013) [30], a plamenom fotometrijom kalijuma (SRPS H.B8.294:1986) [31].

Sadržaj fosfora je određen gravimetrijski i to ukupni (SRPS EN 15956:2012; SRPS EN 15959:2012) [32,33], rastvorljiv u vodi (SRPS EN 15959:2012; SRPS EN 15958:2012) [33,34] i u neutralnom amonijum-citratu (NAC) (SRPS EN 15959:2012; SRPS EN 15957:2012) [33,35]. Sadržaj vlage određen je gravimetrijskom metodom (SRPS EN 12048:2011) [36].

4. REZULTATI I DISKUSIJA

U tabeli 1 su date fizičkohemijske karakteristike ispitivanog pepela i uporedna analiza pepela i dve vrste fosfata različitog kvaliteta koji se koriste u proizvodnim članicama kompanije Eliksir Grupe.

Iz prikazane tabele 1 se može videti da pepeo ima mali sadržaj vlage, hlorida i fluorida, što je veoma bitno pri izboru nove sirovine u proizvodnji mineralnih đubriva. Veći sadržaj hlorida loše utiče na kvalitet zemljišta (ove soli povećavaju kiselost zemljišta), a fluoridi deluju korozivno na procesnu opremu.

Tabela 1. Uporedna analiza pepela dobijenog od mulja nastalog preradom otpadnih komunalnih voda i dve vrste komercijalnih sirovih fosfata

Parametar	Pepeo	Fosfat 1	Fosfat 2
Sadržaj vlage, mas.%	0,44	5,60	4,67
Sadržaj hlorida, mas.%	< 0,10	0,08	0,08
Sadržaj fluorida, mas.%	0,16	3,45	2,65
Sadržaj Fe_2O_3, mas.%	7,66	0,18	3,68
Sadržaj Al_2O_3, mas.%	7,89	0,3	1,13
Sadržaj SiO_2, mas.%	44,25	9,87	6,4
Ukupan sadržaj P_2O_5 , mas.%	12,86	29,98	28,15
Sadržaj P_2O_5 rastvoran u NAC, mas.%	7,12	3,37	3,96
Sadržaj P_2O_5 rastvoran u vodi, mas.%	0,00	0,00	0,00
Sadržaj K_2O, mas.%	0,00	0,07	0,06
Ukupan sadržaj CaO, mas.%	15,75	48,72	41,72
Sadržaj As, mg/kg	10,59	3,03	27,04
Sadržaj Cd, mg/kg	1,53	7,18	2,44
Sadržaj Cr, mg/kg	71,14	102,22	38,96
Sadržaj Ni, mg/kg	49,91	21,72	30,58
Sadržaj Pb, mg/kg	65,83	1,89	20,56
Sadržaj Hg, mg/kg	< 0,10	< 0,10	< 0,10
Sadržaj Se, mg/kg	< 0,10	< 0,10	< 0,10

Velika vrednost ukupnog sadržaja CaO i SiO_2 ukazuje na prisustvo karbonata i peska. Takođe, uočene su i velike vrednosti sadržaja Fe_2O_3 i Al_2O_3. Prisustvo ovih oksida u zbiru do 2 mas.% je poželjno jer poboljšavaju granulaciju mineralnog đubriva, ali oni takođe deluju tako da smanjuju vodorastvorljivost P_2O_5 gradeći nerastvorne komplekse.

Rezultati u tabeli 1 pokazuju da korišćeni pepeo nema vodorastvorljivog fosfora, a da je prisutan P_2O_5 rastvorljiv neutralnom amonijum-citratu (NAC), koji biljke mogu direktno uzimati iz zemljišta. Pepeo sa ovakvim sadržajem aktivne materije poseduje određenu mogućnost primene kao samostalno đubrivo.

Fosfati imaju veće vrednosti fluorida u odnosu na pepeo, a sličan sadržaj hlorida, što predstavlja prednost pepela kao potencijalnih sirovina u odnosu na fosfate. Sadržaji oksida aluminijuma, gvožđa i silicijuma su veći kod pepela u odnosu na posmatrane fosfate.

Prisustvo kalijuma, izraženo preko K_2O, je prilično malo kod fosfata, gotovo da ga i nema, što je slučaj i sa pepelom.

Iz tabele 1 se može takođe uočiti da nijedna sirovina ne sadrzi vodorastvorljivi P_2O_5, a da najmanju vrednost ukupnog P_2O_5 ima pepeo, što je i bilo očekivano. Međutim, korišćenjem pepela kao zamene dela fosfata postigla bi se ušteda ove značajne sirovine za proizvodnju fosforne kiseline i mineralnih đubriva, a koja je na listi kritičnih u pogledu dostupnih zaliha. Pepeo ima veći sadržaj P_2O_5 rastvornog u NAC-u nego fosfati što je naročito značajno za gotov proizvod.

U pogledu prisustva teških metala, može se uočiti da sve sirovine imaju jako male vrednosti sadržaja selena i žive. Najveću vrednost arsena ima fosfat 2 (27,04 mg/kg), dok ostale sirovine imaju znatno manje vrednosti. Najmanji sadržaj kadmijuma ima pepeo i u poređenju sa fosfatima to predstavlja veliku prednost, jer je regulativa EC 2019/1009 [21] uvela dodatna ograničenja u pogledu sadržaja teških metala u đubrivu. Najveći sadržaj hroma ima fosfat 1, a za njim odmah i pepeo, mada prema Regulativi EC 2019/1009 [21], propisano je isključivo praćenje šestovalentnog hroma u mineralnim đubrivima. Prema Pravilniku o uslovima za razvrstavanje i utvrđivanje kvaliteta sredstava za ishranu bilja, odstupanjima sadržaja hranljivih materija i minimalnim i maksimalnim vrednostima dozvoljenog odstupanja sadržaja hranljivih materija i o sadržini deklaracije i načinu obeležavanja sredstava za ishranu bilja Republike Srbije [37], maksimalan sadržaj hroma u neorganskom đubrivu sa više od 5 mas.% P_2O_5 iznosi 500 mg/kg. Najviše vrednosti nikla i

olova se uočavaju kod pepela. Ipak treba imati u vidu da po Regulativi EC 2019/1009 [21] maksimalno dozvoljene koncentracije olova i nikla u mineralnom đubrivu iznose 100, odnosno 120 mg/kg redom, dok prema ranije pomenutom Pravilniku [37], maksimalan propisan sadržaj nikla i olova u neorganskom đubrivu sa više od 5 mas.% P_2O_5 iznosi 100 mg/kg. U tabeli 2 je prikazan sastav hipotetičke smeše, iz koje se može uočiti da zamena dela sirovog fosfata pepelom neće dovesti do prekoračenja zakonom dozvoljenih maksimalnih koncentracije za teške metale kako po Pravilniku RS, tako i po Regulativi EC 2019/1009 [21].

Tabela 2. Hipotetički sastav smeše pepela i fosfata

Parametar	Smeša fosfata 2 i pepela, razmera 90:10	Smeša fosfata 2 i pepela, razmera 85:15	EC regulation 2019/1009 [21]
Sadržaj As, mg/kg	25,40	24,57	40
Sadržaj Cd, mg/kg	2,35	2,30	/
Sadržaj Cr, mg/kg	42,18	43,79	/
Sadržaj Ni, mg/kg	32,51	33,48	100
Sadržaj Pb, mg/kg	25,09	27,35	120
Sadržaj Hg, mg/kg	< 0,10	< 0,10	1
Sadržaj Se, mg/kg	< 0,10	< 0,10	/

5. ZAKLJUČAK

Nova regulativa Evropskog parlamenta i veća (EC 2019/1009) [21] za đubriva, koja se primenjuje od jula 2022. godine, daje snažan podsticaj za ponovnu upotrebu fosfora iz otpada u proizvodnji mineralnih đubriva. Eliksir Grupa posluje po principima cirkularne ekonomije, te istražuje nove alternative sirovinama koje su okarakterisane kao kritične sa aspekta zaliha u svetu.

Analizirani pepeo koji je nastao insineracijom mulja iz prerade komunalnih otpadnih voda ima mali sadržaj vlage, hlorida i fluorida, što ga čini poželjnom sirovinom za mineralna đubriva. S druge strane, nešto veće vrednosti sadržaja Fe_2O_3 i Al_2O_3 mogu poboljšati granulaciju đubriva. Takođe, posmatrani pepeo ima veću koncentraciju P_2O_5 rastvorljivog u NAC u odnosu na referentne sirovine (fosfate) sa kojima je poređen, što ga čini potencijalnim đubrivom.

Zamena fosfatne komponente pepelom ne bi dovela do prekoračenja zakonom propisane dozvoljene maksimalne koncentracije teških metala koji se mogu naći u đubrivu kao gotovom proizvodu. U skladu sa navedenim zamena dela fosfata pepelom mogla bi uštedeti važnu sirovinu za proizvodnju đubriva.

Ovim radom daje se doprinos afirmaciji cirkularne ekonomije i ponovne upotrebe. Takođe, promoviše se primena termičkog tretmana nereciklabilnog opasnog i neopasnog otpada. Postrojenja koja se bave ovom delatnošću zahtevaju jako visoke investicione i operativne troškove, kao i izuzetno zahtevan, time i skup, obavezan tretman otpadnih gasova i monitoring njihovog kvaliteta kao preduslov zaštite životne sredine, a pre svega zdravlja stanovništva u okolini. Rezultati predstavljeni u ovom radu ukazuju na mogućnost korišćenja dobijenog pepela u daljoj proizvodnji mineralnih đubriva kao zamenske sirovine čime se opravdava ulaganje zahtevanih sredstava za izgradnju energana kakva će biti u Prahovu u Srbiji.

LITERATURA

[1] Kovačić M. Tehnološke zabilješke: Predstoji li nam fosforna kriza? *Kem Ind.* 2020; 69: 52-53 https://hrcak.srce.hr/232591

[2] Boskey AL. Bone composition: relationship to bone fragility and antiosteoporotic drug effects. *Bonekey Rep.* 2013; 2: 447 https://doi.org/10.1038/bonekey.2013.181

[3] Childers DL, Corman J, Edwards M, Elser JJ. Sustainability challenges of phosphorus and food: solutions from closing the human phosphorus cycle. *Bioscience*. 2011; 61: 117-124. https://doi.org/10.1525/bio.2011.61.2.6

[4] Van Kauwenbergh SJ, Stewart M, Mikkelsen R. World reserves of phosphate rock - a dynamic and unfolding story. *Better Crops.* 2013; 97: 18-20 http://www.ipni.net/publication/bettercrops.nsf/0/C3AB0523A890EBC685257BD50055E09A/$FILE/BC3%202013%20-%20p18.pdf

[5] Salkunić A, Vuković J, Smiljanić S. Review of Technologies for the Recovery of Phosphorus from Waste Streams. *Chem Biochem Eng Q. 2022;* 36: 91-116 https://doi.org/10.15255/CABEQ.2022.2066

[6] Bogdanović D. Hemizacija-potrošnja mineralnih đubriva u proizvodnji hrane. *Letopis naučnih radova Poljoprivrednog fakulteta.* 2010; 34: 32-45 https://scindeks-clanci.ceon.rs/data/pdf/0546-8264/2010/0546-82641001032B.pdf

[7] Bogdanović D. *Mineralna đubriva i đubrenje*, Novi Sad: Univerzitet u Novom Sadu, Poljoprivredni fakultet; 2010 http://www.agroekologija.com/agri-conto-cleen/wp-content/uploads/2015/02/Mineralna_djubriva.pdf

[8] Vaccari DA. Phosphorus: a looming crisis. *Sci Am.* 2009; 300: 54-59 https://doi.org/10.1038/scientificamerican0609-54

[9] Daneshgar S, Callegari A, Capodaglio AG, Vaccari D. The potential phosphorus crisis: resource conservation and possible escape technologies: a review. *Resources.* 2018; 7: 37 https://doi.org/10.3390/resources7020037
[10] Cooper J, Lombardi R, Boardman D, Carliell-Marquet C. The future distribution and production of global phosphate rock reserves. *Resour Conserv Recycl.* 2011; 57: 78-86. https://doi.org/10.1016/j.resconrec.2011.09.009
[11] European Commission. European Critical Raw Materials Act (2023) https://single-market-economy.ec.europa.eu/publications/european-critical-raw-materials-act_en (23. 4. 2023.)
[12] Kümmerer K, Clark JH, Zuin VG. Rethinking chemistry for a circular economy. *Science.* 2020; 367: 369-370 https://doi.org/10.1126/science.aba4979
[13] Keijer T, Bakker V, Slootweg JC. Circular chemistry to enable a circular economy. *Nature Chem.* 2019; 11: 190-195 https://doi.org/10.1038/s41557-019-0226-9
[14] Guarieiro LL, Rezende MJ, Barbosa WT, Rocha GOD, Pereira PAP, Fernandes DR, Lopes WA, Mota CJA, Andrade JBD. Reaching Circular Economy through Circular Chemistry: The Basis for Sustainable Development. *J Braz Chem Soc.* 2022; 33: 1353-1374 https://doi.org/10.21577/0103-5053.20220119
[15] Li R, Yin J, Wang W, Li Y, Zhang Z. (2014). Transformation of phosphorus during drying and roasting of sewage sludge. *Waste Manag.* 2014; 34: 1211-1216. https://doi.org/10.1016/j.wasman.2014.03.022
[16] Ottosen LM, Kirkelund GM, Jensen PE. Extracting phosphorous from incinerated sewage sludge ash rich in iron or aluminum. *Chemosphere.* 2013; 91: 963-969 https://doi.org/10.1016/j.chemosphere.2013.01.101
[17] Cordell D, Rosemarin A, Schreoder JJ, Smit AL. Towards global phosphorus security: a systems framework for phosphorus recovery and reuse options, *Chemosphere.* 2011; 84: 747-758 https://doi.org/10.1016/j.chemosphere.2011.02.032
[18] Franz M. Phosphate fertilizer from sewage sludge ash (SSA). *Waste Manag.* 2008; 28: 1809-1818 https://doi.org/10.1016/j.wasman.2007.08.011
[19] Fang L, Wang Q, Li JS, Poon CS, Cheeseman CR, Donatello S, Tsang DC. Feasibility of wet-extraction of phosphorus from incinerated sewage sludge ash (ISSA) for phosphate fertilizer production: A critical review. *Crit. Rev. Environ. Sci. Technol.* 2021; 51: 939-971 https://doi.org/10.1080/10643389.2020.1740545
[20] Ohtake H, Tsuneda S. *Phosphorus recovery and recycling*. Springer Singapore, Singapore, 2019 ISBN: 978-981-10-8031-9
[21] Regulation (EU) 2019/1009 of the European Parliament and of the Council of 5 June 2019 laying down rules on the making available on the market of EU fertilising products and amending Regulations (EC) No 1069/2009 and (EC) No 1107/2009 and repealing Regulation (EC) No 2003/2003 https://eur-lex.europa.eu/eli/reg/2019/1009/oj
[22] Đubriva — Određivanje hlorida u odsustvu organskog materijala, SRPS EN 16195:2013 https://iss.rs/sr_Cyrl/project/show/iss:proj:43774
[23] Određivanje sadržaja fluorida, VM002 (Mineralna đubriva – određivanje fluoride (potenciometrija) izdanje 01 od 10.01.2023. zasnovano na EPA 9214:1996 Potentiometric Determination of Fluoride in Aqueous Samples with Ion-Selective Electrode, Modifikovana u delu pripreme) https://www.epa.gov/hw-sw846/sw-846-test-method-9214-potentiometric-determination-fluoride-aqueous-samples-ion
[24] Đubriva i krečni materijali – Određivanje kadmijuma, hroma, olova i nikla atomskom emisionom spektrometrijom sa induktivno spregnutom plazmom (ICP-AES) nakon rastvaranja carskom vodom, SRPS EN 16319:2016 https://iss.rs/sr_Cyrl/project/show/iss:proj:55067
[25] Đubriva – Određivanje kobalta, bakra, gvožđa, mangana i cinka primenom plamene atomske apsorpcione spektrometrije (FAAS), SRPS EN 16965:2018, https://iss.rs/sr_Cyrl/project/show/iss:proj:59451
[26] Snyder GH. *Methods for silicon analysis in plants, soils, and fertilizers*. In Studies in plant science 2001; 8: 185-196 https://doi.org/10.1016/S0928-3420(01)80015-X
[27] Đubriva — Određivanje elemenata u tragovima — Određivanje žive tehnikom generisanja pare (VG) nakon rastvaranja carskom vodom, SRPS EN 16320:2014 https://iss.rs/sr_Cyrl/project/show/iss:proj:46690
[28] Određivanje arsena hidridnom tehnikom atomske apsorpcione spektrometrije (HG/AAS), EPA 7061A:1992 https://www.epa.gov/hw-sw846/sw-846-test-method-7061a-arsenic-atomic-absorption-gaseous-hydride
[29] Određivanje selena hidridnom tehnikom atomske apsorpcione spektrometrije (HG/AAS), EPA EPA 7741A https://www.epa.gov/hw-sw846/sw-846-test-method-7741a-selenium-atomic-absorption-gaseous-hydride
[30] Đubriva - Manganometrijsko određivanje ekstrahovanog kalcijuma nakon taloženja u obliku oksalata, SRPS EN 16196:2013 https://iss.rs/sr_Cyrl/project/show/iss:proj:43775
[31] Veštačka đubriva - Određivanje sadržaja kalijuma - Plamenofotometrijska metoda, SRPS H.B8.294:1986 https://iss.rs/sr_Cyrl/project/show/iss:proj:4509
[32] Mineralna đubriva — Ekstrakcija fosfora rastvorljivog u mineralnim kiselinama, SRPS EN 15956:2011 https://iss.rs/sr_Cyrl/project/show/iss:proj:33698
[33] Mineralna đubriva - Određivanje ekstrahovanog fosfora, SRPS EN 15959:2012 https://iss.rs/sr_Cyrl/project/show/iss:proj:40185
[34] Đubriva – Ekstrakcija vodorastvorljivog fosfora, SRPS EN 15958:2012 https://iss.rs/sr_Cyrl/project/show/iss:proj:69700
[35] Mineralna đubriva — Ekstrakcija fosfora rastvorljivog u neutralnom amonijum-citratu, SRPS EN 15957:2011 https://iss.rs/sr_Cyrl/project/show/iss:proj:33699

[36] Čvrsta mineralna đubriva i materije za kalcifikaciju - Određivanje sadržaja vlage - Gravimetrijska metoda sušenjem na (105±2) °C, SRPS EN 12048:2011 https://iss.rs/sr_Cyrl/project/show/iss:proj:29380

[37] Pravilnik o uslovima za razvrstavanje i utvrđivanje kvaliteta sredstava za ishranu bilja, odstupanjima sadržaja hranljivih materija i minimalnim i maksimalnim vrednostima dozvoljenog odstupanja sadržaja hranljivih materija i o sadržini deklaracije i načinu obeležavanja sredstava za ishranu bilja („Sl. glasnik RS", br. 30/2017 i 31/2018) https://pravno-informacioni-sistem.rs/eli/rep/sgrs/ministarstva/pravilnik/2018/31/6

SUMMARY

Circular chemistry in response to the phosphate crisis

Alija Salkunić[1], Ljiljana Stanojević[2], Nikola Belobaba[1], Slavica Bogdanović[1] and Bajro Salkunić[2]

[1]*Elixir Zorka – Mineral fertilizers, Hajduk Veljkova 1, Šabac, Serbia*
[2]*Elixir Group, Hajduk Veljkova 1, Šabac, Serbia*

(Technical paper)

Raw phosphate is used as a raw material to produce phosphorus-based fertilizers, and its supply shortage could negatively impact the global food supply. The European Commission has classified this raw material as critical in terms of estimated stocks. For years, new resources have been explored as substitutes for the phosphate component in fertilizer production and other phosphorus-containing products. An alternative has emerged in the possibility of using ash obtained from incineration of sludge generated in the process of municipal wastewater treatment. This work presents analyses of such ash as a case study for determination of potentials for partial replacement of raw phosphates in mineral fertilizers. It was shown that the ash contains high P_2O_5 content, which indicates this type of sludge as a promising alternative raw material in fertilizer production. The obtained results are significant for the Republic of Serbia as it is planned to construct over 300 wastewater treatment plants by 2041, with projection of about 135,000 t/year sludge generation. The presented analysis of ash obtained from this type of sludge justifies construction of incineration plants as the one planned in Prahovo, Serbia, which will by waste treatment contribute to circular economy and chemistry.

Keywords: mineral fertilizers, circular economy, phosphorus component, ash valorization

Modelling of sanitary wastewater composition and operation of a small membrane bioreactor wastewater treatment plant with denitrification and nitrification

David S. Mitrinović[1], Marija S. Perović[1], Srđan R. Kovačević[2], Miodrag R. Popović[1] and Zorana Z. Radibratović[1]

[1]*Jaroslav Černi Water Institute, Belgrade, Serbia*
[2]*Faculty of Technical Sciences, University of Novi Sad, Novi Sad, Serbia*

Abstract

The ratio of concentrations of total nitrogen and five-day biochemical oxygen demand in the sanitary wastewater of an energy infrastructure facility in Serbia is many times higher than usual, resulting in only half of the total nitrogen being eliminated in wastewater treatment plants (membrane bioreactor with anoxic and aerobic reactors) by denitrification. The first step of analysis was mathematical modelling of the composition and origins of the input wastewater. The model was developed based on the scientific literature data on composition of human excrement and the data on composition of water used for sanitary purposes. Next, it was successfully verified by comparisons to the experimental data of the wastewater composition. In the next step, a model for wastewater treatment simulation was created by using the BioWin software (Envirosim Associates, USA) in order to examine functioning of the plant and test the effects of several possible modifications of the process. A good agreement with the qualities of the influent and effluent determined by laboratory analyses was achieved after model calibration. The results of simulations showed a tenfold decrease in the total nitrogen concentration and a fortyfold decrease in the total phosphorous concentration in the effluent after introducing the following modifications to the simulated process: ferric chloride dosing, increasing dosing of acetate in the anoxic reactor by a factor of seven, increasing of the waste activated sludge rate by a factor of four and increasing the recirculation flow rate by a factor of three.

Keywords: Wastewater treatment simulation software; excrement; urine; acetate; nitrogen.

Available on-line at the Journal web address: http://www.ache.org.rs/HI/

ORIGINAL SCIENTIFIC PAPER

UDC: 632.153:628.19:631.461.3

Hem. Ind. **78(4)** 337-349 (2024)

1. INTRODUCTION

Mathematical modelling of wastewater composition and biological treatment processes is a powerful tool for predicting effluent quality. It can be used in the design process, or even more importantly, in the analysis of the performance of the existing wastewater treatment plants (WWTPs). The performance of plants can be unsatisfactory mostly due to the flaws in the design or substantially different influent quality than that envisaged by the design. Because of the significant impact the effluent characteristics have on the environment and the status of water bodies, and penalties imposed through legislation for non-conformance with emission limit values, finding the most efficient way to improve the functioning of the underperforming WWTPs is of great importance. Modelling of treatment processes is a valuable tool for testing different solutions and choosing the optimal one.

Quality and quantity of the influent is a key input for the design of WWTPs. Often, especially for design of new WWTPs, the influent quality is presumed using expert judgement or an engineering standard [1]. Even when the measurements, sampling and laboratory analyses have been performed on existing facilities, data sets are often quite limited due to the high financial and temporal costs of extended dynamic influent dataset, hindering the widespread utilization of WWTP models [2] and increasing the risk for errors in the design. In the case of sanitary wastewater, various factors influence its composition [3], as there are different uses of drinking water, different efficiencies of

Corresponding authors: David S. Mitrinović, Jaroslav Černi Water Institute, Belgrade, Serbia
Paper received: 25 April 2024; Paper accepted: 17 December 2024; Paper published: 15 January 2025.
E-mail: david.mitrinovic@jcerni.rs
https://doi.org/10.2298/HEMIND240423025M

drinking water use, cultural differences in food diet (ranges of average daily consumption of foods in 266 countries in 2010 were 19.2 to 325.1 g per day for fruits, 34.6 to 493.1 g per day for vegetables, 3.0 to 124.2 g per day for unprocessed red meat and 2.5 to 66.1 g per day for the processed one) [4] and water consumption [5], *etc*.

In order to address the mentioned issues regarding the influent quality and quantity input for the design and modelling, several approaches [6] have been suggested and tested:

- software tools for deriving WWTP influent data given selected properties of the catchment area and the distribution and kinds of emission sources [7,8],
- simple models for generating temporal distribution of influent data for urban WWTPs using available average quantity and quality data, using statistical distributions [9],
- the Fourier-based models, which are generally used to describe the patterns of the wastewater under dry weather conditions; these models are very useful to interpolate hourly values given average daily data, *e.g.* [9-11],
- simple spreadsheet type of calculation of influent quality and quantity, as a part of the analysis of different options for the treatment of source-separated components of wastewater (usually separately collected urine) depending on their composition and level of dilution [12,13], or the analysis of the influence of the quality and quantity of basic components of wastewater on its composition for special cases and specific diets like for example in the envisaged planetary space bases [14]; these kinds of analyses pertain by definition to small numbers of people.

The present study focused on the performance of a small WWTP, designed for 70 population equivalents (PEs), discharging effluent into a small watercourse with intermittent flow (average 0.16 $m^3 s^{-1}$). The wastewater treatment process is based on a membrane bioreactor (MBR) preceded by denitrification and nitrification reactors, with recirculation to the denitrification reactor, organic substrate addition and chemical removal of phosphorous (simulated process is shown in Fig. 1). The process was simulated for several variants of chemicals and organic substrate dosing, recycle ratio and waste activated sludge (WAS) discharge rate. The starting points of the applied calculation were data on basic human physiology and human habits and preferences, with focus on determining the quantity, quality and share of each source of wastewater resulting from all identified drinking water uses, using new model for the calculation of wastewater quality. Founded on those bases, a method for calculation of the composition of sanitary wastewater was developed and tested.

WWTPs comprise two main types of biological processes – suspended growth processes with microorganisms responsible for the treatment maintained in liquid suspension by appropriate mixing methods and attached growth (biofilm) processes [15]. Treated water is separated from the liquid suspension by using settlers or membranes. Performance of the complex array of treatment processes (biological, chemical and physical) applied in WWTPs can be analysed in detail only by using simulation software based on complex set of equations describing the processes. BioWin (Envirosim Associates, USA) is one of the most frequently used software packages, and one of the very few that are based on a coherent set of equations for all main processes in both suspended and attached growth as well as all the processes in the sludge [16-19].

In this work, the BioWin software coupled with the simulation of wastewater production was used to predict effectiveness and potentials for use of a MBR WWTP in treating of real sanitary wastewater. For the scientific analysis a case was chosen based on the composition of wastewater very different from the usual sanitary wastewater, especially regarding the concentration of total nitrogen (TN), which has significant repercussions on the treatment effects and efficiency in this, and future similar facilities.

Mathematical modelling of the composition and origins of wastewater was based on the composition of human excrement and urine reported in literature and data on the composition of water used for sanitary purposes, and on the average daily consumption of sanitary water per person and the share of defecations during work hours in the daily defecation occurrences, which were determined through the calibration. The aim of the study was to provide a helpful asset for mathematical simulation of wastewater composition based on its constituents derived from sanitary water uses, and for simulation of wastewater treatment using specialised software like BioWin, which helps design, improve, and optimize wastewater treatment processes.

1. 1. Legislation on effluent quality

The limits for the effluent quality were adopted according to the Regulation on emission limit values of polluting substances in waters and deadlines for achieving them of the Republic of Serbia [20]. In addition, Regulation on the limit values of pollutants in surface and ground waters and sediment and deadlines for reaching them of the Republic of Serbia [21] specifies the limits of water quality classes of surface water bodies. Wastewater treatment, as stipulated in the Law on Water [22], Article 98, shall be carried out to the level that corresponds to the emission limit values [20] or to the level that does not violate the quality standards of the recipient's environment [21], adopting a more rigorous criterion.

In this case the recipient watercourse is a small intermittent stream for which data on quality were lacking and a mixing zone could not be defined. Due to the vagueness of Article 98 [22], the only criterion that would undoubtedly be in line with legislation is that the effluent quality should correspond to the class II of quality for the type 6 surface water bodies (as per Rule book for determination of ecological and chemical status parameters for surface waters and determination of chemical and quantitative status parameters for groundwater of the Republic of Serbia [23]), which is significantly more stringent than the emission limits.

1. 2. The analyses performed

As mentioned above, the first step was mathematical modelling of the composition and origins of wastewater. The next step was analysis of the possibilities to achieve the limit values for five day biochemical oxygen demand (BOD_5), chemical oxygen demand (COD) and TN and total phosphorus (TP) concentrations for the class II of quality for type 6 surface water bodies and this required modification and optimisation of the WWTP operation. So, in this step, the effects of modifications to the facility operation were tested using the system model created in the software package BioWin 6.0 (Envirosim Associates, USA).

2. Materials and methods

2. 1. Composition of wastewater

The composition of sanitary wastewater of an energy infrastructure facility in Serbia, was expected to be similar to the composition of standard sanitary wastewater – the mixture of toilet, washbasin, shower, laundry and kitchen wastewaters, in the quantity corresponding to 70 workers present at any time, and the existing WWTP (three reactors in series: anoxic, aerobic and MBR) was designed accordingly.

The assumed quality of the untreated wastewater (Table 1) was similar to the average domestic wastewater, as for example defined by the ATV DVWK A 131E standard [1].

Table 1. Quality of the untreated sanitary wastewater from the ToR

Parameter	
Total content of suspended solids, mg dm^{-3}	500
BOD_5, mg O_2 dm^{-3}	500
TN content, mg N dm^{-3}	53
TP content, mg P dm^{-3}	13
pH	6.5 tpo 9.0
Temperature, °C	5 to 45

According to [1], the COD is typically two times larger than BOD_5, while the ratio of BOD_5 to TN is approximately 5.

Effluent and wastewater samples were collected and analyzed within five campaigns, in the February 2022 to March 2023 period (Table 2). pH value, electrochemical conductivity, temperature and dissolved oxygen concentration were measured *in situ*, using the calibrated probes. The physico-chemical analysis and microbiological testing were conducted following the standard procedures outlined by the American Public Health Association (APHA) and the American Water Works Association (AWWA). All applied procedures from water sampling, water quality testing and reporting followed the requirements of the ISO 17025:2015 standard. The results of the WWTP influent and effluent sampling and laboratory analyses show very low BOD_5/TN ratio of close to 1. The effective removal of nitrogen (over 90 %) is possible only when

this ratio is over 4 [24]. The wastewater composition listed in Table 2 is different from the typical compositions as in [1] and Table 1. The difference is particularly obvious in the BOD_5/TN ratio, and to some extent in the COD to BOD_5 ratio, which is high, close to 3, indicating that organic matter in wastewater has a lower biodegradability than expected.

Table 2. Quality parameters of the untreated sanitary wastewater and of the WWTP effluent

Parameter	Untreated sanitary wastewater		WWTP effluent	
	Mean*	Standard deviation	Mean*	Standard deviation
Temperature, °C	18.5	5.9	23.1	7.0
Smell	faecal		none	
Visible subst.	none		none	
pH	7.90	0.28	7.30	0.35
Specific conductivity, µS cm^{-1}	2799	542.8	2194	437.4
Dissolved O_2, $mg0_2$ dm^{-3}	0.7	0.37	7.8	0.43
Colour, °Pt-Co**	557.7	200.7	190.7	96.2
Ammonium ion content, mg N dm^{-3}	139.4	62.4	10.8	6.3
Nitrites content, mg N dm^{-3}	0.041	0.02	0.69	0.82
Nitrates content, mg N dm^{-3}	0.3	0.12	97.7	44.82
Kjeldahl nitrogen content, mg N dm^{-3}	186.3	33.3	11.6	5.9
TN content, mg N dm^{-3}	186.6	33.4	109.9	47.6
Organophosphates content, mg P dm^{-3}	11.6	8.4	10.7	4.9
TP content, mg P dm^{-3}	12.8	8.2	11.8	4.8
Chlorides content, mg dm^{-3}	185.2	66.9	167.3	30.8
Sulphates content, mg dm^{-3}	145.1	37.5	163.3	47.6
Cuntent of settleable matter (Imhoff), ml dm^{-3}	2.1	2.1	<0.7	
Content of total suspended solids, mg dm^{-3}	121.7	48.2	11.1	12.9
Ignition weight loss at 550°C, mg dm^{-3}	109.1	44.3	10.4	12.6
Ignition residue at 550 °C, mg dm^{-3}	3.8	1.5	0.8	0.1
Evaporation residue at 105 °C, mg dm^{-3}	1514	275.6	1624	143.1
COD, mg O_2 dm^{-3}	451.4	154.7	70.9	46.6
BOD_5, mg O_2 dm^{-3}	168.3	69.2	7.7	2.1
TOC, mg dm^{-3}	88.5	46.6	13.8	4.7

*if the value of parameter was below the quantification limit, it was taken as half of quantification limit in calculation of means; **°Pt-Co – platinum-cobalt scale degrees

2. 2. Mathematical modelling of composition of influent wastewater

The actual number of workers in the facility is several times smaller than the planned one, and kitchen and showers for staff are not available or used. The ratio of concentration of TN and BOD_5 is many times higher than that envisaged in ToR, resulting in only half of the TN being eliminated by denitrifycation (Table 2).

Composition of the influent wastewater was explained through its constituents' origins and the scientific literature data. The base assumption was that the only sources of wastewater were washbasins and toilets.

The composition of human urine and excrement (average values) adopted from the literature sources [25-27] is shown in Table 3. The quality parameter mass generated per person is divided by the sanitary water volumetric consumption and summed with the parameter concentration in the sanitary water used for washing and toilet flushing (samples were collected at the groundwater treatment plant outlet in February, March and April 2022, Table 4) to calculate the composition of wastewater by Eqs. (1) and (2).

In order to calculate the excrement contribution to the wastewater composition, the share of defecations during work hours in the daily defecation occurrences in a person had to be determined. If, for example, an average person working one eight-hour shift a day defecates when at work in 20 % of cases, then in three eight-hour shifts in one day, only 60 % of average daily excrement quantity per person is generated per workplace. Considering that the COD to BOD_5 ratio in excrement (which dominates regarding the organic matter in comparison to urine) is approximately 2 based on data shown in Table 3, biodegradability of the excrement organic matter is reduced by a fitting factor in comparison to that ratio to achieve a good fit. Calculation of wastewater BOD_5, and all other parameter concentrations (represented here by COD), is given by Eqs. (1) and (2), respectively:

Table 3. Composition of human urine and excrement adopted from scientific literature sources [25-27]

Parameter	Content, mg dm^{-3} (for urine quantity, dm^3/c/d*)	Content per dry mass of excrement, mg g_{dry}^{-1}	Quantity, g/c/d*
	Urine	Excrement	
COD	12968[1]	1275[1]	65.5[1]
BOD_5	2552[3]		31.7[1]
TN	8858[1]		1.8[1]
Total phosphorus	1200[1]	4.29[1]	0.814[1]
Potassium	1362[1]	3.85[1]	0.919[1]
Calcium	111[1]	3.57[1]	1.103[1]
Magnesium	95[1]	1.71[1]	0.213[1]
Chlorides	4190[2]	0.6[1]	0.09[1]
Sulphur	810[2]	0.87[1]	0.165[1]
Sodium	2820[2]	2.87[1]	0.1[1]
Sulphates	1180[2]		
Urine daily quantity ($UQ_{c,d}$)	1.4[1]		
Excrement (dry mass)			29[1]
Excrement (wet mass)			128[1]

*/c /d - per caput per diem (latin for per head per day); [1]from [25]; [2]from [26]; [3]from [27]

Table 4. Experimentally determined composition of sanitary water (treated groundwater)

Parameter	Mean	Standard deviation
Specific electric conductivity at 20°C, µS cm^{-1}	1365	425
Temperature, °C	23.4	0.54
Colour, °Pt-Co*	<5	
Smell	none	
Taste	none	
Turbidity, NTU**	<1	
pH	7.69	0.081
COD ($KMnO_4$), mg O_2 dm^{-3}	1.42	0.78
Ammonia content, mg dm^{-3}	<0.03	
Nitrites content, mg dm^{-3}	<0.003	
Nitrates content, mg dm^{-3}	2.21	0.55
Chlorides content, mg dm^{-3}	135.3	98
Total iron content, mg dm^{-3}	<0.09	
Active chlorine content, mg dm^{-3}	<0.05	
Manganese content, mg dm^{-3}	<0.05	
Total hardness, mg Ca dm^{-3}	130.6	4.7
Calcium content, mg dm^{-3}	49.4	12.4
Magnesium content, mg dm^{-3}	48.9	14.8
Sulphates content, mg dm^{-3}***	68.4	7.2
Bicarbonates content, mg dm^{-3}***	369.0	14.3
Potassium, mg dm^{-3}***	0.78	0.18
Sodium content, mg dm^{-3}****	100.5	
Total mineralization, mg dm^{-3}	775.5	

*°Pt-Co - platinum-cobalt scale degrees; **NTU – nephelometric turbidity unit; ***taken from the data on untreated groundwater quality; ****calculated based on electric charge balance

$$BOD_{5ww} = \frac{m(BOD_5)_{e,c,d} \times \frac{24}{8} \times SDW \times BRF + UQ_{c,d} \times BOD_{5u}}{Q_{sw,c,d}} + BOD_{5sw} \quad (1)$$

$$COD_{ww} = \frac{m(COD)_{e,c,d} \times \frac{24}{8} \times SDW + UQ_{c,d} \times COD_u}{Q_{sw,c,d}} + COD_{sw} \quad (2)$$

where BOD_{5ww} and COD_{ww} are BOD_5 and COD in wastewater, $m(BOD_5)_{e,c,d}$ and $m(COD)_{e,c,d}$ are daily BOD_5 and COD quantities in human excrement, SDW is a share of defecations during work hours in the daily defecation occurrences, BRF is the biodegradability reduction factor, BOD_{5u} and COD_u are BOD_5 and COD in urine, BOD_{5sw} and COD_{sw} are BOD_5 and COD in sanitary water, $UQ_{c,d}$ is a daily urine quantity, and $Q_{sw,c,d}$ is a daily consumption of sanitary water.

Cations like potassium and sodium, and anions like sulphates and bicarbonates were not a part of the laboratory analyses performed on sanitary water. Concentrations of these ions in sanitary water were derived directly from the data on untreated groundwater quality (except for sodium which was calculated), in order to calculate total mineralization, which is referenced in key legislation [20]. The ion exchanger (regenerated by sodium chloride) is used in the facility for groundwater treatment to lower the magnesium concentration below the limit set by legislation [28] on drinking water quality. Probably due to the use of sodium chloride for ion exchanger regeneration, the chloride ions average concentration was higher in sanitary water than in groundwater by almost 120 mg dm^{-3}. The sodium concentration in sanitary water was calculated based on electric charge balance of the solution (*i.e.* for the calculated sodium concentration net charge of the solution is zero).

2. 3. Wastewater treatment plants treatment process simulation

As the quality of effluent (Table 2) implies, low BOD_5 value in particular, oxidation of biodegradable organic carbon and organic nitrogen by oxygen, and oxidation of biodegradable organic carbon through denitrification and denitritation practically proceed to the end. About a half of total nitrogen in wastewater, 90 % comprised of nitrate, remains in the effluent as there is not enough biodegradable organic carbon for complete nitrogen reduction. The nitrate and nitrite ions are reduced to nitrogen gas by electron donors like wastewater complex organics represented by formula $C_{10}H_{19}O_3N$ (Eqs.(4) and (7)), or basic ions or molecules like acetate (Eqs.(5) and (8)) and glucose (Eqs.(6) and (9)) which can be added if there is insufficient organic carbon for complete denitrification and denitritation in wastewater [29,30].

$$C_{10}H_{19}O_3N + 10NO_3\text{-} + 10H^+ \rightarrow 5N_2 + 9CO_2 + HCO_3^- + NH_4^+ 15H_2O \quad (4)$$

$$5CH_3COO^- + 8NO_3^- + 3H^+ \rightarrow 4N_2 + 10HCO_3^- + 4H_2O \quad (5)$$

$$5C_6H_{12}O_6 + 24NO_3^- \rightarrow 12N_2 + 30HCO_3^- + 6H^+ + 12H_2O \quad (6)$$

$$3C_{10}H_{19}O_3N + 50NO_2^- + 50H^+ \rightarrow 25N_2 + 27CO_2 + 3HCO_3^- + 3NH_4^+ + 46H_2O \quad (7)$$

$$3CH_3COO^- + 8NO_2^- + 5H^+ \rightarrow 4N_2 + 6HCO_3^- + 4H_2O \quad (8)$$

$$C_6H_{12}O_6 + 8NO_2^- + 2H^+ \rightarrow 4N_2 + 6HCO_3^- + 4H_2O \quad (9)$$

After the analysis of the wastewater and effluent compositions, the treatment process and the resulting effluent quality were analysed by using modelling. The system model was created with the use of the software BioWin 6.0, which uses a general activated sludge/anaerobic digestion (ASDM) model, referred to as the BioWin ASDM. The BioWin ASDM has more than fifty state variables and over eighty process expressions [31]. These expressions are used to describe the following biological processes (including substrate and electron-acceptors consumption, hydrolysis, biomass growth) and chemical reactions typically occurring in wastewater treatment plants [31]:

- growth and decay of ordinary heterotrophic biomass,
- growth and decay of methylotrophic biomass,
- growth and decay of ammonia oxidizing biomass,
- growth and decay of nitrite oxidizing biomass,
- growth and decay of anaerobic ammonia oxidizing biomass,
- growth and decay of phosphorus accumulating biomass,
- growth and decay of sulphur oxidizing biomass,
- growth and decay of sulphur reducing biomass,
- hydrolysis, fermentation, oxidation/reduction, adsorption, ammonification and assimilative denitrification processes,
- chemical phosphorus removal with iron and aluminium salts,
- chemical phosphorus removal with salts,
- iron redox reactions and precipitation of vivianite and FeS,
- modelling of pH and alkalinity,
- liquid – gas interaction.

To simulate the enumerated processes, input data have to be set such as flow rate and composition of the influent, geometries of reactors and clarifiers, flow rates in pumps, flow rates of inputs like air or solutions of chemicals *etc*. Composition of influent, in addition to the standard quality parameters, is defined also by wastewater (WW) fractions,

like the fractions of soluble, colloidal and particulate matter, their readily biodegradable, slowly biodegradable and nonbiodegradable fractions *etc.*, and rates (for BOD_5 calculation) of degradation of colloidal slowly biodegradable COD, particulate slowly biodegradable COD and degradable external organics COD. Delimiting the organic matter in this fashion can be important in the analyses of the performance of WWTPs and finding causes of underperformance, especially when there is a significant share of pretreated industrial wastewater in the influent [3].

The simulations can be dynamic and steady state. In the present case, the simulations were performed in the steady state mode, with input defined based on average values of the flow rate and parameters of wastewater quality.

The WWTP configuration is replicated in the model (Figure 1) by using elements enumerated and described in Table 5. The parameter values in the model were, whenever possible, taken from the available data on the WWTP and influent.

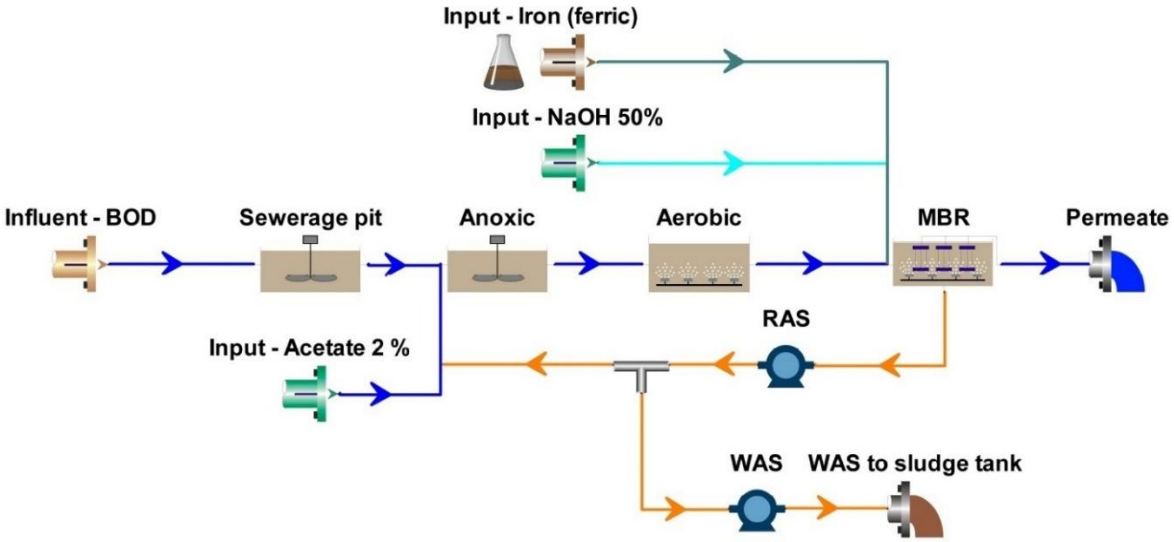

Figure 1. BioWin model flowsheet simulating the WWTP process flowsheet

Table 5. Description of the elements in the BioWin model simulating the current state of the system

Element	Description of the model input
Influent defined with BOD_5 and other parameters (COD is calculated by BioWin)	Flow rate 1.32 $m^3\ day^{-1}$ ($1.53 \cdot 10^{-5}\ m^3\ s^{-1}$), BOD_5 168.3 mg $O_2\ dm^{-3}$, TSS 121.7 mg dm^{-3}, VSS 90.0 mg dm^{-3}, TKN 186.3 mg N dm^{-3}, nitrates 0.3 mg dm^{-3}, TP 12.8 mg dm^{-3}, pH 7.9, alkalinity 7.4 mmol dm^{-3}, calcium 52 mg dm^{-3}, magnesium 51 mg dm^{-3}. WW fractions are default ones, except for the share of nonbiodegradable soluble COD (0.225 instead of 0.1300), and share of non-colloidal slowly biodegradable COD (0.1015 instead of 0.750). The three rates of degradation (for BOD_5 calculation) are all set to 0.2865 instead of default 0.5000. Changes were made in order to replicate the COD of 451.4 mg $O_2\ dm^{-3}$
Sewerage pit	Volume 30 m^3, depth 3 m, width 2.5 m, nonaerated
Anoxic suspended growth bioreactor	Volume 4 m^3, depth 3 m, width 1 m, nonaerated
Aerobic suspended growth bioreactor	Volume 3.7 m^3, depth 3 m, width 1 m, aerated (dissolved oxygen setpoint 1.5 mg dm^{-3}, density of diffusers 10 % (share of active area of diffusers in aeration tank in the area of aeration tank), α 0.500 and β 0.950 (parameters connected to mass transfer calculations)
Suspended growth MBR	Volume 3.5 m^3, depth 3 m, width 1 m, aerated (dissolved oxygen setpoint 6.0 mg dm^{-3}, density of diffusers 10 %, α 0.500 and β 0.950 (parameters connected to mass transfer calculations), number of cassettes 6, displaced volume per cassette 0.043 m^3, membrane surface area per cassette 6.25 m^2. Flow split 7.2 (as return mixed liquor to permeate (effluent) ratio)
Flow splitter for waste activated sludge	Rate in side stream to waste activated sludge tank 10 $dm^3\ d^{-1}$ ($1.16 \cdot 10^{-4}\ dm^3\ s^{-1}$)
Input for dosing of ferric chloride solution	32 wt.% ferric chloride solution, no flow (not added)
Input for dosing of sodium hydroxide solution	50 wt.% sodium hydroxide solution for pH regulation, flow 1 $dm^3\ day^{-1}$ ($1.16 \cdot 10^{-5}\ dm^3\ s^{-1}$)
Input for dosing of acetate salt solution	2 wt.% sodium acetate solution as a carbon source for denitrification (equivalent to 1.5 wt.% glucose solution). Acetate is used in the model as it is available in the BioWin software along with methanol and propionate, glucose is used in the WWTP. Flow rate was 7.3 $dm^3\ day^{-1}$ ($8.45 \times 10^{-5}\ dm^3\ s^{-1}$)

The model was tested and calibrated using data on wastewater quality and quantity, and the quality of the effluent, determined by laboratory analyses. The calibrated model described in Table 5 is a representation of the system in its current state.

The simulations were performed in the steady state mode due to the small average flow rate (approximately 1.3 $m^3\ day^{-1}$) and a large volume of the system (approximately 40 m^3), as well as due to the limited number of temporal data on the qualities of the influent and effluent.

If the legislation is interpreted in the most stringent way (as elaborated in section 1.1), the operation of the WWTP could be modified and optimised to achieve values for BOD_5, COD and nutrients concentrations as close to, or under the limit values for the class II of quality for the type 6 surface water bodies. The effects of modifications to the facility operation were tested using the calibrated model. Testing included several variants of dosing of the 2 wt.% (10, 20, 30, 40, 50, 60, 70 $dm^3\ day^{-1}$, with 50 found optimal) acetate in the anoxic reactor for denitrification, 32 wt.% ferric chloride dosing for phosphorus elimination (1, 2, 3, 5, 2.2, 2.4, 2.6 $dm^3\ day^{-1}$, with 2.4 $dm^3\ day^{-1}$ found optimal) and 50 % sodium hydroxide solution dosing for pH regulation in the MBR (1, 1.5, 2, 3 $dm^3\ day^{-1}$, with 1.5 $dm^3\ day^{-1}$ found optimal), as well as different recirculation rates of mixed liquor from the MBR to the anoxic reactor set as return mixed liquor to permeate (effluent) ratio (5, 10, 15, 20, 25, with 20 found optimal) and rates in the side stream to the waste activated sludge tank (0.01, 0.02, 0.03, 0.04, 0.05, 0.06 $m^3\ day^{-1}$, with 0.04 $m^3\ day^{-1}$ found optimal). The best performing set of flow and dosing rates values in a sense of minimization of TN, TP and COD in the effluent was determined and is shown in the Results section along with the respective effluent quality.

The BioWin model generates output for every model element, down to the effluent discharge. The output is comprised of quality parameters, which are derived from the parameters defining the composition of inputs, by calculation at every successive element.

Other parameters relevant for the comparison with limits set by legislation [20,21] that could not be calculated from the inputs within the BioWin model itself, were calculated by using a Microsoft Excel spreadsheet. Chlorides and sodium ions concentrations are calculated by adding contributions of ferric chloride and sodium hydroxide to contents of chlorides and sodium in wastewater, Eqs. (10) and (11), total mineralization is calculated by summing the dissolved matter, and total organic carbon (TOC) is calculated by using a correlation with COD, Eq. (12) [32].

$$c\left(\mathrm{Cl^-}\right)_{\mathrm{e}} = c\left(\mathrm{Cl^-}\right)_{\mathrm{ww}} + Q_{\mathrm{FeCL_3,d}}\rho\left(\mathrm{FeCL_{3\ (32\ wt.\%)}}\right)0.32\frac{3M(\mathrm{Cl})}{M(\mathrm{FeCL_3})} \tag{10}$$

$$c\left(\mathrm{Na^+}\right)_{\mathrm{e}} = c\left(\mathrm{Na^+}\right)_{\mathrm{ww}} + Q_{\mathrm{NaOH,d}}\rho\left(\mathrm{NaOH_{(50\ wt.\%)}}\right)0.50\frac{M(\mathrm{Na})}{M(\mathrm{NaOH})} \tag{11}$$

$$c(\mathrm{TOC}) = \frac{\mathrm{COD}_e\text{-}7.25}{2.99} \tag{12}$$

where $M(\mathrm{Cl^-})$, $M(\mathrm{Na^+})$, $M(\mathrm{NaOH})$ and $M(\mathrm{FeCl_3})$ are the molar masses of chlorine, sodium, sodium hydroxide and ferric chloride respectively, $\rho(\mathrm{FeCl_{3\ (32\ wt.\%)}})$, $\rho(\mathrm{NaOH_{(50\ wt.\%)}})$, $Q_{\mathrm{FeCl3,d}}$ and $Q_{\mathrm{NaOH,d}}$ are the densities and flow rates of ferric chloride and sodium hydroxide solutions respectively. Subscript e denotes effluent.

3. RESULTS

3. 1. Results of wastewater quality modelling

By using Eqs. (1) and (2) and data from Table 3, the values of key wastewater parameters (BOD_5, COD, TN, TP) and chlorides were calculated, juxtaposed with laboratory analyses results, as those parameters were covered by the analyses performed on the wastewater samples, and values of SDW, BRF and $UQ_{c,d}$ parameters calibrated. The best fitting calculated values are shown in Table 6. The total calcium, magnesium, sodium and potassium concentrations were also calculated in order to calculate total mineralization for the purpose of comparison with the limit set by legislation [20] but were not used for the calibration.

The results presented in Table 6 show a very good fit of calculated to measured values for the key quality parameters of influent wastewater (root-mean-square deviation is 14.7 mg dm^{-3}). The values of BRF, SDW and $Q_{\mathrm{sw,c,d}}$ that were fitted

in order to achieve the best agreement of calculated with the measured values, are all within the logical and acceptable ranges (biodegradability smaller than average by a third, and defecation two times less likely at work than at home).

Table 6. Results of parameter fitting and wastewater quality calculation

Parameter	Calculated	Average	Fitted
COD, mg O_2 dm^{-3}	452	451.4	
BOD_5, mg O_2 dm^{-3}	168	168.3	
TN content, mg N dm^{-3}	172	186.6	
TP content, mg P dm^{-3}	23	12.8	
Chlorides content, mg dm^{-3}	212	185.2	
Calcium content, mg dm^{-3}	52		
Magnesium content, mg dm^{-3}	51		
Sulphur content, mg dm^{-3}	38	48.4 (SO_4^{2-})	
Sodium content, mg dm^{-3}	152		
Potassium content, mg dm^{-3}	26		
$Q_{sw,c,d}$ / l /c/d*			77
BRF, %			66
SDW, %			15

*/c/d – per caput per diem (latin for per head per day)

3. 2. Wastewater treatment plants treatment process simulations

The system model was first tested and calibrated by using data from the laboratory testing of influent and effluent quality, and then its parameters modified to achieve the optimal performance of the simulated WWTP (Table 7). A good agreement with the quality of the effluent determined by laboratory analyses was achieved in the model (Table 8, columns 2 and 3). In order to achieve values for BOD_5, COD and nutrients concentrations as close as possible, or under the limit values for the class II of quality for the type 6 surface water bodies (Table 8, column 6), modifications in the operation of the WWTP were proposed to optimise it, especially in the sense of maximizing nutrients reduction. The effects of modifications to the facility operation were tested by using the model. The values of optimised parameters (flow rates of inputs of solutions, recirculation ratio and discharge of waste activated sludge) are shown in Table 7. The composition of the effluent is shown in Table 8, column 4.

Table 7. Description of the elements in the BioWin model of the optimized system with regard to parameters that were changed in comparison with the current state (Table 5)

Element	Description of model input
Suspended growth MBR	Flow split 20 instead of 7.2 (as return mixed liquor to permeate (effluent) ratio)
Flow splitter for waste activated sludge	Rate in side stream to waste activated sludge tank is 0.04 m^3 day^{-1} ($4.63\cdot10^{-4}$ dm^3 s^{-1}) instead of 0.01 m^3 day^{-1} ($1.16\cdot10^{-4}$ dm^3 s^{-1})
Input for dosing of ferric chloride solution	32 wt.% ferric chloride solution, 2.4 dm^3 day^{-1} ($2.78\cdot10^{-5}$ dm^3 s^{-1}) instead of no flow (not added)
Input for dosing of sodium hydroxide solution	50 wt.% sodium hydroxide solution for pH regulation, flow 1.5 dm^3 day^{-1} ($1.74\cdot10^{-5}$ dm^3 s^{-1}) instead of 1 dm^3 d^{-1} ($1.16\cdot10^{-5}$ dm^3 s^{-1})
Input for dosing of acetate salt solution	2 wt.% sodium acetate solution as carbon source for denitrification (equivalent to 1.5 wt.% glucose solution). Flow is 50 dm^3 day^{-1} ($5.79\cdot10^{-4}$ dm^3 s^{-1}) instead of 7.3 dm^3 d^{-1} ($8.45\cdot10^{-5}$ dm^3 s^{-1})

Table 8. Results of the effluent quality obtained experimentally and by the calibrated BioWin model simulations for the current and optimized states of the system along with the limits set by legislation

1	2	3	4	5	6	7
Parameter	Effluent, current state, laboratory results (Reduction, %)	Effluent, current state, simulation (Reduction, %)	Effluent, best performance, simulation (Reduction, %)	Change between the current (3) and optimized (4), %	Values for class II from Regulation on the limit values of pollutants [21]	Regulation on emission limit values (Reduction, %) [20]
pH[1]	7.3	7.51	7.29	-3	6.5 8.5	
TSS[1], mg dm^{-3}	11.1	0.0	0.0	0	25 + ✓	100 + ✓
BOD_5[1], mg O_2 dm^{-3}	7.7 (95.4)	0.71 (99.6)	0.63 (99.6)	-11	4.0 + ✓	80 (75) + ✓
COD (bichromate)[1], mg O_2 dm^{-3}	70.9 (84)	23.4 (95)	27.93 (94)	19	15	70 + ✓
TOC[2], mg C dm^{-3}	13.8	5.41	6.92	30	5.0	

1	2	3	4	5	6	7
Parameter	Effluent, current state, laboratory results (Reduction, %)	Effluent, current state, simulation (Reduction, %)	Effluent, best performance, simulation (Reduction, %)	Change between the current (3) and optimized (4), %	Values for class II from Regulation on the limit values of pollutants [21]	Regulation on emission limit values (Reduction, %) [20]
TN content[1], mg N dm^{-3} [1]	109.9	109.9	11.27	**-90**	2,0	
Nitrates content[1], mg N dm^{-3}	97.7	105.5	6.83	**-94**	3,0	
Nitrites content[1], mg N dm^{-3}	0.688	0.007	0.016	129	0.03 ✓	
Ammonium ion content[1], mg N dm^{-3}	10.8	0.032	0.065	103	0.1 ✓	
Molecular ammonia content[1], mg NH_3 dm^{-3}		0.000025	0.00003	20	0.025 ✓	
TP content[1], mg P dm^{-3}	11.8	10.4	0.25	**-98**	0.15	
Orthophosphates content[1], mg P dm^{-3}	10.7	10.4	0.25	**-98**	0.1	
Chlorides content[2], mg dm^{-3}	167.3	211.7	726.7	243	100	
Sulphates content[2], mg dm^{-3}	163.3	90.3	90.3	0	100 **+** ✓	
Total mineralization[2], mg dm^{-3}		1865	2065	34	1000	

✓ - under the limit (for the optimized WWTP simulation results); **+** - under the limit (for the current state WWTP simulation results);
[1]BioWin simulation results; [2]Spreadsheet calculation results (Eqs. (10) to (12) and summing for total mineralization)

The results for the best performing variant showed a tenfold decrease in the TN concentration and a fortyfold decrease in the TP concentration in the effluent in comparison to the current state.

4. DISCUSION

4. 1. Wastewater quality modelling

The results present a very good fit of calculated to measured values for the key quality parameters of the influent wastewater, which points strongly to the usefulness of the presented model for the calculation of wastewater quality. As expected, share of defecations during work hours in the total defecation occurrences (15 %) is much smaller than the share of working hours in 24 hours (33 %), as most people obviously prefer using the toilet at home. Biodegradability reduction factor (66 %) reflects the higher COD to BOD_5 ratio than the standard one for sanitary wastewater. It is quite possible that this reflects the diet that deviates from the average one in a number of workers, as this is possible within a small group of people. The daily sanitary water consumption per person of 77 dm^3 is in accordance with the very limited number of waters uses in the facility – drinking, hand washing and toilet and urinal flushing, as it is a half of the standard domestic daily consumption per person [1].

4. 2. Wastewater treatment plants treatment process simulations

Despite the tenfold decrease in the TN concentration and a fortyfold decrease in the TP concentration in the effluent in comparison to the current state (after the changes in dosing rates of input solutions, recirculation rate and waste activated sludge discharge rate), concentrations of nutrients are still somewhat above the very stringent limits for the class II quality. Even if they could be reached with further adjustments to the WWTP, the best results would be near the limits, and compliance with the Regulation on the limit values of pollutants in surface and ground waters and sediment and deadlines for reaching them of the Republic of Serbia [21] could not be guarantied. The large volume of 32 wt.% ferric chloride needed for almost complete phosphorus removal creates problems as it releases large quantities of chlorides (for the set of model parameters given in Table 7 it is 515 mg dm^{-3} in addition to the influent concentration, Eq. (10)). The alternative of adding ferric sulphate would create similar problem with the sulphates. The large increase in the contents of chlorides and sulphates would cause the equivalent increase in specific electric conductivity and mineralization (2065 mg dm^{-3}), too. Even without the modifications, the use of sodium hydroxide for pH control causes a high sodium concentration, which together with nitrate and chloride ions originating from the human waste raise the total mineralization to 1865 mg dm^{-3}. The limits of class II quality from the Regulation on the limit values of pollutants of the Republic of Serbia [21] obviously could not be reached by any modification to the existing equipment.

5. CONCLUSIONS

Wastewater composition in the case of small facilities, as demonstrated in this paper, especially with the restricted number of sanitary waters uses, can be very different than the typical domestic, or more generally, communal wastewater. To set the appropriate baseline quality and quantity of wastewater for the WWTP design purposes, the recommendation based on the analysis performed in this paper is that the data on per person excrement and urine production and their compositions should be used with the data on sanitary water quality and consumption to predict the quantity and quality of wastewater. If there are any significant water uses apart from wash basins and toilets/urinals, they should be addressed in the same manner. The utility of the presented methodology was demonstrated in this work, as well as its potential for use with the broader set of water uses.

The modelling of processes in a WWTP using software like BioWin was shown to be of great utility and value. The model was built based on the data obtained from the WWTP functioning, and from all, or most of key parameters regarding the inputs of influents and chemicals solutions. After the calibration by using the results of laboratory testing of the influent and effluent, the model was proved to be a very useful tool for testing several variants of dosing rates of input solutions, recirculation rate and waste activated sludge discharge rate, in order to obtain the best performing set of values in a sense of minimization of TN, P, BOD_5 and COD in the effluent.

The need to check for the compliance with the legislation necessitated additional spreadsheet calculations, which depend on the available parameters from the existing results of laboratory analyses of influent and sanitary water.

The developed approach comprises characterisation of wastewater based on precise knowledge of drinking water uses, modelling software use, and basic spreadsheet calculations to supplement the missing parameters in laboratory results and software ouput. This methodology, developed on the basis of experimental data and modelling simulations and calculations is beneficial for further extension to other wastewater types and treatment systems.

REFERENCES

[1] ATV-DVWK-A 131E: Dimensioning of Single-Stage Activated Sludge Plants. 2000. ISBN 3-935669-96-8

[2] Rieger L, Takacs I, Villez K, Siegrist H, Lessard P, Vanrolleghem PA, Comeau Y. Data reconciliation for WWTP simulation studies and planning for high quality data and typical sources of errors. *Water Environ Res.* 2010; 82: 426-433 https://doi.org/10.2307/25679798.

[3] Choi Y-Y, Baek S-R, Kim J-I, Choi J-W, Hur J, Lee T-U, Park C-J, Lee BJ. Characteristics and Biodegradability of Wastewater Organic Matter in Municipal Wastewater Treatment Plants Collecting Domestic Wastewater and Industrial Discharge. *Water.* 2017; 9(6): 409 https://doi.org/10.3390/w9060409.

[4] Micha R, Khatibzadeh S, Shi P, Andrews KG, Engell RE, Mozaffarian D. Global Burden of Diseases Nutrition and Chronic Diseases Expert Group (NutriCoDE). Global, regional and national consumption of major food groups in 1990 and 2010: a systematic analysis including 266 country-specific nutrition surveys worldwide. *BMJ Open.* 2015; 5(9): e008705 https://doi.org/10.1136/bmjopen-2015-008705.

[5] Moncaleano DCC, Saket P, Rietveld L. Water Use Efficiency: A Review of Contextual and Behavioral Factors. *Front Water.* 2021; 3: 685650 https://doi.org/10.3389/frwa.2021.685650.

[6] Martin C, Vanrolleghem PA. Analysing, completing, and generating influent data for WWTP modelling: A critical review, *Environ Modell Softw.* 2014; 60: 188-201 https://doi.org/10.1016/j.envsoft.2014.05.008.

[7] Gernaey KV, Flores-Alsina X, Rosen C, Benedetti L, Jeppsson U. Dynamic influent pollutant disturbance scenario generation using a phenomenological modelling approach. *Environ Modell Softw.* 2011; 26: 1255-1267 https://doi.org/10.1016/j.envsoft.2011.06.001.

[8] De Keyser W, Gevaert V, Verdonck F, De Baets B, Benedetti L. An emission time series generator for pollutant release modelling in urban areas. *Environ Modell Softw.* 2010; 25: 554-561 https://doi.org/10.1016/j.envsoft.2009.09.009

[9] Devisscher M, Ciacci G, Fe L, Benedetti L, Bixio D, Thoeye C, De Gueldre G, Marsili-Libelli S, Vanrolleghem PA. Estimating costs and benefits of advanced control for wastewater treatment plants - the MAgIC methodology. *Wat Sci Tech.* 2006; 53 (4-5): 215-223 https://doi.org/10.2166/wst.2006.126.

[10] Mannina G, Cosenza A, Vanrolleghem PA, Viviani G. A practical protocol for calibration of nutrient removal wastewater treatment models. *J Hydroinform.* 2011; 13: 575-595 https://doi.org/10.2166/hydro.2011.041.

[11] Langergraber G, Alex J, Weissenbacher N, Woerner D, Ahnert M, Frehmann T, Halft N, Hobus I, Plattes M, Spering V, Winkler S. Generation of diurnal variation for influent data for dynamic simulation. *Wat Sci Tech.* 2008; 57 (9): 1483-1486 https://doi.org/10.2166/wst.2008.228.

[12] Faust V, Markus P, Schielke-Jenni S, Timmer MJ, De Paepe J, Ganigué R. Conditions for successful nitrogen removal from source-separated urine by partial nitritation/anammox. *PLOS Water* 2024; 3(5): e0000235 https://doi.org/10.1371/journal.pwat.0000235.

[13] Niwagaba CB. Treatment Technologies for Human Faeces and Urine. PhD Thesis, Swedish University of Agricultural Sciences, Sweden, Uppsala 2009. https://pub.epsilon.slu.se/2177/1/niwagaba_c_091123.pdf.

[14] Shrestha B, Hernandez R, Fortela DLB, Sharp W, Chistoserdov A, Gang D, Revellame E, Holmes WE, Zappi ME. Formulation of a Simulated Wastewater Influent Composition for Use in the Research of Technologies for Managing Wastewaters Generated during Manned Long-Term Space Exploration and Other Similar Situations-Literature-Based Composition Development. BioTech (Basel) 2023; 12 (1): 8 https://doi.org/10.3390/biotech12010008.

[15] Yildiz BS. Chapter 18 - Water and wastewater treatment: biological processes. In: Zeman F, ed. *Metropolitan Sustainability*: Woodhead Publishing Series in Energy, Woodhead Publishing; 2012: 406-428 https://doi.org/10.1533/9780857096463.3.406.

[16] Oleyiblo OJ, Cao J, Feng Q. Evaluation and improvement of wastewater treatment plant performance using BioWin. *Chin J Ocean Limnol.* 2015; 33: 468–476 https://doi.org/10.1007/s00343-015-4108-8.

[17] Moragaspitiya J, Rajapakse C, Senadeera W, Ali I. Simulation of Dynamic Behaviour of a Biological Wastewater Treatment Plant in South East Queensland, Australia using Bio-Win Software. *Eng J.* 2017; 21(3): 1-22 https://doi.org/10.4186/ej.2017.21.3.1.

[18] Lei L, Gharagozian A, Start B, Roth G, Emmett R. Process alternative comparisons assisted with Biowin modelling. In: *Proceedings of the Water Environment Federation; 2006*(9): 3274-3289 https://doi.org/10.2175/193864706783751573.

[19] Huang S, Pooi CK, Shi X, Varjani S, Ng HY. Performance and process simulation of membrane bioreactor (MBR) treating petrochemical wastewater, *Sci Total Environ.* 2020; 747:141311 https://doi.org/10.1016/j.scitotenv.2020.141311.

[20] Regulation on Emission Limit Values of Polluting Substances in Waters and Deadlines for Achieving Them. The Official Gazette of Republic Serbia. 2011; 67, 2012; 48, 2016; 1. https://www.paragraf.rs/propisi/uredba-granicnim-vrednostima-emisije-zagadjujucih-materija-u-vode.html.

[21] Regulation on the limit values of pollutants in surface and ground waters and sediment and deadlines for reaching them. The Official Gazette of Republic of Serbia. 2012; 50. https://www.paragraf.rs/propisi/uredba-granicnim-vrednostima-zagadjujucih-materija-vodama.html.

[22] Law on Water. The Official Gazette of Republic Serbia. 2010; 30, 2012; 93, 2016; 101, 2018; 95, 2018; 95. https://www.paragraf.rs/propisi/zakon_o_vodama.html.

[23] Rule book for determination of ecological and chemical status parameters for surface waters and determination of chemical and quantitative status parameters for groundwater. The Official Gazette of Republic of Serbia. 2011; 74. https://www.paragraf.rs/propisi/pravilnik-o-parametrima-ekoloskog-i-hemijskog-statusa-povrsinskih-voda-podzemnih-voda.html.

[24] Gajewska M. Influence of composition of raw wastewater on removal of nitrogen compounds in multistage treatment wetlands. *Environ Prot Eng.* 2015; 41(3): 19-30 https://doi.org/10.37190/epe150302.

[25] Rose C, Parker A, Jefferson B, Cartmell E. The Characterization of Feces and Urine: A Review of the Literature to Inform Advanced Treatment Technology. *Crit Rev Environ Sci Technol.* 2015; 45: 1827–79 https://doi.org/10.1080/10643389.2014.1000761.

[26] Kuntke P. Nutrient and energy recovery from urine. PhD thesis, Wageningen University, Wageningen, NL; 2013 https://edepot.wur.nl/254782.

[27] Hassan SSM, Abdel-Shafy HI, Mansour MSM. Removal of pharmaceutical compounds from urine via chemical coagulation by green synthesized ZnO-nanoparticles followed by microfiltration for safe reuse. *Arab J Chem.* 2019; 12(8): 4074-4083 http://dx.doi.org/10.1016/j.arabjc.2016.04.009.

[28] Rulebook on quality of drinking water. The Official Gazette of Republic of Serbia. 1998; 42, 1999; 44 and 2019; 28 https://www.paragraf.rs/propisi/pravilnik-higijenskoj-ispravnosti-vode-pice.html.

[29] Hollingham M. Effect of organic carbon substrates on denitrification rates in sediment. PhD thesis, University of Waterloo, Ontario, Canada; 2013 https://uwspace.uwaterloo.ca/bitstream/handle/10012/8217/Hollingham_Melisa.pdf?sequence=5&isAllowed=y.

[30] Inc. Metcalf & Eddy, Tchobanoglou G, Stensel H, Tsuchihashi R, Burton F, Abu-Orf M, Bowden G, Pfrang W. Wastewater Engineering: Treatment and Resource Recovery. 5th ed., New York, NY, USA: McGraw-Hill Education; 2014: 634. https://www.amazon.com/Wastewater-Engineering-Treatment-Resource-Recovery/dp/0073401188

[31] Inc. EnviroSim Associates. BioWin Help Manual https://www.envirosim.com/downloads/BW5Manual.pdf.

[32] Dubber D, Gray NF. Replacement of chemical oxygen demand (COD) with total organic carbon (TOC) for monitoring wastewater treatment performance to minimize disposal of toxic analytical waste. *J Environ Sci Health, Part A Tox Hazard Subst. Environ Eng.* 2010; 45(12): 1595-1600 http://dx.doi.org/10.1080/10934529.2010.506116.

Modeliranje sastava sanitarnih otpadnih voda i rada malog membranskog bioreaktorskog postrojenja za prečišćavanje otpadnih voda sa denitrifikacijom i nitrifikacijom

David S. Mitrinović[1], Marija S. Perović[1], Srđan R. Kovačević[2], Miodrag R. Popović[1] i Zorana Z. Radibratović[1]

[1]*Institut za vodoprivredu Jaroslav Černi, Beograd, Srbija*
[2]*Fakultet tehničkih nauka, Univerzitet u Novom Sadu, Novi Sad, Srbjia*

(Naučni rad)

Izvod

Odnos koncentracija ukupnog azota i petodnevne biohemijske potrošnje kiseonika u sanitarnoj otpadnoj vodi jednog objekta energetske infrastrukture u Srbiji je višestruko veći nego što je uobičajeno za ovaj tip otpadnih voda, zbog čega se u postrojenju za prečišćavanje otpadnih voda (membranski bioreaktor sa anoksičnim i aerobnim reaktorom) denitrifikacijom eliminiše samo polovina ukupnog azota iz otpadne vode. Prvi korak analize je predstavljalo matematičko modelovanje geneze otpadnih voda da bi se ustanovio uzrok neuobičajeno velikog udela organskog i neorganskog azota. Prema projektnom zadatku za postrojenje bio je predviđen skoro deset puta veći broj radnika od sada prisutnih, kao i kuhinja i tuševi za osoblje, kojih nema ili se ne koriste. Na osnovu podataka iz naučne literature o sastavu ljudskih ekskremenata i podataka o sastavu vode koja se koristi za piće, određena je potrošnja vode za piće po čoveku i faktor umanjenja produkcije fecesa tokom radnog vremena u odnosu na srednju dnevnu vrednost uz dobro poklapanje za utvrđenim kvalitetom otpadnih voda. Osim azota, u efluentu je prisutna praktično ista koncentracija ukupnog fosfora kao u influentu. Da bi se ispitalo funkcionisanje postrojenja i isprobali efekti različitih mogućih modifikacija u procesu, napravljen je model u programu BioWin (Envirosim Associates Ltd.). U modelu je i bez značajnije kalibracije postignuto dobro poklapanje sa kvalitetom efluenta određenim laboratorijskim analizama. Ispitano je više varijanti doziranja rastvora acetatne soli u anoksičnom reaktoru, doziranja feri-hlorida u membranskom bioreaktoru radi eliminacije fosfata kao i 50 % rastvora natrijum-hidroksida radi regulacije pH. Rezultati simulacija pokazuju dvadesetostruko smanjenje koncentracije ukupnog azota i tridesetostruko smanjenje koncentracije ukupnog fosfora u efluentu (permeatu)

Ključne reči: softver za simulaciju tretmana otpadnih voda, ekskrement, urin, acetat, azot

Luminescence intensity ratio by three thermalized levels in YAG:Er^{3+}/Yb^{3+} nanoparticles

Aleksandar Ćirić, Mina Medić, Jovana Periša, Željka Antić and Miroslav D. Dramićanin

Centre of Excellence for Photoconversion, Vinča Institute of Nuclear Sciences - National Institute of the Republic of Serbia, University of Belgrade, Belgrade, Serbia

Abstract

Luminescence thermometry is a remote temperature sensing method by observing temperature dependent spectral changes for temperature readout. Chase for increasing temperature readout sensitivity motivated research of employing 3rd thermalized level of Er^{3+} emission in Yb^{3+}/Er^{3+} upconversion photoluminescence. For this purpose, highly stable and efficient yttrium aluminium garnet (YAG): Yb^{3+}/Er^{3+} nanoparticles were prepared by a modified Pechini method. The emission spectra were recorded from 300 to 800 K, and two luminescence intensity ratios between emissions of $^4S_{3/2}$, $^2H_{11/2}$, and $^4F_{7/2}$ were obtained. Apart from excellent matching theoretical predictions, the readout by using the $^4F_{7/2}$ method provided a 3.5-fold increased relative sensitivity over the luminescence intensity ratio by $^2H_{11/2}$ level, which is limited by being usable only above 600 K. The method by emission from $^2H_{11/2}$ is to be used from 300 to 600 K, while emission from $^4F_{7/2}$ provides the best luminescence intensity ratio at temperatures from 600 K to 800 K. YAG:Yb^{3+}/Er^{3+} nanoparticles proved to be an excellent sensor material for the luminescence intensity ratio method by employing multiple thermalized levels.

Keywords: Luminescence thermometry; upconversion nanoparticles; fluorescence intensity ratio; Pechini method.

Available on-line at the Journal web address: http://www.ache.org.rs/HI/

ORIGINAL SCIENTIFIC PAPER

UDC: 536.51:52-628:620.3

Hem. Ind. **78(4)** 351-357 (2024)

1. INTRODUCTION

Luminescence is the emission of light that occurs when a substance absorbs energy, such as photons or electrons, and then releases that energy in the form of light emission. This phenomenon is commonly observed in various contexts, including fluorescence, phosphorescence, and bioluminescence, and it is essential in fields like lighting, materials science, and biological imaging.

Luminescence thermometry is a remote temperature measurement technique that relies on the temperature induced spectral changes of luminescence from a material to determine its temperature. By analysing the emitted luminescence, it is possible to accurately and remotely measure the temperature of the material, making the method valuable for various applications, including in industrial processes and scientific research [1]. The read-out method and its probe are unperturbed even by high electromagnetic fields, radiation, and are often resistant to corrosive environments. Luminescence thermometry has an advantage over infrared (IR) cameras and pyrometers in its ability to provide highly accurate and non-contact temperature measurements even for materials with low or variable emissivity, as it relies on the intrinsic properties of luminescent materials rather than surface characteristics like infrared radiation [2]. Additionally, it can be employed from the nanoscale up to measuring the temperature of a large surface. Thus, luminescent thermometry is used in niche applications where other contact methods, like thermocouples, or remote methods, like IR cameras, fail.

The most frequently used method for luminescence thermometry is called luminescence intensity ratio (LIR), which uses the ratio of emission intensities (*I*) for the read-out. LIR is ratiometric, *i.e.* it does not depend on the fluctuations in excitation. Usually, LIR is taken as a ratio of emissions from two thermally coupled levels. Thermally coupled levels are

Corresponding authors: Aleksandar Ćirić, Affiliation Centre of Excellence for Photoconversion, Vinča Institute of Nuclear Sciences - National Institute of the Republic of Serbia, University of Belgrade, P.O. Box 522, Belgrade 11001, Serbia

Paper received: 27 february 2024; Paper accepted: : 6 October 2024; Paper published: 21 October 2024.

E-mail: aleksandar.ciric@ff.bg.ac.rs

https://doi.org/10.2298/HEMIND240227021C

those in which the energy difference is sufficient for the thermal energy to produce excitation from the lower (L) to the higher (H) thermally coupled energy level. LIR then follows Boltzmann distribution according to Equation (1) [3]:

$$\mathrm{LIR} = \frac{I_\mathrm{H}}{I_L} = Be^{-\frac{\Delta E}{kT}} \quad (1)$$

where B is the temperature invariant constant that depends on the material properties, I_H is the intensity from H level, I_L is the intensity from the L level, and ΔE is the energy difference between the thermally coupled levels, and k = 0.695 cm^{-1} K^{-1} is the Boltzmann constant. The performance of a temperature probe material is estimated by the figure of merit called relative sensitivity [4], Equation (2):

$$S_\mathrm{r} = \frac{100}{\mathrm{LIR}}\left|\frac{\partial \mathrm{LIR}}{\partial T}\right| = 100\frac{\Delta E}{kT^2} \quad (2)$$

The relative sensitivity (% K^{-1}) is the normalized rate of change of LIR and can be used for comparison with other sensor probes or even other readout methods.

Upconversion luminescence is a process in which a material absorbs multiple lower-energy photons and then emits a single higher-energy photon. This phenomenon is used in various applications, such as upconversion nanoparticles, where it enables the conversion of low-energy near-infrared light into visible light for purposes like biological imaging and energy-efficient photovoltaic devices [5]. It also has advantages in luminescence thermometry as it eliminates background radiation and autofluorescence that could appear under UV excitation of the probe material. The most famous upconverting pair of lanthanide ions are erbium and ytterbium, as they have excited energy levels with similar energies, thus there is an efficient energy transfer from Yb^{3+} to Er^{3+}. Yb^{3+} has an order of magnitude larger absorption cross-section than Er^{3+}, thus the upconversion efficiency by Yb^{3+} co-doping is increased multiple times [6]. After two energy transfers from Yb^{3+} (which is excited by near-infrared (NIR) light) to Er^{3+}, Er^{3+} exhibits visible, green emission. Er^{3+} is also the most frequently used ion in luminescence thermometry as there is an excellent thermal coupling between its thermalized levels $^4S_{3/2}$ and $^2H_{11/2}$ and the latter is unusually very intense due to its favourable radiative properties [7]. However, the energy separation of about 700 cm^{-1} between those two levels limits the relative sensitivity according to Eq. 2. The current trend in luminescence thermometry is either finding sensor materials that exhibit higher relative sensitivities or finding methods or their improvements that enable the same [8]. The recent improvement in the LIR readout method, presented in literature [9,10], enable the use of energetically higher thermalized levels at elevated temperatures for reaching larger relative sensitivities. As the relative sensitivity, according to Eq. 2, linearly depends on the energy gap, using this 3rd excited level in LIR produces higher sensitivity than conventional LIR [9].

Ultimately, high stability of the host matrix is of utmost importance for luminescence thermometry. Oxide crystals are considered the most thermally and chemically stable hosts, among which yttrium aluminium garnet (YAG, $Y_3Al_5O_{12}$) is well known for both its stability and its optical properties, as it is used in the most prominent of solid-state lasers, Nd:YAG, and as a phosphor in commercial white LED chips. The Pechini method offers several advantages for synthesizing YAG, including excellent homogeneity, precise compositional control, and the production of fine powders with enhanced properties such as mechanical strength. Additionally, it allows for easy integration of dopant ions, making it ideal for tailoring YAG's luminescence and other properties for specific applications [11]. The only previous research employing the 3rd thermalized level in Er^{3+} is in a less stable fluoride matrix [10]. Here we present the investigation of using the 3 thermalized levels for luminescence thermometry by upconverting pair of Yb^{3+}/Er^{3+} in the YAG matrix, report on its performance, and demonstrate the increase in sensitivity by employing the 3rd thermalized emissive level.

2. EXPERIMENTAL

Herein, the sample with the following formula: $Y_{2.64}Yb_{0.3}Er_{0.06}Al_5O_{12}$ (YAG:10Yb2Er) was synthesized *via* a modified Pechini method [12,13]. The doping ions concentration of 10 (Yb^{3+}), and 2 mol % (Er^{3+}) were chosen arbitrary based on our previous extensive experience in working with lanthanide activated garnet type of materials, based on the well known fact that the optimal ratios of Yb/Er for upconversion process are 4:1 or 5:1 [14,15]. The concentrations do not affect the ratios of thermalized emissions employed for thermometry. Metal nitrates (yttrium(III) nitrate hexahydrate, $Y(NO_3)_3{\times}6H_2O$;

ytterbium(III) nitrate pentahydrate, $Yb(NO_3)_3{\times}5H_2O$; erbium (III)-nitrate pentahydrate, $Er(NO_3)_3{\times}5H_2O$; aluminium(III) nitrate nonahydrate, $Al(NO_3)_3{\times}9H_2O$; Alfa Aesar, USA, purity 99.9, 99.9, 99.99+ and 98+ %, respectively); citric acid - CA ($HOC(COOH)(CH_2COOH)_2$, Sigma Aldrich, USA, ACS reagent, ≥99.5 %) and ethylene glycol - EG ($HOCH_2CH_2OH$, Sigma Aldrich, country, anhydrous, 99.8 %) were used as starting materials without further purification. In a typical procedure, calculated amounts of metal nitrate precursors were added to the solution of citric acid in ethylene glycol (M: CA: EG = 1: 5: 25) and stirred for 30 min at 80 °C. After rising temperature to 120 °C, stirring was continued until a yellow brownish gel was obtained, which was then transferred into a alumina crucible and placed into a furnace at 600 °C for 2 h, followed by annealing at 1100 °C for 2 h. The powder sample obtained after annealing was cooled to room temperature and ground in a mortar.

Crystal structure and phase purity of the material were assessed by X-ray diffraction (XRD) measurements conducted by using a Rigaku SmartLab instrument (Rigaku, Japan), utilizing Cu-Ka radiation with a wavelength of 15.40 nm. The sample morphology was analysed by transmission electron microscopy (TEM) using Philips CM-20 SuperTwin TEM (Philips, Holland). After placing the sample powder inside the holder of the heating stage the emission spectra were recorded by, *via* Andor Kymera 193i spectrometer (Oxford Instruments, UK) with a CCD detector. Single emission/excitation spectrum was obtained at each temperature, from 300 to 800 K, with step 25 K. Excitation was performed by Ekspla NT342B OPO laser (producer, country). The sample was heated by the Linkam THMS600 stage (Linkam, UK).

3. RESULTS AND DISCUSSION

XRD measurements demonstrated that the YAG:10Yb2Er crystallizes in a body-centred cubic structure with $Ia\bar{3}d$ (230) space group (ICDD card no. 01-073-3184), as presented in Figure 1a. A TEM image shows that the YAG:Er^{3+}/Yb^{3+} sample consists of agglomerated nanoparticles of size between 30 nm and 40 nm (Figure 1b).

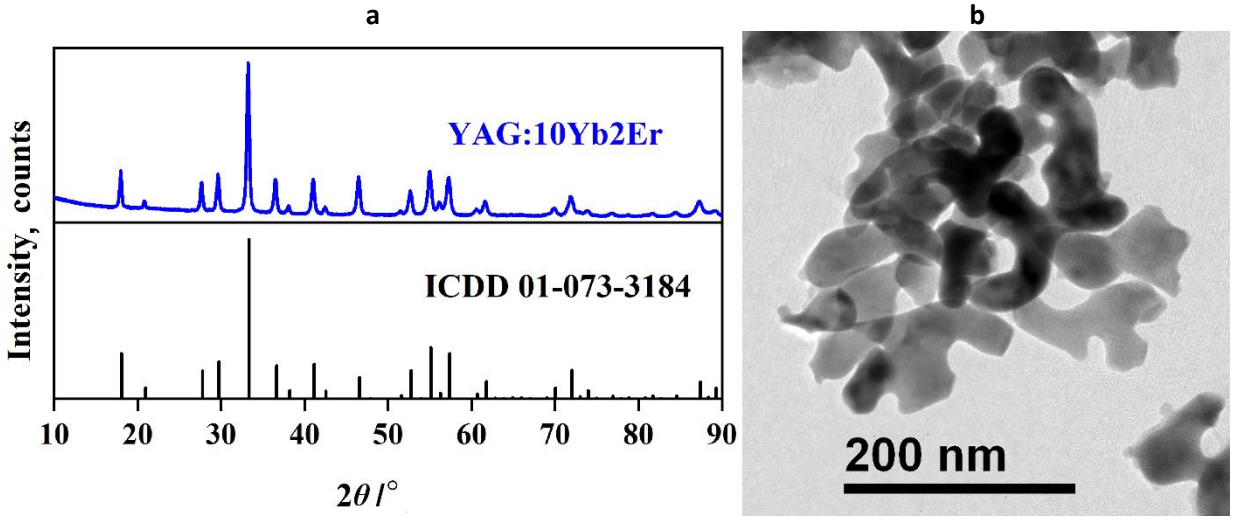

Figure 1 Characterization of YAG:Yb^{3+}/Er^{3+} powder: a) XRD, b) TEM micrograph (scale bar: 200 nm)

The excitation spectrum obtained by monitoring the most intense emission at room temperature, $^4S_{3/2}{\rightarrow}{}^4I_{15/2}$, is presented in Figure 2a. The spectra are featured by the excitations from the ground multiplet of Yb^{3+} and a small peak originating from direct excitation of Er^{3+} to the $^4I_{11/2}$ level. The Stark splitting of Yb^{3+} $^2F_{7/2}$ and $^2F_{5/2}$ levels in the YAG matrix is well known [13]: the ground level is split into 4 sublevels, and the excited level into 3 sublevels. Due to the thermalization of the Stark sublevels of the ground level of Yb^{3+}, there is also a possible excitation from the 2nd and 3rd Stark sublevels into the $^2F_{5/2}$ [16]. After excitation into $^2F_{5/2}$, the non-radiative energy transfer from Yb^{3+} to Er^{3+} occurs, populating the $^4I_{11/2}$ level, with a much higher probability than excitation directly from the Er^{3+} ground level [17]. After the second energy transfer from the Yb^{3+} ion, Er^{3+} gets excited to the $^4F_{7/2}$ level. From $^4F_{7/2}$ the electron can de-excite radiatively or non-radiatively to the lower levels. Due to the small energy gap between $^4F_{7/2}$ and its neighbouring level $^2H_{11/2}$, and somewhat energetically lower $^4S_{3/2}$, multiphonon de-excitation is the most probable mechanism [18]. As the

energy difference between those 3 levels, $^4F_{7/2}$, $^2H_{11/2}$, and $^4S_{3/2}$ are small enough, the relative optical centre population between them is given by the Boltzmann distribution, and those 3 levels are said to be thermalized (see Figure 2b). Due to the larger energy gap between $^4S_{3/2}$ and its next energetically lower level the probability for multiphonon de-excitation significantly drops, and the $^4S_{3/2}$ level is highly efficient for radiative emission.

The emission spectra under 916 nm excitation (1-7 Stark levels of Yb^{3+}) from 300 K to 800 K, with a step of 25 K, are presented in Figure 2c. $^4S_{3/2}\rightarrow{}^4I_{15/2}$ emission uniformly decreases with increasing temperature. The $^2H_{11/2}\rightarrow{}^4I_{15/2}$ emission first increases with temperature because of obtaining optical centres from the $^4S_{3/2}$ level according to the Boltzmann distribution, and then decreases due to the temperature quenching and increased share of electrons to the even higher level, $^4F_{7/2}$. $^4F_{7/2}\rightarrow{}^4I_{15/2}$ emission uniformly increases with increasing temperature.

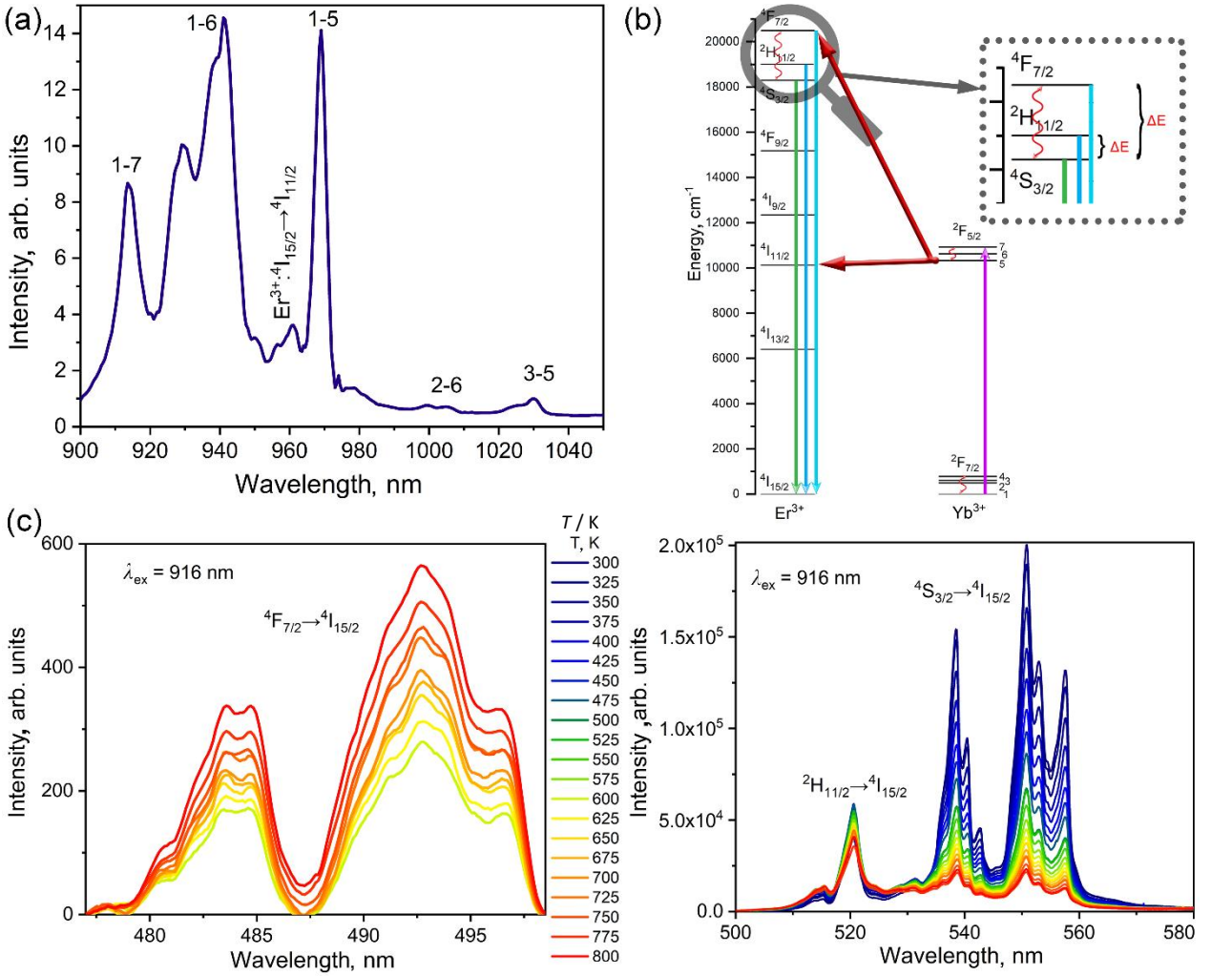

Figure 2. Luminescence of YAG:Er^{3+}/Yb^{3+} (a) NIR excitation spectrum obtained by monitoring $^4S_{3/2}\rightarrow{}^4I_{15/2}$ emission. (b) Energy level diagram of excitation, energy transfers, thermalizations, and emissions in Yb^{3+}/Er^{3+} upconversion. (c) Upconversion emission spectra of YAG:Er^{3+}/Yb^{3+} at various temperatures.

The integrated emission intensities of $^4S_{3/2}\rightarrow{}^4I_{15/2}$, $^2H_{11/2}\rightarrow{}^4I_{15/2}$, and $^4F_{7/2}\rightarrow{}^4I_{15/2}$ are given in Figure 3a. From the integrated intensities and Eq. 1 two LIRs are obtained: between the 1st and 2nd thermalized levels (Figure 3b), and between the 1st and 3rd thermalized levels (Figure 3c). Conventional LIR between the 1st and 2nd thermalized levels, obtained by fitting to the Boltzmann distribution, provided for an energy gap of 633 cm^{-1} between the $^2H_{11/2}$ and $^4S_{3/2}$, which is a value close to the one given in the literature [19]. The relatively high value of the *B* parameter is an indication of a high intensity of emission from the $^2H_{11/2}$ level. By using the emissions from $^4F_{7/2}$ and $^4S_{3/2}$ levels the fitted energy gap is equal to 2197 cm^{-1}. Due to the low intensity of $^4F_{7/2}$ emissions LIR using the 3rd thermalized level is impractical at

temperatures below 600 K. An excellent fit qualities and fitting to the Boltzmann relation without added offset are proof of good thermalization and adequate experimental conditions without stray light [3].

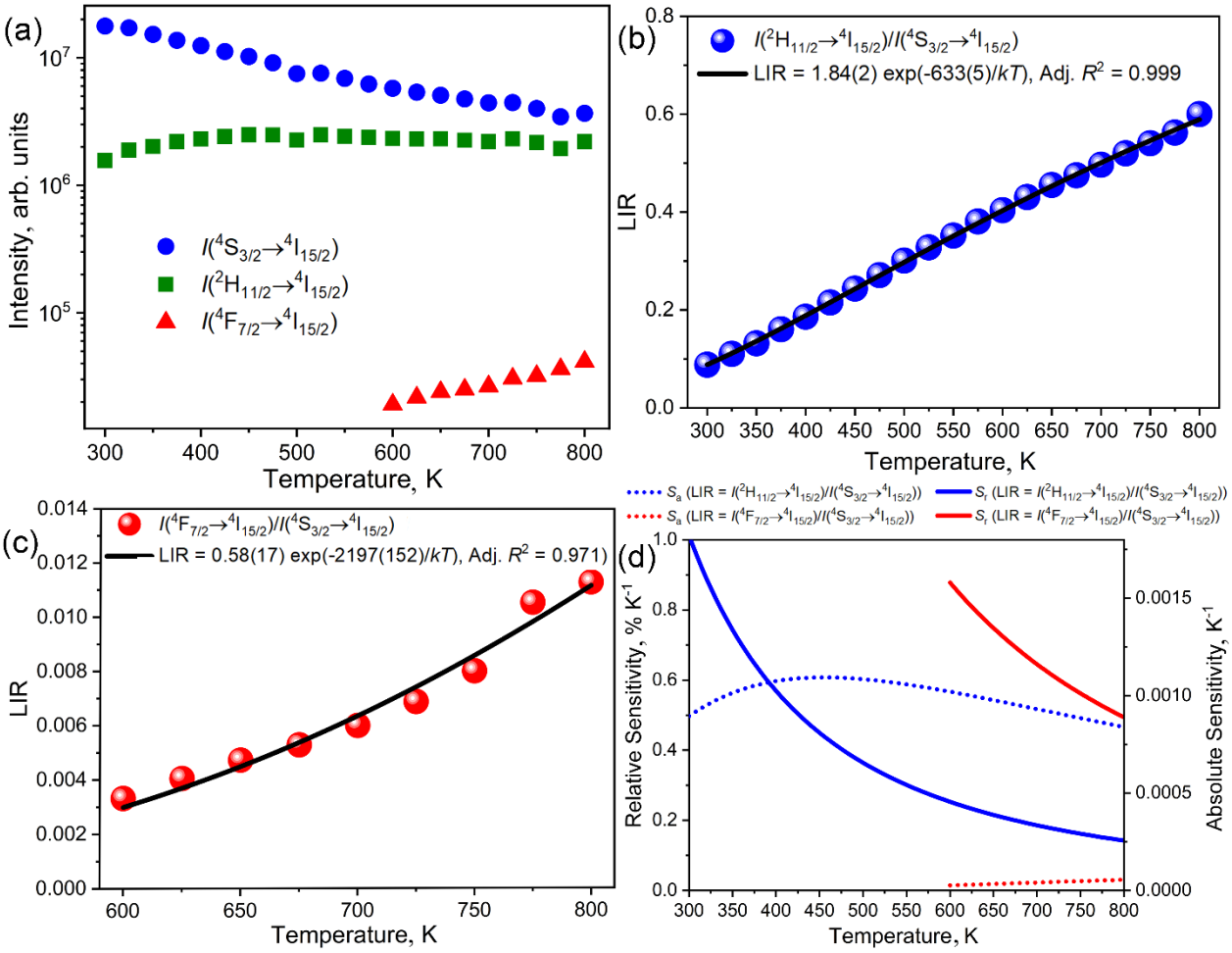

Figure 3. Thermometric analysis of YAG:Er^{3+}/Yb^{3+} by LIR methods. (a) Integrated intensities of $^4S_{3/2}\rightarrow{}^4I_{15/2}$, $^2H_{11/2}\rightarrow{}^4I_{15/2}$, and $^4F_{7/2}\rightarrow{}^4I_{15/2}$ emissions; (b) LIR of $^2H_{11/2}\rightarrow{}^4I_{15/2}$ and $^4S_{3/2}\rightarrow{}^4I_{15/2}$ emissions; (c) LIR of $^4F_{7/2}\rightarrow{}^4I_{15/2}$ and $^4S_{3/2}\rightarrow{}^4I_{15/2}$ emissions; (d) Comparison of absolute sensitivities (S_a) and relative sensitivities (S_r) of LIRs given under (b) and (c)

Relative sensitivities of those two LIRs are calculated from the fitted relations and according to Eq. 2. The results are shown in Figure 3d. Note that this figure also features the absolute sensitivity (S_a), which is a non-normalized rate of change of LIR, given by Equation (3):

$$S_a = \left|\frac{\mathrm{d\ LIR}}{\mathrm{d}T}\right| = \mathrm{LIR}\, S_r \tag{3}$$

Figure 3d demonstrates that LIR by using 1st and 3rd thermalized levels is significantly more sensitive than the conventional LIR at temperatures above 600 K where this method is practical. The improvement of sensitivity is directly proportional to the rate of energy gaps, Equation (4):

$$\frac{\Delta E\left(3^{rd}-1^{st}\right)}{\Delta E\left(2^{nd}-1^{st}\right)} = \frac{S_r\left(3^{rd}-1^{st}\right)}{S_r\left(2^{nd}-1^{st}\right)} \approx 3.5 \tag{4}$$

meaning that the relative sensitivity of the YAG:Er^{3+}/Yb^{3+} sensor by using the 3rd thermalized level is 3.5-fold greater than the conventional LIR by using only the 2nd level. At temperatures below 600 K, conventional LIR thermometry has to be used. Thus, this broad-temperature range sensor should employ two LIR variants for temperature readouts with the best performance, depending on the temperature range.

4. CONCLUSION

Luminescence thermometry by upconversion nanoparticles is a novel, prospective, and industrially relevant remote temperature sensing technique for niche applications. Due to the advantages over other methods, it is important to perfect the signal (spectrum) information processing to obtain the highest possible sensitivity. This problem was addressed by employing emission from the 3rd thermalized level in a highly stable YAG matrix doped by the most recognized upconverting pair Yb^{3+}/Er^{3+}. YAG:Yb^{3+}/Er^{3+} nanoparticles were prepared by a modified Pechini method after which their pure phase was confirmed, while the average nanoparticle diameter was determined as around 35 nm.

Under NIR excitation the Er^{3+} exhibited efficient green upconversion emission consisting of emissions from $^4S_{3/2}$, $^2H_{11/2}$, and $^4F_{7/2}$ levels. Spectra were recorded in a wide temperature range, from room temperature up to 800 K. From the integrated intensities two LIR relations were obtained, by the ratio of emissions from $^2H_{11/2}$ and $^4S_{3/2}$, and by $^4F_{7/2}$ and $^4S_{3/2}$ levels. Fitting to the Boltzmann relation by both LIRs the obtained energy gaps are similar to those reported in the literature. The energy gap in the LIR by using $^4F_{7/2}$ and $^4S_{3/2}$ levels is 3.5-fold greater than that obtained by the conventional LIR by using the first two thermalized levels, providing several times greater relative sensitivity. However, low intensity from the 3rd thermalized level prevents this method from being used at relatively lower temperatures. Thus, for the best utilization of YAG:Yb^{3+}/Er^{3+} nanoparticles, it is recommended to combine both LIRs depending on the measured temperature range.

Acknowledgements: *This work is supported by the Ministry of Science, Technological Development, and Innovation of the Republic of Serbia, under contract 451-03-47/2023-01/200017. The authors acknowledge Dr. Thomas van Swieten and Prof. Andries Meijerink for help in obtaining photoluminescence spectra.*

REFERENCES

[1] Wang X, Wolfbeis OS, Meier RJ. Luminescent probes and sensors for temperature. *Chem Soc Rev.* 2013; 42(19): 7834. https://doi.org/10.1039/c3cs60102a

[2] Wade SA. Temperature Measurement Using Rare Earth Doped Fibre Fluorescence. *Victoria.* 1999:169. https://vuir.vu.edu.au/id/eprint/15723

[3] Wade SA, Collins SF, Baxter GW. Fluorescence intensity ratio technique for optical fiber point temperature sensing. *J Appl Phys.* 2003; 94(8):.743. https://doi.org/10.1063/1.1606526

[4] Wang X, Liu Q, Bu Y, Liu C-S, Liu T, Yan X. Optical temperature sensing of rare-earth ion doped phosphors. *RSC Adv.* 2015; 5(105): 86219–36. https://doi.org/10.1039/C5RA16986K

[5] Sun Q-C, Ding YC, Sagar DM, Nagpal P. Photon upconversion towards applications in energy conversion and bioimaging. *Prog Surf Sci.* 2017; 92(4): 281–316. https://doi.org/10.1016/j.progsurf.2017.09.003

[6] Auzel F. Compteur quantique par transfert d'energie entre deux ions de terres rares dans un tungstate mixte et dans un verre. *CR Acad Sci Paris.* 1966; 262: 1016–1019.

[7] Suta M, Meijerink A. A Theoretical Framework for Ratiometric Single Ion Luminescent Thermometers—Thermodynamic and Kinetic Guidelines for Optimized Performance. *Adv Theory Simulations.* 2020; 3(12): 2000176. https://doi.org/10.1002/adts.202000176

[8] Marciniak L, Bednarkiewicz A, Kowalska D, Strek W. A new generation of highly sensitive luminescent thermometers operating in the optical window of biological tissues. *J Mater Chem C.* 2016; 4(24): 5559–5563. https://doi.org/10.1039/C6TC01484D

[9] Ćirić A, Periša J, Zeković I, Antić Ž, Dramićanin MD. Multilevel-cascade intensity ratio temperature read-out of Dy^{3+} luminescence thermometers. *J Lumin.* 2022 ;245: 118795. https://doi.org/10.1016/j.jlumin.2022.118795

[10] Ćirić A, Aleksić J, Barudžija T, Antić Ž, Đorđević V, Medić M, Periša J, Zeković I, Mitrić M, Dramićanin MD. Comparison of three ratiometric temperature readings from the Er^{3+} upconversion emission. *Nanomaterials.* 2020; 10(4): 627. https://doi.org/10.3390/nano10040627

[11] Shi H, Zhu C, Huang J, Chen J, Chen D, Wang W, Wang F, Cao Y, Yuan X. Luminescence properties of YAG:Ce, Gd phosphors synthesized under vacuum condition and their white LED performances. Optical Materials Express. 2014; 4 (4): 649-655. https://doi.org/10.1364/OME.4.000649

[12] Pechini M. Method of preparing lead and alkaline earth titanates and niobates and coating method using the same to form a capacitor. US Patent No. 3330697., 1967

[13] Periša J, Ristić Z, Piotrowski W, Antić Ž, Marciniak L, Dramićanin MD. All near-infrared multiparametric luminescence thermometry using Er^{3+}, Yb^{3+}-doped YAG nanoparticles. *RSC Advances.* 2021; 11(26): 15933. https://doi.org/10.1039/d1ra01647d

[14] Yin HJ, Feng JS, Liang N, Liu XM, Liu JX, Wang KZ, Yao CJ. Boosting Photo Upconversion in Electropolymerised Thin Film with Yb/Er Complexes. *Adv. Opt. Mat.* 2023; 11(6), 2202550. https://doi.org/10.1002/adom.202202550

[15] Yoshikawa A, Boulon G, Laversenne L, Canibano H, Lebbou K, Collombet A, Guyot Y, Fukuda T. Growth and spectroscopic analysis of Yb^{3+}-doped $Y_3Al_5O_{12}$ fiber single crystals. *J Appl Phys.* 2003; 94(9): 5479–88. https://doi.org/10.1063/1.1597763

[16] Ćirić A, van Swieten T, Periša J, Meijerink A, Dramićanin MD. Twofold increase in the sensitivity of Er^{3+}/Yb^{3+} Boltzmann thermometer. *J Appl Phys.* 2023; 133(19): 194501 https://doi.org/10.1063/5.0149757

[17] Auzel F. Upconversion and Anti-Stokes Processes with f and d Ions in Solids. *Chem Rev.* 2004; 104(1): 139-174. https://doi.org/10.1021/cr020357g

[18] Ćirić A, Dramićanin MD. LumTHools - Software for fitting the temperature dependence of luminescence emission intensity, lifetime, bandshift, and bandwidth and luminescence thermometry and review of the theoretical models. *J Lumin.* 2022; 252: 119413. https://doi.org/10.1016/j.jlumin.2022.119413

[19] Ćirić A, Gavrilović T, Dramićanin MD. Luminescence Intensity Ratio Thermometry with Er^{3+}. *Crystals.* 2021; 11(2): 189. https://doi.org/10.3390/cryst11020189

Odnos intenziteta luminescencije tri termalizovana nivoa u YAG:Er^{3+}/Yb^{3+}nanočesticama

Aleksandar Ćirić*, Mina M. Medić, Jovana V. Periša, Željka M. Antić and Miroslav D. Dramićanin

Centar izvrsnosti za fotokonverziju, Institut za nuklearne nauke Vinča - institut od nacionalnog značaja za Republiku Srbiju, Univerzitet u Beogradu, Beograd, Srbija

(Naučni rad)

Izvod

Luminiscentna termometrija je metoda za očitavanje temperature pomoću daljinskog senzora temperature posmatranjem temperaturno zavisnih spektralnih promena. Potraga za povećanom osetljivosti očitavanja temperature motivisala je istraživanje korišćenja trećeg termalizovanog nivoa Er^{3+} emisije u fotoluminiscenciji Yb^{3+}/Er^{3+}. Za ovu svrhu pripremljene su veoma stabilne i efikasne nanočestice YAG:Yb^{3+}/Er^{3+} modifikovanom Pećinijevom metodom. Emisioni spektri su snimljeni u temperaturnom opsegu od 300 K do 800 K i dobijena su dva odnosa intenziteta luminiscencije između emisija $^4S_{3/2}$, $^2H_{11/2}$ i $^4F_{7/2}$. Pored odličnog poklapanja sa teorijskim predviđanjima, očitavanje korišćenjem $^4F_{7/2}$ metode je omogućilo 3,5 puta povećanje relativne osetljivosti u odnosu na odnos intenziteta luminiscencije za nivo $^2H_{11/2}$, uz ograničenje upotrebljivosti samo iznad 600 K. Metoda emisije iz $^2H_{11/2}$ treba da se koristi od 300 K do 600 K, dok emisija od $^4F_{7/2}$ obezbeđuje najbolji odnos intenziteta luminiscencije od 600 K do 800 K. YAG:Yb^{3+}/Er^{3+} nanočestice su se pokazale kao odličan senzorski materijal za luminescentnu metodu odnosa intenziteta korišćenjem više termalizovanih nivoa.

Ključne reči: luminiscentna termometrija; apkonvertujuće nanočestice; odnos intenziteta fluorescencije; Pećini metod

Fenton-like oxidative degradation of Orange G dye and binary dye mixtures using Oxone® activated with cobalt-doped alumina catalysts

Sanja R. Marinović[1], Tihana M. Mudrinić[1], Marija J. Ajduković[1], Nataša P. Jović-Jovičić[1], Dimitrinka A. Nikolova[2], Predrag T. Banković[1] and Tatjana B. Novaković[1]

[1]*University of Belgrade - Institute of Chemistry, Technology and Metallurgy, Department of Catalysis and Chemical Engineering, Belgrade, Serbia*

[2]*Institute of Catalysis, Bulgarian Academy of Sciences, Sofia, Bulgaria*

Abstract

Two texturally and structurally different Co-doped aluminas were obtained by using the sol-gel method followed by calcination at temperatures of 1000 °C and 1100 °C. The obtained materials were tested as catalysts in anionic textile dye Orange G (OG) degradation using Oxone® as a precursor of sulfate anion radicals, the main reactive oxygen species. Effects of temperature and initial pH on degradation efficiency was investigated. The increase in temperature accelerated the reaction rate and the maximal degradation efficiency was obtained at 60 °C. Different kinetic models were applied and pseudo-first order rate was found to be the most appropriate. Both catalysts showed the optimal performance in the pH range around neutral. Coexisting cations (Ca^{2+}, Mg^{2+}, K^+ and Na^+) enhanced the OG degradation rate, as well as anions: Cl^- and $H_2PO_4^-$, while NO_3^-, $SO_4^{2-}$and HCO_3^- inhibited the degradation. The catalysts were also proved effective in degradation of the other investigated dyes: Methylene blue, Basic blue 41, and Remazol brilliant blue R. Finally, simultaneous degradation of OG in binary dye mixtures was investigated showing that the synthesized catalysts can be also used in simultaneous processes of dye degradation. However, differences in structural and textural properties of the two catalysts affected their catalytic performance.

Keywords: Sol-gel alumina; anionic and cationic dyes, peroxymonosulfate; advanced oxidation processes; simultaneous dye degradation.

Available on-line at the Journal web address: http://www.ache.org.rs/HI/

ORIGINAL SCIENTIFIC PAPER

UDC: 667:778.665

Hem. Ind. **78(4)** 359-370 (2024)

1. INTRODUCTION

Aluminum (III) oxide, often called “alumina” belongs to the group of surface-active metal oxides [1]. The synthesis method used to obtain aluminas affects the surface properties of the synthesized material. Sol-gel method is one of the often-used preparation methods by which the structural and textural properties of aluminas can be altered in a desired manner. By synthesizing alumina with specific physicochemical properties its catalytic activity can be controlled [2,3]. Several metastable crystalline structures of alumina can be obtained: η-, γ-, δ-, θ-, β-, κ-, χ, and α-alumina (thermodynamically most stabile phase) [4], while by rising the calcination temperature one phase will transform to another. At calcination temperatures above 800 °C, γ-Al_2O_3 transforms to δ-Al_2O_3 followed by further transformation to θ-Al_2O_3 above 1000 °C, and above 1100 °C the α- Al_2O_3 phase is obtained [5]. Yet, if the impurities are present, the phase transformation temperatures will be altered [4]. Therefore, a material with desired properties can be designed by doping alumina with different metals, which changes the properties of the new surface compared to the parent alumina. Metal-doped aluminas have shown good potential as adsorbents and catalysts in wastewater treatments to remove different organic pollutants [6,7]. This is important as removal of organic pollutants is often not possible by conventional processes and therefore, oxidative degradation using Fenton-like processes is more applicable [8,9,10]. To the best of our knowledge, using transition metal-doped aluminas as catalysts in catalytic oxidative degradation of organic

Corresponding authors: Sanja R. Marinović, University of Belgrade - Institute of Chemistry, Technology and Metallurgy, Department of Catalysis and Chemical Engineering, Njegoševa 12, 11000 Belgrade, Republic of Serbia

Paper received: 26 January 2023; Paper accepted: 17 August 2024; Paper published: 26 August 2024.

E-mail: sanja.marinovic@ihtm.bg.ac.rs

https://doi.org/10.2298/HEMIND240126016M

pollutants in wastewater in the presence of Oxone® was first investigated by our research group [7]. We have investigated degradation of the food dye Tartrazine using three alumina catalysts with different crystalline structures and different textural properties. Oxone® was used as a source of sulfate anion radicals, proven to be superior to hydroxyl radicals in Fenton-like processes for degradation of different organic pollutants [11,12].

Apart from food dyes, textile dyes, are often found in industrial wastewaters. The textile industry produces large amounts of wastewater containing genuine reactive textile dyes [13,14]. One of the representatives, and often used textile dyes is Orange G (OG). OG is a synthetic acidic azo-dye, which is toxic and non-biodegradable [15]. Due to its high solubility in water, OG can be present in wastewater from textile, leather, and printing industries at high concentrations. Given OG's potentially carcinogenic nature, it is a high priority to find an efficient way for removal from wastewater [16]. Since Co-doped alumina catalysts (CoA) tested in Tartrazine degradation showed excellent performance, two selected catalysts with different alumina phases and different textural properties were investigated in this work for catalytic OG degradation in the presence of Oxone®. The first catalyst labeled CoA-1000 was calcined at 1000 °C containing the γ-Al_2O_3phase. On the other hand, the second catalyst labeled CoA-1100 calcined at 1100 °C has shown the presence of α- Al_2O_3. Several reaction parameters were investigated to determine the effects of different material structures and properties on the catalytic performance in Oxone® induced OG dye degradation. Apart from OG degradation, simultaneous degradation of OG and three other dyes: Methylene blue, Remazol brilliant blue R, and Basic blue 41 were tested to get an insight in the interactions of different dyes and to assess if the catalyst efficiency changes in a complex system.

2. EXPERIMENTAL

2. 1. Materials and synthesis

Oxone® (potassium triple salt - $KHSO_5 \cdot 0.5 \cdot KHSO_4 \cdot 0.5 \cdot K_2SO_4$), Orange G (OG), Methylene blue (MB), Remazol brilliant blue R (RB), Basic blue 41 (BB), NaCl (*p.a.*), $NaHCO_3$ (*p.a.*), $NaNO_3$ (*p.a.*), Na_2SO_4 (*p.a.*), $NaH_2PO_4 \cdot H_2O$ (*p.a.*), KCl (*p.a.*), $CaCl_2$ (anhydrous >98 %), and $MgCl_2$ (anhydrous >98 %), were supplied by Sigma Aldrich (USA) and were used as received. Structural formulas of the dyes are presented in Figure S1 (Supplementary material).

Two Co-doped alumina catalysts were synthesized using the sol-gel method and calcined at 1000 °C (CoA-1000) and 1100 °C (CoA-1100). The synthesis and characterization of the synthesized materials were presented previously [7]. In addition to previous characterization, the morphology of both catalysts was studied using scanning electron microscopy with energy dispersive spectroscopy (SEM-EDS). The samples were characterized by a dual beam scanning electron/focused ion beam system (SEM/FIB LYRA I XMU, TESCAN, Czech Republic), equipped with an EDX detector (Quantax 200, Bruker, Germany). SEM-EDS analyses were performed under the following conditions: tungsten filament, resolution: 3.5 nm at 30 kV, accelerating voltage: 200 V - 30 kV, EDX detector: spectroscopic resolution at Mn-Kα was 126 eV. The maximum input count range was 1 kcps.

2. 2. Catalytic tests

In all catalytic tests, 200 cm^3 of aqueous solution of a dye was introduced into a thermostated Pyrex reactor. The stirring was provided by a mechanical stirrer. After reaching the desired reaction temperature, 1 cm^3 of Oxone solution (40 mg of Oxone®) was added to the dye solution, and 10 mg of catalyst was added right after that initial moment (0 min of the reaction). The aliquots (2 cm^3) were taken at predetermined time intervals after the reaction started. Supernatant solutions were separated from the catalyst by centrifugation. Degradation of dyes was determined by measuring the decrease in the peak maximum at 478 nm, for OG, and at 665, 592 and 609 nm for MB, RB, and BB respectively, using UV-Vis spectrophotometry (Evolution 220, Thermo Scientific, USA).

For OG, the effects of temperature and the initial pH on the degradation efficiency were monitored. The starting OG concentration was 50 mg dm^{-3} in all experiments. The effect of temperature was investigated in the range from 30 °C to 60 °C at unadjusted pH 3.7 and the effect of the initial pH was followed in the pH range 2 to 9, at 30 °C. The experimentally obtained data were modeled by the zero, pseudo-first, and pseudo-second order kinetic models in order to determine reaction kinetics.

Prior to catalytic tests, the adsorption of each of the dyes on the CoA-1000 and CoA-1100 as adsorbents was examined, without the presence of Oxone®, and the amount of adsorbed dyes was less than 3 %. Degradation of OG with Oxone® without a catalyst under the same experimental conditions was negligible meaning that the presence of a catalyst for Oxone® activation was necessary.

To examine the influence of coexisting anions and cations, each ion was added (as a water-soluble salt) to the OG solution ($C_{0,OG}$ = 50 mg dm^{-3}), so that the concentration of that ion in the dye solution was 5 mmol dm^{-3}. For investigations of the effects of Cl^- and NO_3^- ions, additional experiments were performed with the ion concentration of 20 mmol dm^{-3}. In all these experiments, the reaction temperature was 50 °C and the CoA-1000 catalyst was used. All other experimental conditions were the same as stated above.

For experiments using MB, RB, and BB, the starting dye concentration was 20 mg dm^{-3} in single dye experiments. In binary system degradation experiments, 20 mg dm^{-3} of each dye was applied. The degradation degree of investigated dyes was calculated by comparing the absorbance at the characteristic wavelengths at predefined reaction times with the initial absorbance values. In these experiments, the reaction temperature was 30 °C.

3. RESULTS AND DISCUSSION

The catalysts' characterization results were previously published [7]. However, an overview of the structural, phase and textural properties of the catalysts is presented here to facilitate the interpretation of the obtained results.

The X-ray powder diffraction (XRPD) analysis confirmed that the main phase in both catalysts was some type of Co-spinel (Co_3O_4, $CoAl_2O_4$, Co_2AlO_4), and the second phase was identified to be γ-Al_2O_3 stabilized by cobalt for CoA-1000, and α-Al_2O_3 for CoA-1100. H_2-temperature programmed reduction (H_2-TPR) confirmed the presence of Co_3O_4/$CoAl_2O_4$ in CoA-1000, and $CoAl_2O_4$ in CoA-1100. Using the N_2 physisorption technique textural parameters of synthesized catalysts were obtained. The specific surface area of the CoA-1000 (S_{BET} = 43 m^2 g^{-1}) was over 4 times higher than that of CoA-1100 (S_{BET} = 10 m^2 g^{-1}). Similar results were observed for the total pore volume ($V_{0.98}$ = 0.122 cm^3 g^{-1} for CoA-1000, and $V_{0.98}$ = 0.057 cm^3 g^{-1} for CoA-1100) [7].

In this paper, the morphology of CoA-1000 and CoA-1100 catalysts was examined using the SEM-EDS characterization technique. The surface chemical composition of catalysts is presented in Table 1. The analysis of the results revealed enrichment of the CoA-1100 catalyst surface with cobalt by 7 % as compared to that of CoA-1000. At the same time, a decrease in surface oxygen concentration is observed for CoA-1100. Calculation of the Co/Al mass ratio and EDS element mapping, for the same image of magnification used for quantity control, confirmed differences between the two catalysts (Figs. 1a, 1d, 2a, and 2d). These observations are in accordance with different phase structures of CoA-1000 and CoA-1100. It is obvious that the complete formation of $CoAl_2O_4$ during calcination at 1100 °C led to an increase in cobalt distribution on the surface.

Table 1. Surface chemical compositions of CoA-1000 (in Fig. 1a) and CoA-1100 (in Fig. 2a)

Sample	Surface concentration, wt.%			Co/Al mass ratio
	O	Al	Co	
CoA-1000	30.87	32.04	37.09	1.16
CoA-1100	25.72	30.08	44.20	1.47

The images of selected areas at higher magnifications showed very different morphology of the two catalysts (Figs. 1b, 1c, 2b, and 2c). The surface microstructure of the CoA-1000 catalyst is characterized by plate-like formations of different sizes and the presence of white spherical particles of similar sizes. These results are consistent with the findings from low-temperature N_2 physisorption. The obtained morphology of CoA-1000 corresponds to aggregated planar particles and slit type pores [7]. The presence of Co_3O_4/$CoAl_2O_4$ phases at the CoA-1000 surface is also recognized indirectly by the EDX technique. The increase in the calcination temperature of 100 °C led to more homogeneous morphology and plate formation was not observed in the case of the CoA-1100 catalyst. The agglomeration of spherical particles was observed for CoA-1100 as well as for CoA-1000. However, CoA-1100 exhibited a more pronounced effect when observed at higher magnification (Fig. 2c). Comparison of EDS mapping images of Co for both catalysts (Figs. 1f and 2f) reveals the enrichment of cobalt on the CoA-1100 surface.

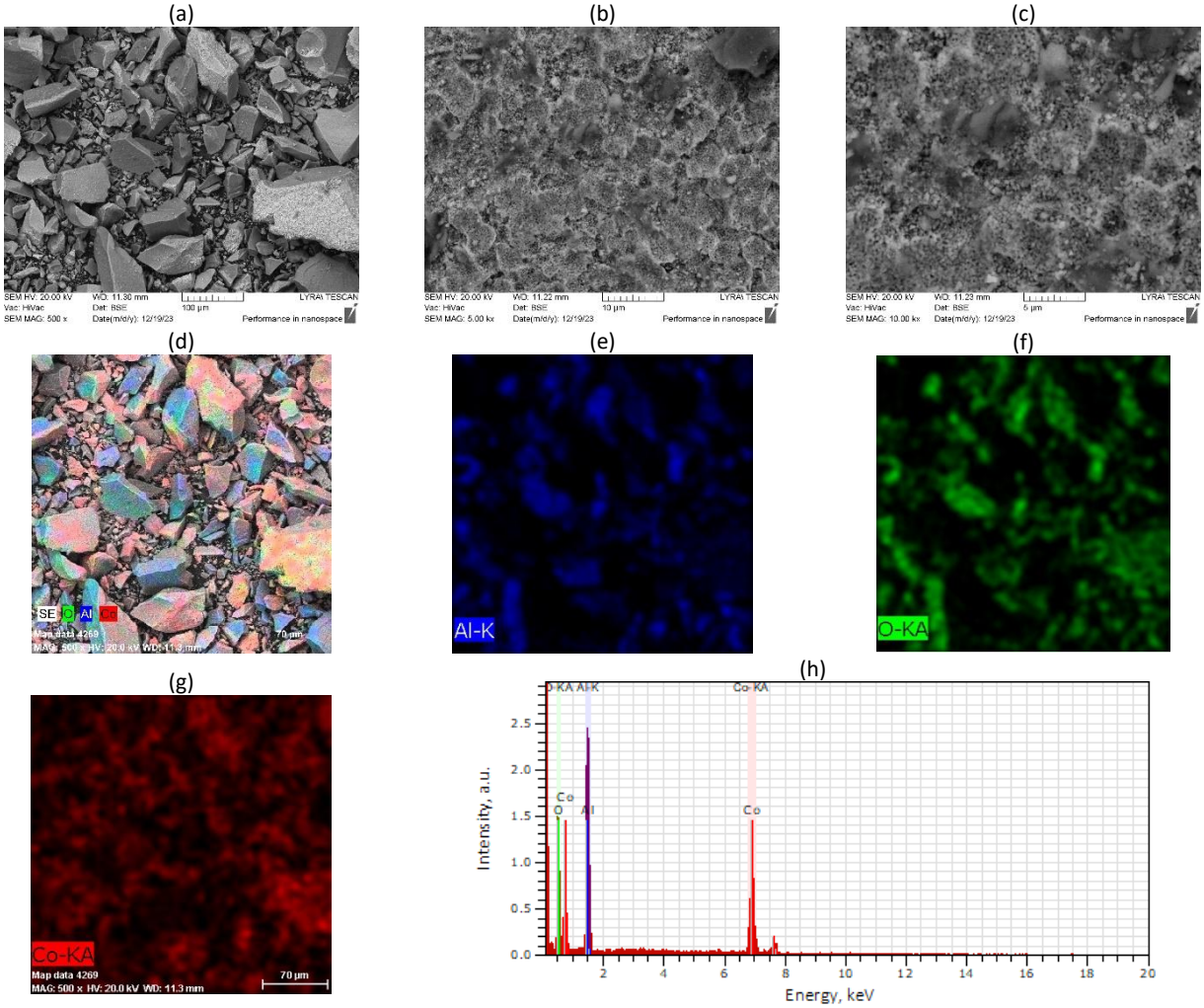

Figure 1. SEM images of CoA-1000: a-c - different magnifications; d-g - EDS elemental mapping of Co, Al, O; h - EDX spectrum determined for the image a

3. 1. Catalytic tests

3. 1. 1. Influence of temperature

The influence of temperature on the catalytic degradation of the OG was investigated for 120 min in the temperature range from 30 °C to 60 °C. The reaction extent was followed by measuring the characteristic OG's UV adsorption peak at 478 nm originating from the azo group in the OG molecule. With the increase in the reaction temperature, the degradation rate increased, as expected, being significantly higher for CoA-1000 (Fig. 3a) as compared to that for CoA-1100 (Fig. 3b) at all investigated temperatures. The OG dye was completely degraded after 120 min in the presence of CoA-1000 at temperatures above 45 °C. On the other hand, for CoA-1100, the complete degradation was achieved only at 60 °C in the investigated period. The proposed degradation mechanism for the catalyst CoA-1000 at the temperature of 60 °C is presented in Chapter S3 (Supplementary material).

Zero (Eq. (1)), pseudo-first (PFO) (Eq. (2)), and pseudo-second order (PSO) (Eq. (3)) kinetic models in linear forms were applied to the obtained experimental data (Fig. 4 for PFO and Figs S2-S5 for zero and PSO models in Supplementary material).

$$C_t = C_0 - k_0 t \quad (1)$$

$$\ln C_t = \ln C_0 - k_1 t \quad (2)$$

$$1/C_t = 1/C_0 + k_2 t \quad (3)$$

C_t is the dye concentration in aqueous solution at any time t, C_0 is the starting dye concentration, and k_0, k_1, and k_2 are zero, pseudo-first, and pseudo-second order rate constants respectively.

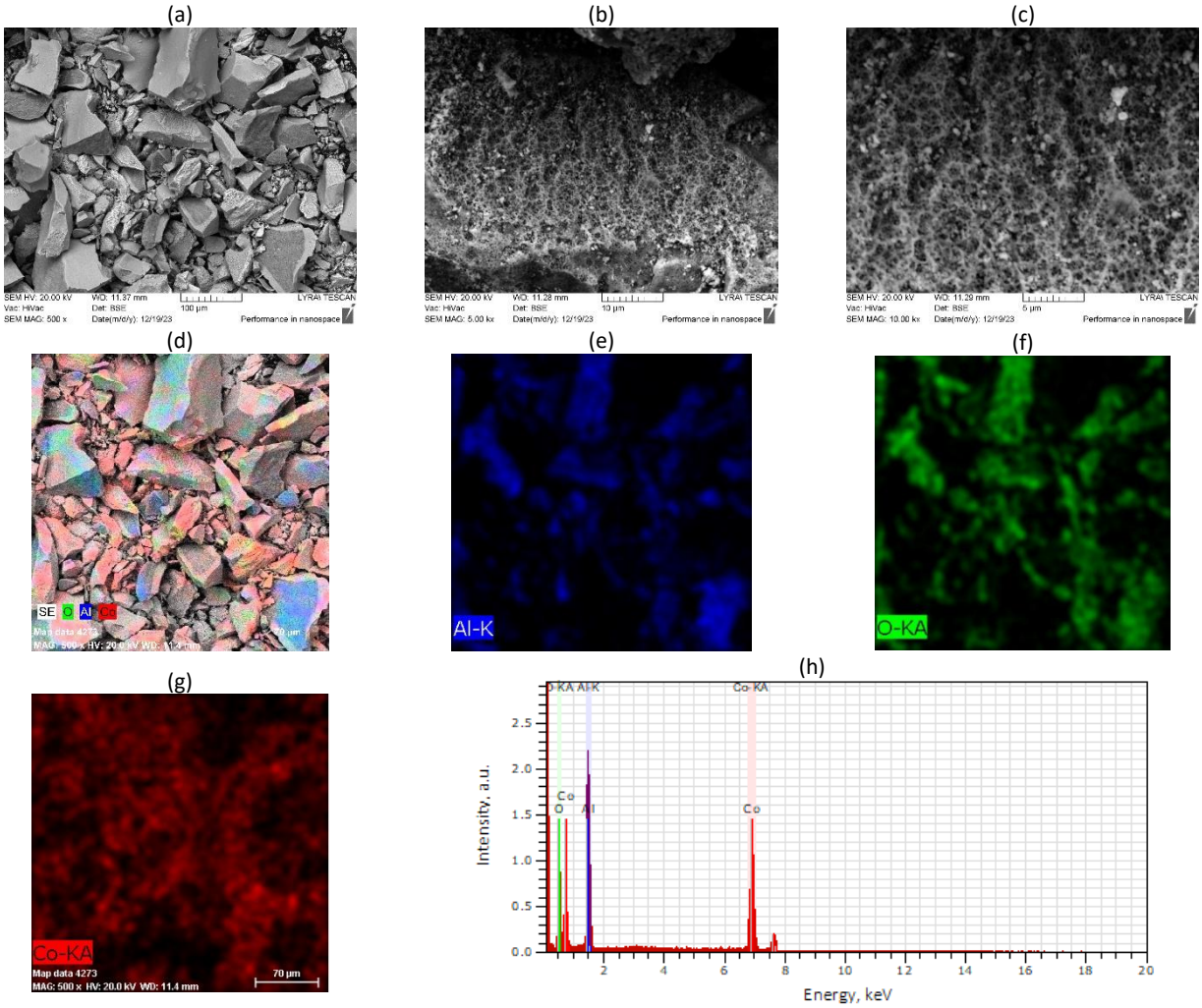

Figure 2. SEM images of CoA-1100: a-c - different magnifications; d-g - EDS elemental mapping of Co, Al, O; h - EDX spectrum determined for the image a

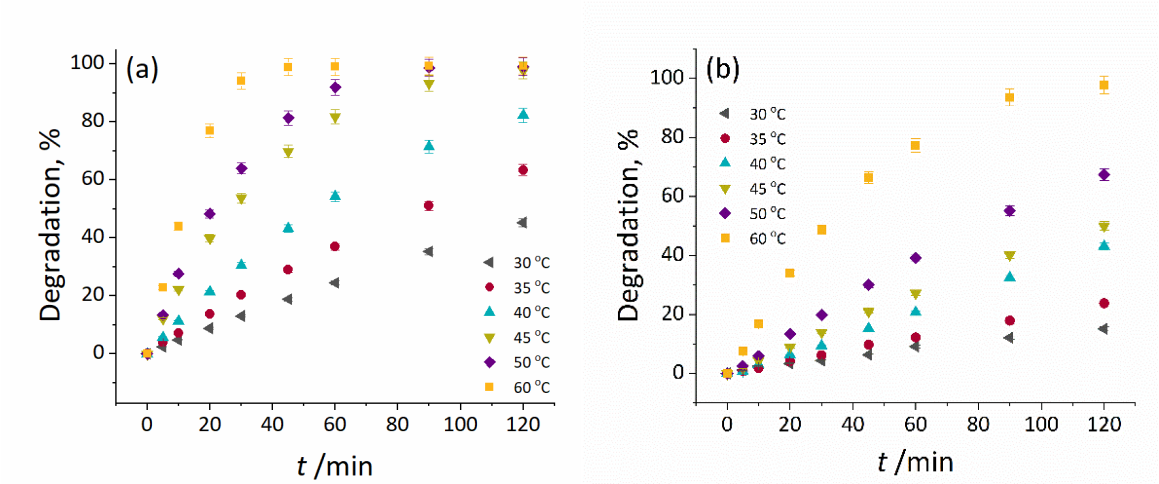

Figure 3. Influence of the temperature on the OG degradation extent for: a) CoA-1000 and b) CoA-1100 ($C_{0,OG}$ = 50 mg dm^{-3}; $V_{OGsolution}$ = 200 cm^3; $m_{Oxone®}$ = 40 mg; m_{cat} = 10 mg)

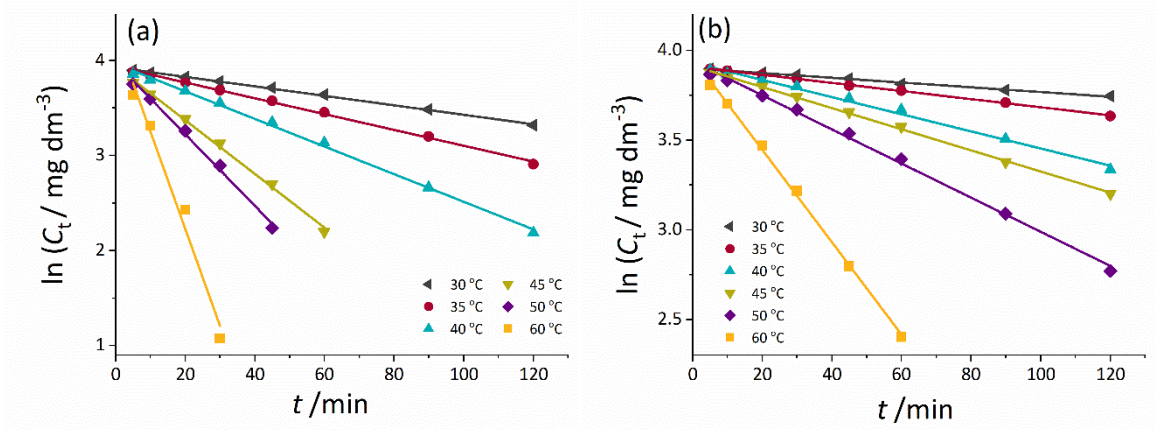

Figure 4. Application of the PFO kinetic model (lines) on experimental data (symbols) for OG degradation at different temperatures for:(a) CoA-1000 and (b) CoA-1100 ($C_{0,OG}$ = 50 mg dm^{-3}; $V_{OGsolution}$ = 200 cm^3; $m_{Oxone®}$ = 40 mg; m_{cat} = 10 mg).

For lower temperatures, both zero and PFO showed good agreement between experimental data and applied models, with slightly better fitting obtained with the PFO model. At higher temperatures, it becomes evident that the PFO kinetic model aligns better with the experimental data. The PSO model did not fit the data well, as expected. This trend is also noticeable when comparing kinetic model parameters shown in Table 2.

Table 2. Kinetic model parameters

			Temperature, °C					
Catalyst	Kinetic model		30	35	40	45	50	60
CoA-1000	Zero	k_0×10^2 / mg dm^{-3} min^{-1}	18.75	24.79	33.93	52.16	82.81	139.50
		R^2	0.9982	0.9941	0.9709	0.9082	0.9783	0.9700
	Pseudo-first	k_1×10^2 / min^{-1}	0.50	0.83	1.45	2.83	3.77	10.22
		R^2	0.9984	0.9975	0.9972	0.9968	0.9953	0.9802
	Pseudo-second	k_2×10^2 / dm^3 mg^{-1} min^{-1}	0.01	0.03	0.08	0.11	0.2	1.22
		R^2	0.9852	0.9657	0.9272	0.9673	0.9253	0.8355
CoA-1100	Zero	k_0×10^2 / mg dm^{-3} min^{-1}	6.21	9.90	18.01	20.97	28.16	64.68
		R^2	0.9901	0.9985	0.9989	0.9964	0.9906	0.9795
	Pseudo-first	k_1×10^2 / min^{-1}	0.13	0.23	0.48	0.59	0.95	2.58
		R^2	0.9932	0.9991	0.9923	0.9987	0.9970	0.9985
	Pseudo-second	k_2×10^2 / dm^3 mg^{-1} min^{-1}	0.003	0.005	0.010	0.020	0.030	0.110
		R^2	0.9932	0.9967	0.9739	0.982	0.9591	0.9421

R^2 - square of coefficient of correlation; k- rate constants

Although at lower temperatures, especially for CoA-1100, R^2 values for zero and for PFO are similar, small differences in favor of PFO are noticeable. This behavior is expected and reported in similar systems, where even a zero kinetic model is more applicable at lower temperatures. PFO is expected to be the best fit for the experimental data because Oxone® is present in great excess.

To check whether the application of the kinetic models in linear and non-linear forms fit the data equally well, the data were also fitted with the PFO model in non-linear form. The obtained kinetic parameters for the PFO model applied in the nonlinear form are presented in Table S1 in Supplementary material. Application of the PFO model in both linear and non-linear forms provided very similar results confirming that in the present case, linear fitting was sufficiently good. PFO rate constants (k_1) increased with increasing the reaction temperature for both catalysts. The k_1 values for CoA-1000 were more than 3 times higher than for CoA-1100, for all investigated temperatures, leading to the conclusion of higher catalyst efficiency of CoA-1000. The differences in textural and structural characteristics between CoA-1000 and CoA-1100 can explain the differences in their activity as catalysts in investigated reactions. The textural properties of CoA-1000 were much better compared to CoA-1100, with four times higher specific surface area, and twice as high the total pore volume. Also, the presence of the *γ*-alumina phase in CoA-1000, stabilized with a small amount of cobalt, provided more accessible active sites leading to higher activity of this catalyst. But the most important feature of CoA-1000

is the presence of Co_3O_4 which is much more active in Oxone® activation reaction than $CoAl_2O_4$ (the only Co phase identified in CoA-1100) where cobalt is strongly attached to the alumina matrix making it harder to promote Oxone® activation [7].

To calculate activation energy (E_a / J mol^{-1}), obtained pseudo-first order rate constants were applied in the Arrhenius equation (Eq. 4):

$$\ln k_1 = \ln A - \frac{E_a}{RT} \quad (4)$$

A: constant related to the geometry; *T* / K: thermodynamic temperature and *R*: universal gas constant (8.314 J / mol^{-1} K^{-1}).

From the ln k_1 *vs.* T^{-1} plot (Fig. 5) activation energy was calculated.

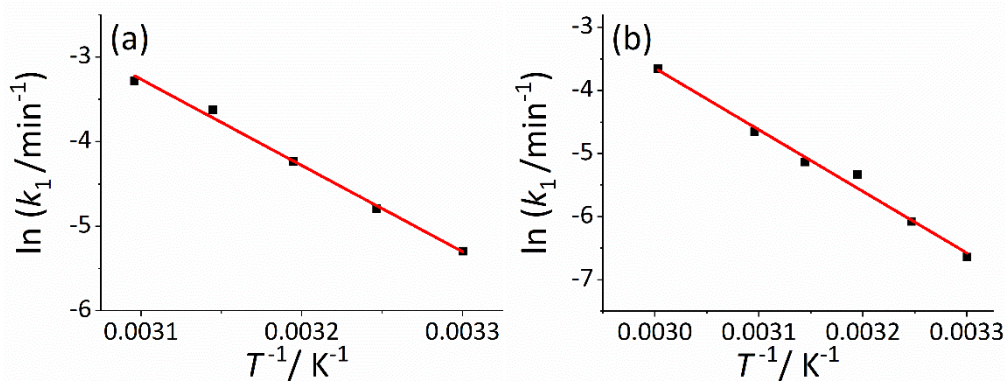

Figure 5. Arrhenius plot for the degradation of OG using a) CoA-1000 and b) CoA-1100 as catalyst

E_a was found to be 82.98 kJ mol^{-1} and 81.28 kJ mol^{-1} for CoA-1000 and CoA-1100 respectively. These values are of the same order of magnitude as those reported in the literature for OG degradation in the presence of sulfate ion radicals [16,17].

3. 1. 2. Influence of pH

The influence of the pH of the initial solution (pH_i) on the degradation of OG was investigated for different pH_i from 2 to 9 for both investigated catalysts. The unadjusted initial pH value of pH_i 3.7 was included in these graphs. In Figure 6 degradation of OG at different initial pH values is shown.

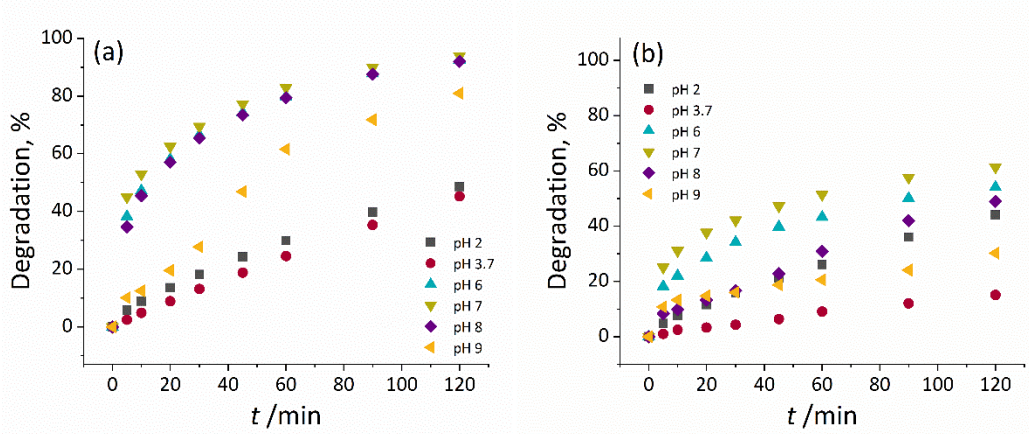

Figure 6. Degradation of OG monitored at different initial pH values for a) CoA-1000 and b) CoA-1100 ($C_{0,OG}$ = 50 mgdm^{-3}; $V_{OG\ solution}$ = 200 cm^3; $m_{Oxone®}$ = 40 mg; m_{cat} = 10 mg; θ = 30 °C)

The highest degradation rate was obtained for pH_i 7, for both catalysts. For CoA-1000 for pH_i 6-8, reaction rate was almost the same, and more than 90 % of degradation was achieved after 120 min of the reaction. On the other hand, for CoA-1100, differences in reaction rate were more pronounced in this pH_i range. After 120 minutes, the highest degradation of 60 % was obtained at pH_i 7. At pH_i 8 the reaction was slow at the beginning, and then it became faster

reaching 45 % of degradation at the end. Similar behaviour was obtained for Tartrazine degradation using investigated catalyst [7]. For all pH_i the degradation of OG for CoA-1100 was much lower than for CoA-1000.

3. 1. 3. The effect of coexisting ions

Since real wastewater usually contains various inorganic ions, it is important to investigate their effect on OG degradation efficacy in the presence of Oxone®, as these ions can interfere with the activation of Oxone®. In this work, the effects of the most common anions: Cl^-, HCO_3^-, NO_3^-, SO_4^{2-}, and $H_2PO_4^-$ on OG degradation were investigated. Apart from anions, the effect of cations K^+, Mg^{2+}, and Ca^{2+} was also tested. The tests were performed at 50 °C to allow better monitoring of the change in the absorbance peak at 478 nm and because complete decolorization was achieved after 60 min only at that temperature. The concentration of the added anion (in water solution) was 5 mmol dm^{-3}, chosen in accordance with the literature as well as the estimation of concentrations in the real water [18,19,20]. For $Cl^-$and NO_3^- anions an additional higher concentration (20 mmol dm^{-3}) was also investigated to confirm the influence of these species. The results are presented in Figure 7 (*i.e.* effects of anions and cations are presented in Fig. 7a and 7b, respectively).

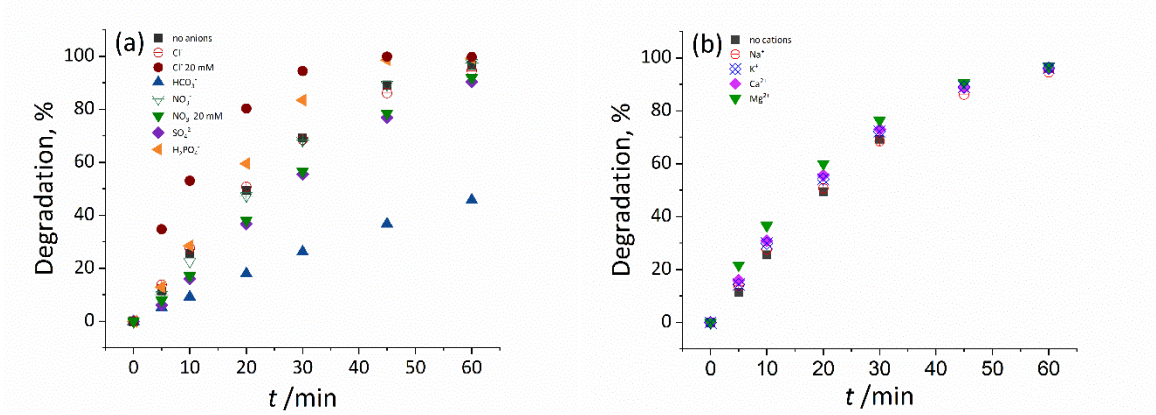

Figure 7. Influence of the coexisting ions on degradation of OG for CoA-1000 catalyst: (a) effects of anions, (b) effects of cations ($C_{0,OG}$ = 50 mg dm^{-3}; $V_{OG\ solution}$ = 200 cm^3; $m_{Oxone®}$ = 40 mg; $m_{CoA-1000}$ = 10 mg; θ = 50 °C)

It is noticeable that some anions speed up and others slow down the degradation of OG, while all the investigated cations had a positive effect on the reaction rate. The experiments showed that HCO_3^- had the most significant influence on OG degradation causing a decrease in the reaction rate of approximately 2.5 times. Only 45 % of degradation was achieved after 60 min, while in the system without the added ions almost complete degradation was observed at the same reaction time. This phenomenon is expected according to literature, since the HCO_3^- can scavenge free radicals and impede the degradation process by generating carbonate radical ($CO_3^{\cdot-}$), which has a lower oxidation ability [18,19,21]. Still, it can react with $SO_4^{\cdot-}$ and $HO^{\cdot}$ leading to lowering their concentrations in the reaction system. Sulfate anions (SO_4^{2-}) have also suppressed degradation of OG but for the investigated concentration this effect was less pronounced than that observed for HCO_3^-. Since SO_4^{2-} is produced in one of the steps of Oxone® decomposition, the existence of SO_4^{2-} in the system will inhibit the formation of SO_4^{2-} from HSO_5^- by reducing the formation of reactive species $SO_4^{\cdot-}$ [22]. On the other hand, $H_2PO_4^-$ showed an accelerating effect on reaction rate since these anions promote Oxone® degradation according to the literature [21,23]. Nitrate and chloride anions only slightly affected the reaction rate. Since the effect of these anions was not sufficiently clear for the investigated concentration of 5 mmol dm^{-3}, a higher concentration of 20 mmol dm^{-3} was also applied. It was concluded that NO_3^- anions inhibited OG degradation because they can rapidly react with $SO_4^{\cdot-}$ to form $NO_3^{\cdot}$ [20]. On the other hand, the enhancing effect of Cl^- ions on OG degradation was confirmed. This was in line with literature findings for similar systems, where even an inhibitory effect of Cl^- ions was found for very low concentrations such as 1 mmol dm^{-3}, but at higher concentrations, a promoting effect of these anions on the degradation process in Oxone® systems was reported [9,24,25,26]. It is assumed that chloride ions directly react with Oxone® to form active chlorine species that participate in dye degradation. Chloride ions can combine with hydroxyl radicals to generate chloride radicals whose oxidability is superior to hydroxyl radicals and even similar to sulfate ion radicals. This is the main cause of increasing the degradation efficiency by Cl^- ions.

The effect of non-redox metal cations Ca^{2+}, Mg^{2+}, K^{+}, and Na^{+} on the degradation of OG in the Co/Oxone® system was also studied by using 5 mmol dm^{-3} concentrations of aqueous solutions of chloride salts. The examined cations showed a slight influence on the reaction rate at the examined cation concentration. Still, it is clear that these cations have an accelerating effect that can be presented in the following sequence: $Na^{+}< K^{+}< Ca^{2+}< Mg^{2+}$. This suggests that the reaction rate increased with increasing the Lewis acidity of non-redox metal ions. Similar results were obtained by other authors [27].

It can be concluded that the effects of coexisting ions are complex. The overall effect of the coexistence of several ions in the Co/Oxone® system depends on many factors, such as the ion type, concentrations of each species, *etc*.

3. 1. 4. Simultaneous dye degradation

Since more than one pollutant is usually present in real wastewater, it was important to investigate the simultaneous degradation of dyes to see how their interaction changes the degradation efficiency.

Prior to simultaneous degradation tests, the degradation experiments of single dyes were performed under the same reaction conditions as in a binary mixture. The starting concentrations of dyes were 20 mg dm^{-3} for each dye in binary dye mixed solutions. Three combinations of two dyes systems were investigated: OG-MB, OG-RB, and OG-BB. The reaction time was extended to 240 min so that degradation of both dyes could be followed.

In Figures 8 and 9 the results obtained for degradation of single dyes are presented together with degradation efficiencies obtained for binary dye mixtures under the same experimental conditions using CoA-1000 and CoA-1100.

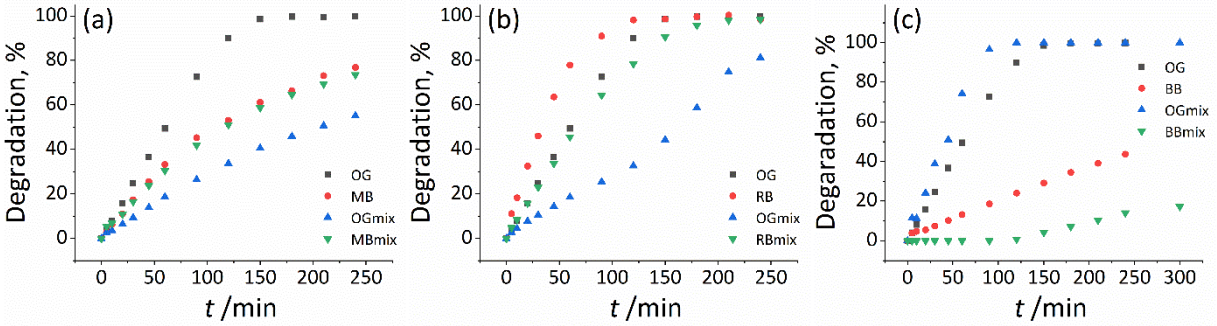

Figure 8. Degradation efficiency for single dyes and binary dye mixtures for CoA-1000 catalyst: (a) OG and MB, (b) OG and RB, and (c) OG and BB ($C_{0,dye}$ = 20 mg dm^{-3} ; $C_{0,dye\ mix}$ = 20 mg dm^{-3}; $V_{dye\ solution}$ = 200 cm^3 ; $m_{Oxone®}$ = 40 mg; $m_{CoA\text{-}1000}$ = 10 mg; θ = 30 °C).

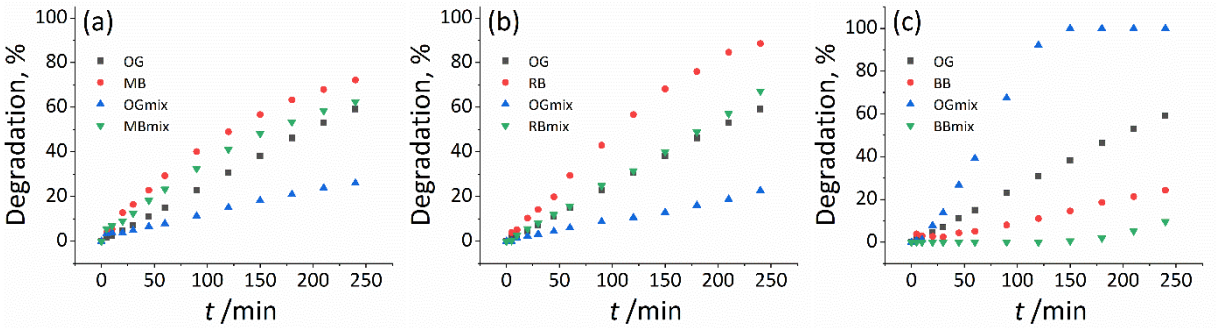

Figure 9. Degradation efficiency for single dyes and binary dye mixtures for CoA-1100 catalyst: (a) OG and MB, (b) OG and RB, and (c) OG and BB ($C_{0,dye}$ = 20 mg dm^{-3}; $C_{0,dye\ mix}$ = 20 mg dm^{-3}; $V_{dye\ solution}$ = 200 cm^3; $m_{Oxone®}$ = 40 mg; $m_{CoA\text{-}1100}$ = 10 mg; θ = 30 °C)

Differences in the results obtained for CoA-1000 and CoA-1100 are very pronounced. The efficiency of CoA-1100 was much lower for the degradation of single dyes and binary dye mixtures, but also the degradation profiles are noticeably different as compared to those obtained for CoA-1000.

For OG and MB combination of dyes, CoA-1000 was the most effective catalyst in OG single dye degradation, with complete degradation achieved after 150 min. In contrast, for MB as a single dye about 80 % of degradation was obtained during the entire investigated period. On the other hand, CoA-1100 was found to be the most effective in MB single dye degradation, achieving similar degradation of this dye as with CoA-1000 as the catalyst.

Degradation of OG (OG_{mix}) in the binary dye mixture with MB was significantly slower than in the single dye solution and compared to the MB_{mix} degradation for both catalysts, but with CoA-1000 the degradation percent of OG_{mix} was about twice as high as that obtained for CoA-1100. The effectiveness of MB_{mix} degradation with CoA-1000 as a catalyst was very similar to MB degradation in a single dye system, while for CoA-1100, degradation of the MB_{mix} was a bit lower.

In the OG and RB system, both catalysts had the best performance for RB single dye degradation, but the degradation rate of RB was significantly higher with CoA-1000. The complete degradation of this dye was achieved after 120 min for CoA-1000, while for CoA-1100 approximately 90 % degradation was reached after 240 min. When it comes to degradation in the binary dye mixture, a significantly higher rate was obtained for RB_{mix} for both catalysts. Degradation of OG and OG_{mix} was the slowest process for both investigated catalysts. Also, in the case of the CoA-1000 catalyst degradation of OG_{mix} has accelerated when most of the RB_{mix} amount was degraded.

In the OG and BB combination of dyes, the noticed behaviour was pronouncedly different than that observed in the other two systems. Firstly, both investigated catalysts showed selective degradation of OG_{mix}. It was observed that the degradation of the BB had not started before the degradation of OG was completed and even after that BB degradation was very slow for both catalysts. It was assumed that the interaction of OG and BB in a mixed dye system led to a significantly faster and selective degradation of OG_{mix}. Even CoA-1100, which was less effective for the other tested dye systems, showed excellent degradation efficiency. Also, the degradation of BB as a single dye was slower than for all other dyes tested in this study, indicating that the tested catalysts were the least effective for the degradation of this dye.

Since the adsorption of all investigated dyes was negligible, the observed degradation efficiency for single dye degradation can be probably attributed to differences in the molecular structure of the dyes [28,29]. OG and RB are anionic dyes, while MB and BB are cationic. Besides, OG and BB are azo dyes, MB is a heterocyclic aromatic chemical compound, while RB is an anthraquinone dye. On the other hand, degradation in a dye mixture involves interactions and competition between dyes [30].

4. CONCLUSION

Oxone® induced catalytic oxidative degradation of Orange G (OG) was investigated using two structurally and texturally different cobalt-doped alumina catalysts (CoA-1000 - calcined at 1000 °C and CoA-1100 - calcined at 1100 °C). The catalysts were characterized by using scanning electron microscopy. The surface microstructure of the CoA-1000 catalyst showed plate-like formations of different sizes and the presence of white spherical particles of similar sizes. A more homogeneous morphology without plate formations was observed in the case of CoA-1100. The presence of $Co_3O_4/CoAl_2O_4$ phases at CoA-1000 was also recognized indirectly by applying the EDX technique.

Influences of temperature and initial pH value on the degradation efficiency of OG were followed. It was found that the reaction rate increased with the temperature increase both for CoA-1000 and CoA-1100. The highest degradation rate was obtained at 60 °C. The pseudo-first order kinetic model was proved to be the most applicable, and the activation energy was about 80 kJ mol^{-1} for both catalysts. It was also shown that the reaction rate was the highest at an initial pH 7 for both catalysts, but they can be used in a wide range of initial pH values. Effects of coexisting cations and anions on the degradation rate were investigated in an attempt to simulate the real situation in practice. It was shown that all non-metal redox cations (Ca^{2+}, Mg^{2+}, K^{+}, and Na^{+}) as well as anions: Cl^{-} and $H_2PO_4^{-}$ enhanced the OG degradation rate, while NO_3^{-}, $SO_4^{2-}$and HCO_3^{-} inhibited OG degradation. Apart from OG degradation, the degradation of three other dyes (Methylene blue, Remazol brilliant blue, and Basic blue 41) was also investigated. Both studied catalysts were found to be efficient in these reactions, but a better performance of CoA-1000 was noticeable for all investigated dyes. Such finding is the consequence of differences in the structural and textural properties of the two catalysts, but most importantly of different cobalt phases present.

In the end, degradation of dyes in three binary dye mixtures was tested showing that the investigated catalysts can be used in complex systems with more than one organic pollutant present in wastewater.

Supplementary material: Additional data are available electronically on the article page on the journal's website: www.ache-pub.org.rs/index.php/HemInd/article/view/1218, or from the corresponding author on request.

Acknowledgments: This research was financially supported by the Ministry of Science, Technological Development and Innovation of the Republic of Serbia (Contract No: 451-03-66/2024-03/200026).

REFERENCES

[1] Busca G. Structural, surface, and catalytic properties of aluminas. In: Jentoft F, ed. Advances in Catalysis, Norman, Oklahoma, USA, Elsevier Inc. 2014; 57: 2-412, ISSN 0360-0564; http://dx.doi.org/10.1016/B978-0-12-800127-1.00003-5

[2] Maldonado CS, De la Rosa JR, Lucio-Ortiz C, Hernández-Ramírez A, Castillón Barraza F, Valente J. Low concentration Fe-doped alumina catalysts using sol-gel and impregnation methods: The synthesis, characterization and catalytic performance during the combustion of trichloroethylene. *Materials.* 2014; 7: 2062-2086. http://dx.doi.org/10.3390/ma7032062

[3] Jiratova K, Beranek L, Properties of modified aluminas. *Appl Catal.* 1982; 2: 125-138. http://doi.org/10.1016/0166-9834(82)80196-6

[4] Matori KA, Wah LC, Hashim M, Ismail I, Mohd Zaid MH. Phase transformations of α-alumina made from waste aluminum via a precipitation technique., *Int J Mol Sci.* 2012; 13: 16812-16821 doi:10.3390/ijms131216812

[5] Gitzen WH. Alumina as a ceramic material; Wiley-American Ceramic Society, Columbus, OH, USA, 1970.

[6] Khattak AK, Afzal M, Saleem M, Yasmeen G, Ahmad R, Surface modifcation of alumina by metal doping, Colloid surf A 2000; 162: 99-106 https://doi.org/10.1016/S0927-7757(99)00218-6.

[7] Marinović S, Mudrinić T, Dojčinović B, Barudžija T, Banković P, Novaković T, Cobalt-doped alumina catalysts in catalytic oxidation of tartrazine induced by Oxone®. J Environ Chem Eng. 2021; 9: 106348 (8 pages). https://doi.org/10.1016/j.jece.2021.106348

[8] Jovanović A, Bugarčić M, Sokić M, Barudžija T, Pavićević V, Marinković A, Photodegradation of thiophanate-methyl under simulated sunlight by utilization of novel composite photocatalysts. *Hem Ind.* 2024. https://doi.org/10.2298/HEMIND230523004J

[9] Hu P, Long M, Cobalt-catalyzed sulfate radical-based advanced oxidation: A review on heterogeneous catalysts and applications. *Appl Catal.* 2016; 181: 103-117.http://dx.doi.org/10.1016/j.apcatb.2015.07.024

[10] Nfodzo P, Choi H, Triclosan decomposition by sulfate radicals: Effects of oxidant and metal doses. *Chem Eng J.* 2011; 174: 629-634.http://dx.doi.org/10.1016/j.cej.2011.09.076

[11] Zhou ZG, Du HM, Dai Z, Mu Y, Tong LL, Xing QJ, Liu SS, Ao Z, Zou JP, Degradation of organic pollutants by peroxymonosulfate activated by MnO2 with different crystalline structures: Catalytic performances and mechanisms. *Chem Eng J.* 2019; 374: 170-180. https://doi.org/10.1016/j.cej.2019.05.170

[12] Stevanović G, Jović-Jovičić N, Popović A, Dojčinović B, Milutinović-Nikolić A, Banković P, Ajduković M, Degradation of textile dyes by Oxone® activated by cobalt supported chitosan-derived carbon-smectite catalyst. *Sci Sinter.* 2024; https://doi.org/10.2298/SOS2304270375

[13] KulićMandić A, Bečelić Tomin M, PucarMilidrag G, Rašeta M, Kerkez Đ, Application of impregnated biocarbon produced from soybean hulls in dye decolorization. Hem Ind. 2021; 75: 307-320. https://doi.org/10.2298/HEMIND210427023K

[14] Ganesan S, Kokulnathan T, Sumathi S, Palaniappan A, Efficient photocatalytic degradation of textile dye pollutants using thermally exfoliated graphitic carbon nitride (TE-g-C3N4). Sci Rep. 2024; 14: 2284. https://doi.org/10.1038/s41598-024-52688-y

[15] Far HS, Hasanzadeh M, Najafi M, Rabbani M, Highly porous organoclay-supported bimetal-organic framework (CoNi-MOF/OC) composite with efficient and selective adsorption of organic dyes. Environ Sci Pollut Res. 2023; 30: 43714-43725

[16] https://doi.org/10.1007/s11356-023-25374-1

[17] Thao LT, Nguyen TV, Nguyen VQ, Phan NM, Ki Jae Kim, Huy NN, Dung NT, Orange G degradation by heterogeneous peroxymonosulfate activation based on magnetic MnFe2O4/α-MnO_2 hybrid, J Environ Sci. 2023; 124: 379-396 https://doi.org/10.1016/j.jes.2021.10.008.

[18] Zhang J, Zhua MCL, Activation of peroxymonosulfate by iron-based catalysts for orange G degradation: role of hydroxylamine. RSC Adv. 2016; 6: 47562-47569 https://doi.org/10.1039/C6RA07231C

[19] Wu M, Wang Y, Lu B, Xiao B, Chen R, Liu H, Efficient activation of peroxymonosulfate and degradation of Orange G in iron phosphide prepared by pickling waste liquor. Chemosphere. 2021; 269: 129398.https://doi.org/10.1016/j.chemosphere.2020.129398

[20] Yu B, Li Z, Zhang S, Zero-valent copper-mediated peroxymonosulfate activation for efficient degradation of azo dye Orange G. Catalysts. 2022; 12: 700. https://doi.org/10.3390/catal12070700

[21] Madihi-Bidgoli S, Asghari F, Cheraghi S, Hamidinia H, Shagerdi E, AsadnezhadS, UV/periodate and UV/chlorine for dye degradation and real wastewater treatment: a comparative study, Water Pract Technol. 2023; 18: 2453-2468.https://doi.org/10.2166/wpt.2023.160

[22] Li C, Huang Y, Dong X, Sun Z, Duan X, Ren B, Zheng S, Dionysiou DD, Highly efficient activation of peroxymonosulfate by natural negatively-charged kaolinite with abundant hydroxyl groups for the degradation of atrazine, ApplCatal B: Environ. 2019; 247: 10-23. https://doi.org/10.1016/j.apcatb.2019.01.079

[23] Zhou G, Xu Y, Zhang X, Sun Y, Wang C, Yu P, Efficient Activation of Peroxymonosulfate by Cobalt Supported Used Resin Based Carbon Ball Catalyst for the Degradation of Ibuprofen. Materials. 2022; 15:5003. https://doi.org/10.3390/ma15145003
[24] Li N, Wang Y, Cheng X, Dai H, Yan B, Chen G, Hou L, Wang S, Influences and mechanisms of phosphate ions onto persulfate activation and organic degradation in water treatment: A review, Water Res. 2022; 222: 118896. https://doi.org/10.1016/j.watres.2022.118896
[25] Sheng B, Huang Y, Wang Z, Yang F, AiL, Liu J,On peroxymonosulfate-based treatment of saline wastewater: When phosphate and chloride co-exist,RSC Adv.2018; 8: 13865. http://doi.org/10.1039/c8ra00600h
[26] Zhao X, Ana QD, Xiao ZY, Zhai SR, Shi Z, Seaweed-derived multifunctional nitrogen/cobalt-co doped carbonaceous beads for relatively high-efficient peroxymonosulfate activation for organic pollutants degradation, Chem Eng J. 2018; 353: 746-759. https://doi.org/10.1016/j.cej.2018.07.171
[27] Yuan R, Ramjaun SN, Wang Z, Liu J, Effects of chloride ion on degradation of Acid Orange 7 by sulfate radical-based advanced oxidation process: Implications for formation of chlorinated aromatic compounds, J Hazard Mater. 2011; 196: 173-179. https://doi.org/10.1016/j.jhazmat.2011.09.007
[28] Xu A, Wei Y, Zou Q, Zhang W, Jin Y, Wang Z, Yang L, Li X, The effects of nonredox metal ions on the activation of peroxymonosulfate for organic pollutants degradation in aqueous solution with cobalt based catalysts: A new mechanism investigation, J Hazard Mater. 2020; 382: 121081. https://doi.org/10.1016/j.jhazmat.2019.121081
[29] Lončarević D, Dostanić J, Radonjić V, ŽivkovićLj, Jovanović D, Simultaneous photodegradation of two textile dyes usingTiO2 as a catalyst, React Kinet Mech Cat. 2016; 118: 153-164. http://doi.org/ 10.1007/s11144-016-0990-0
[30] Lin KYA, Lin TY, Degradation of Acid Azo Dyes Using Oxone Activated by Cobalt Titanate Perovskite, Water Air Soil Pollut. 2018; 229:10. https://doi.org/10.1007/s11270-017-3648-2
[31] Verma S, Rao BT, Singh R, Kaul R, Photocatalytic degradation kinetics of cationic and anionic dyes using Au-ZnO nanorods: Role of pH for selective and simultaneous degradation of binary dye mixtures, Ceram Int. 2021; 47: 34751-34764.https://doi.org/10.1016/j.ceramint.2021.09.014

Fentonov tip oksidativne degradacije boje Orange G i binarnih smeša boja pomoću Oksona® aktiviranog katalizatorima na bazi aluminijum oksida dopiranih kobaltom

Sanja R. Marinović[1], Tihana M. Mudrinić[1], Marija J. Ajduković[1], Nataša P. Jović-Jovičić[1], Dimitrinka A. Nikolova[2], Predrag T. Banković[1] i Tatjana B. Novaković[1]

[1]Univerzitet u Beogradu-Institut za hemiju, tehnologiju i metalurgiju, Centar za katalizu i hemijsko inženjerstvo, Beograd, Srbija
[2]Institut za katalizu, Bugarske akademije nauka, Sofija, Bugarska

(Naučni rad)

Izvod

Dva kobaltom dopirana katalizatora na bazi aluminijum oksida, sa ra zličitim teksturalnim i strukturnim karakteristikama, dobijena su sol-gel postupkom sinteze, nakon koje su uzorci žareni na tempreturi od 1000 °C odnosno 1100 °C. Dobijeni materijali su ispitani kao katalizatori u procesu degradacije anjonske tekstilne boje *Orange* G (OG) uz korišćenje Oksona kao prekursora sulfatnih anjon radikala, koji su glavna oksidativna vrsta. Ispitan je uticaj temperature i početnog pH na efikasnost degradacije, i uočeno je da porast temperature povećava brzinu reakcije. Maksimalna efikasnost degradacijeje dobijena na 60 °C. Primenjeni su različiti kinetički modeli i pokazalo se da kinetički model pseudo-prvog reda najbolje opisuje kinetiku ispitanog procesa. Takođe je za oba katalizatora utvrđeno da je optimalna vrednost pH za ispitivanu reakciju u oblasti blizu neutralne. Koegzistirajući katjoni (Ca^{2+}, Mg^{2+}, K^+ and Na^+) i anjoni Cl^- and $H_2PO_4^-$ su ubrzavali degradaciju OG, dok su je anjoni NO_3^-, SO_4^{2-} i HCO_3^- usporavali. Katalizatori su se pokazali efikasnii u degradaciji boja: metilensko plavo, osnovno plavo 41 i boje "Remazol brilliant blue", kao i u degradaciji boja u binarnim smešama. Ipak, razlike u strukturnim i teksturalnim svojstvima su uticale na razlike u katalitičkoj efikasnosti ova dva katalizatora.

Ključne reči: sol-gel aluminijum oksid; anjonske i katjonske boje; peroksimonosulfat; napredni oksidativni procesi; simultana degradacija bojai

SPISAK RECENZENATA

Spisak recenzenata radova čije je procesiranje završeno tokom 2024. godine

List of reviewers of papers whose processing has been completed during 2024

1. **Ioannis Anastopoulos,** *Department of Agriculture, University of Ioannina, Arta, Greece*
2. **Eleonora Aneggi,** *Università Di Udine, Udine, Italy*
3. **Desalegn Atalie**, *Bahir Dar University, Bahir Dar, Amhara, Ethiopia*
4. **Jelena Bajat***, Tehnološko-metalurški fakultet, Univerzitet u Beogradu, Srbija*
5. **Ivana Banković Ilić***, Tehnološki fakultet u Leskovcu, Univerzitet u Nišu, Srbija*
6. **Dejan Bezbradica***, Tehnološko-metalurški fakultet, Univerzitet u Beogradu, Srbija*
7. **Siniša Bikić,** *Fakultet tehničkih nauka, Univerzitet u Novom Sadu, Srbija*
8. **Danica Brzić,** *Tehnološko-metalurški fakultet, Univerzitet u Beogradu, Srbija*
9. **Estefania Canzian,** *Centre of Agrarian Sciences and Engineering, Federal University of Espirito Santo, Alegre, Brazil*
10. **Girish Chikmagalur,** *Manipal Institute of Technology, Manipal, Mahé, India*
11. **Gradimir Cvetanović,** *Tehnološki fakultet u Leskovcu, Univerzitet u Nišu, Srbija*
12. **Iana Ćubela,** *Metalurško-tehnološki fakultet, Univerzitet u Zenici, Bosna i Hercegovina*
13. **Aleksandar Dekanski,** *Institut za hemiju tehnologiju i metalurgiju, Univerzitet u Beogradu, Srbija*
14. **Jelena Dikić,** *Tehnološko-metalurški fakultet, Univerzitet u Beogradu, Srbija*
15. **Natalija Dolić,** *Metalurški fakultet Sisak, Univerzitet u Zagrebu, Sisak, Hrvatska*
16. **Ivana Drvenica**, *Institut za medicinska istraživanja, Univerzitet u Beogradu, Srbija*
17. **Maja Đolić,** *Tehnološko-metalurški fakultet, Univerzitet u Beogradu, Srbija*
18. **Aleksandar Đukić,** *Građevinski fakultet, Univerzitet u Beogradu, Srbija*
19. **Mihal Đuriš,** *Institut za hemiju, tehnologiju i metalurgiju, Univerzitet u Beogradu, Srbija*
20. **Radmila Garić Grulović,** *Institut za hemiju, tehnologiju i metalurgiju, Univerzitet u Beogradu, Srbija*
21. **Olalla González Sas,** *Department of Chemical Engineering University of Vigo, Spain*
22. **Branimir Grgur,** *Tehnološko-metalurški fakultet, Univerzitet u Beogradu, Srbija*
23. **Miha Grilc,** *Kemijski inštitut, Ljubljana, Slovenia*
24. **Branka Hadžić***, Institut za fiziku, Univerzitet u Beogradu, Srbija*
25. **Jordan Hristov,** *University of Chemical Technology and Metallurgy, Sofia, Bulgaria*
26. **Špiro Ivošević,** *Pomorski fakultet Kotor, Univerzitet Crne Gore, Kotor, Crna Gora*
27. **Aleksandar Jovović,** *Mašinski fakultet, Univerzitet u Beogradu, Srbija*
28. **Nikola Karličić,** *Mašinski fakultet, Univerzitet u Beogradu, Srbija*
29. **Stjepan Kožuh,** *Metalurški fakultet, Sveučilište u Zagrebu, Sisak, Hrvatska*
30. **Tibela Landeka Dragičević***, Prehrambeno-biotehnološki fakultet, Sveučilište u Zagrebu, Hrvatska*
31. **Zhi-Yong Liu,** *Key Laboratory of Green Chemical Technology and Efficient Energy Saving of Hebei Province, Hebei University of Technology, Tianjin, China*
32. **Davor Lončarević,** *Institut za hemiju, tehnologiju i metalurgiju, Univerzitet u Beogradu, Srbija*
33. **Zorica Lopičić,** *Institut za tehnologiju nuklearnih i drugih mineralnih sirovina, Beograd, Srbija*
34. **Ivana Lukić,** *Tehnološko-metalurški fakultet, Univerzitet u Beogradu, Srbija*
35. **Nataša Lukić,** *Tehnološki fakultet, Univerzitet u Novom Sadu, Srbija*
36. **Vesna Maksimović,** *Institut za nuklearne nauke Vinča, Univerzitet u Beogradu, Srbija*
37. **Branislav Marković**, *Institut za tehnologiju nuklearnih i drugih mineralnih sirovina, Beograd*
38. **Radmila Marković,** *Institut za rudarstvo i metalurgiju, Bor, Srbija*
39. **Gordana Matijašić,** *Fakultet hemijskog inženjerstva tehnologije, Sveučilište u Zagrebu, Hrvatska*
40. **Jelena Milojković,** *Institut za tehnologiju nuklearnih i drugih mineralnih sirovina, Beograd, Srbija*
41. **Dušan Mijin***, Tehnološko-metalurški fakultet, Univerzitet u Beogradu, Srbija*

42. **Milica Mladenović,** *Institut za nuklearne nauke Vinča, Univerzitet u Beogradu, Srbija*
43. **Marija Nikolić***, Tehnološko-metalurški fakultet, Univerzitet u Beogradu, Srbija*
44. **Branislava Nikolovski,** *Tehnološki fakultet, Univerzitet u Novom Sadu, Srbija*
45. **Bojana Obradović,** *Tehnološko-metalurški fakultet, Univerzitet u Beogradu, Srbija*
46. **Marko Obradović,** *Mašinski fakultet, Univerzitet u Beogradu, Srbija*
47. **Snežana Papović,** *Prirodno-matematički fakultet, Univerzitet u Novom Sadu, Srbija*
48. **Vladimir Pavičević**, *Tehnološko-metalurški fakultet, Univerzitet u Beogradu, Srbija*
49. **Lidija Peić Tukuljac***, Institut za prehrambene tehnologije, Univerzitet u Novom Sadu, Srbija*
50. **Rada Petrović,** *Tehnološko-metalurški fakultet, Univerzitet u Beogradu, Srbija*
51. **Jasna Prlić Kardum,** *Fakultet hemijskog inženjerstva tehnologije, Sveučilište u Zagrebu, Hrvatska*
52. **Nenad Radić,** *Centar za katalizu i hemijsko inženjerstvo, Institut za hemiju, tehnologiju i metalurgiju, Univerzitet u Beogradu, Srbija*
53. **Ivona Radović,** *Tehnološko-metalurški fakultet, Univerzitet u Beogradu, Srbija*
54. **Ana Rita Lado Ribeiro,** *University of Porto, Portugal*
55. **Ivica Ristović,** *Rudarsko-geološki fakultet, Univerzitet u Beogradu, Srbija*
56. **Jorge Rodriguez-Chueca,** *Technical University of Madrid, Spain*
57. **Maja Sremački,** *Fakultet tehničkih nauka, Univerzitet u Novom Sadu, Srbija*
58. **Snežana Stanković,** *Tehnološko-metalurški fakultet, Univerzitet u Beogradu, Srbija*
59. **Srećko Stopić,** *IME Metallurgische Prozesstechnik und Metallrecycling, RWTH Aachen, Germany*
60. **Ewa Strzałkowska,** *Department of Applied Geology, Faculty of Mining, Silesian University of Technology, Gliwice, Poland*
61. **Anna Szelwicka,** *Department of Chemistry, Technical University of Darmstadt, Germany*
62. **Predrag Škobalj,** *Institut za nuklearne nauke Vinča, Univerzitet u Beogradu, Srbija*
63. **Anita Štrkalj,** *Faculty of Metallurgy, University of Zagreb , Sisak, Croatia*
64. **Lidija Peić Tukuljac,** *Institute of Food Technology, University of Novi Sad, Serbia*
65. **Andromachi Tzani,** *School of Chemical Engineering, National Technical University of Athens, Greece*
66. **Đorđe Veljović,** *Tehnološko-metalurški fakultet, Univerzitet u Beogradu, Srbija*
67. **Tatjana Volkov-Husović,** *Tehnološko-metalurški fakultet, Univerzitet u Beogradu, Srbija*
68. **Milan Vraneš,** *Prirodno-matematički fakultet, Univerzitet u Novom Sadu, Srbija*
69. **Jian-Ping Zou***, Nanchang Hangkong University, Nanchang, PR China*
70. **Anton Zubrik,** *Institute of Geotechnics SAS, Košice, Slovak Republic*
71. **Emila Živković***, Tehnološko-metalurški fakultet, Univerzitet u Beogradu, Srbija*
72. **Nikola Živković,** *Institut za nuklearne nauke Vinča, Univerzitet u Beogradu, Srbija*